Operation and Control of Hybrid Power Plants in LV Isolated Microgrid

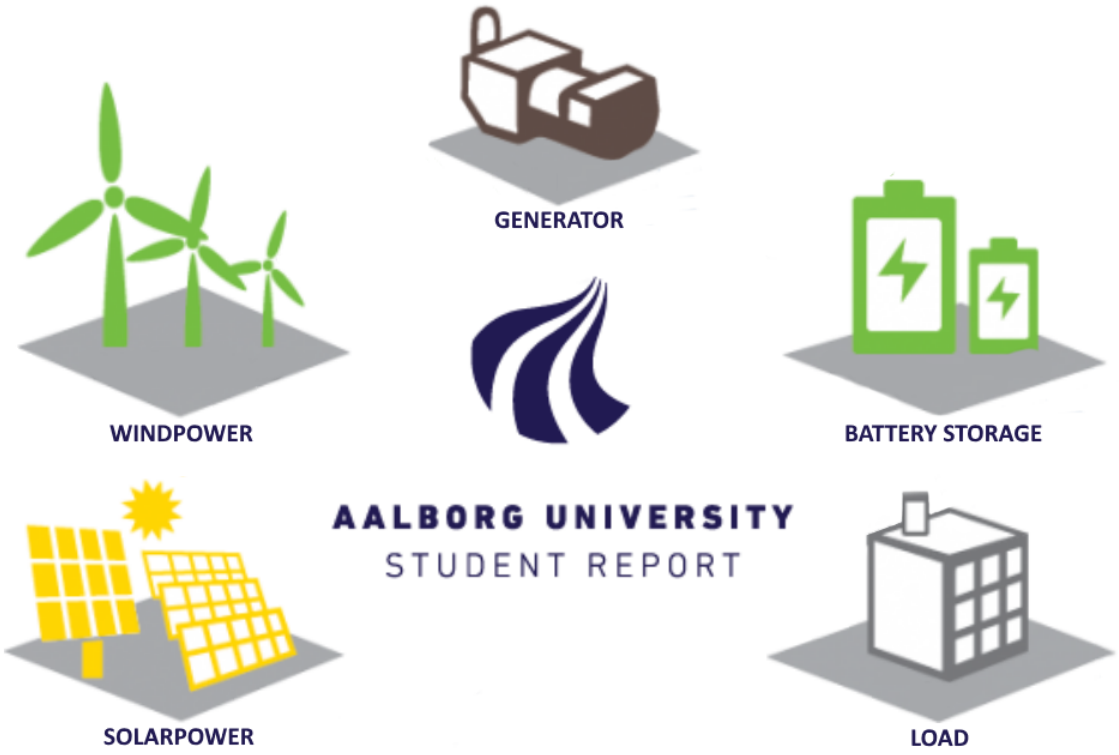

P10 Master Thesis
Group EPSH4-1031
Electrical Power System
and High Voltage Engineering
Aalborg University
June 1ST 2018

AALBORG UNIVERSITY

School of engineering and science
Energy Engineering
Pontoppidanstraede 111
9000 Aalborg
http://www.ses.aau.dk/

Titel:
Operation and Control of Hybrid Power Plants in LV Isolated Microgrid

Project:
P10-project

Project period:
February 2018 - June 2018

Project group:
EPSH4-1031

Group members:
Adrian Expethit
Morten Virklund Pedersen
Sebastian Bille Sørensen

Supervisor:
Florin Iov

Co-supervisor:
Lennart Petersen

Number printed: 3
Pages: 186
Appendixes: 5
Finished 1-06-2018

Synopsis:

Following the increasing penetration of distributed energy resources (DER), the conventional power system is changing. These changes requires new control strategies for future power systems. This has lead to a high interest of the microgrid topic. This project focuses on developing microgrids with high penetration of DERs meant for mainly or solely isolated operation. Recent studies propose a wide range of solutions, however the practical aspects of implementing suggested control architecture are rarely included, and specific types of DERs are often not considered. Furthermore, a properly structured approach towards designing the grid, usable by DSOs is found lagging. This project therefore develops microgrid voltage and frequency control from a simple and practical approach. Emphasis is put on the specific DER units, their behaviour from grid perspective and suited functions. State space models are made of the grid and generation/load units, these are used to analyse grid behaviour in various scenarios and design control, which ensures stable grid operation. Device level control of all units and network level control which removes steady state errors in voltage and frequency, is designed. Finally, dynamic model of the grid is used to show stable operation during large load changes. A step wise guide for how to design DLC and NLC microgrid control is proposed, and the design in this report is an example of the performance of this guide.

Preface

This report has been made during the 4th semester on the Electrical Power Systems and High Voltage Engineering MSc. programme at Aalborg University.

The individual chapters in the report are introduced and concluded with a section written in the *italic* font. Throughout the report there will be stated references all listed by the end of the paper in the Bibliography. The references are denounced cf. the Harvard method hence a statement will be referred by [Surname, year]. If more than one reference from the same year has the same author, these will be denoted with a, b, c and so forth. This reference refers to the bibliography where books are referred by author, title, ISBN-number, publisher, edition and year while websites are referred by author, title, year, URL and time of last visit. Technical papers are referred by author, title and year. If the source is added before a full stop it implies that it belongs to the contents of that sentence. However, if the source is added after a full stop, it covers the contents of the entire previous paragraph.
Figures, tables and equations are numbered according to the particular chapter they're placed in. The first figure in chapter three will herefore be assigned with figurenumber 3.1 and the second 3.2 etc. Descriptive captions for tables and figures are found above relevant tables and under figures.

The report is made in collaboration with all of the group's members, thus all the members are equally accountable for its contents.

Adrian Expethit	Sebastian Bille Sørensen	Morten V. Pedersen

Abstract

With the increase of renewable energy and thereby intermittent power sources in the power system, the need for coordination and control of such devices in local areas are needed. The concept of microgrids is also gaining interest due to its use in rural areas and small communities that are disconnected from the main grid and has to operate on their own. The combination of being able to utilize more renewable energy sources and to operate in islanded mode is highly attractive.

This thesis therefore deals with the topic of operation and control of such LV hybrid isolated microgrids, with the main focus of giving a step-wise guide on how to design the device and network level control of these power plants. This therefore includes control of voltage and frequency in the grid.

When looking at the existing rural areas versus the ones that are run as microgrids, a huge difference occurs. This suggests that microgrids are not yet the go-to solution for such areas. The reason for this is the many cumbersome tasks with regards to control. An isolated microgrid is dependent on equalizing supply and demand at all times. Hence, with renewable energy sources this become cumbersome, due to their intermittent behaviour. The state of the art in this field is therefore studied, with regards to device and network level control, as this will be the fundamental control layers in a functioning hybrid isolated microgrid. 56 papers are analysed and the relevant ones are presented in this study.

From the state of the art literature, it is seen that almost none of the papers fulfil the state of the art criteria that are defined before studying the papers. As the criteria are based on practical issues in such microgrids, it is concluded, that the literature is more keen on novelty and complex algorithms rather than practical and simple solutions to the problems. A guideline for how to design device and network level control is not present, which therefore further motivates this study. The literature is seen to use a specific method without considering the system at hand. This project therefore reverses this process by looking at the system in hand and thereby deducing the relevant control methods and strategies.

This is therefore firstly done, by looking at the system components, their capabilities with regards to V and f control, the microgrid main goal and the critical scenarios

that can occur in such system. The units are wind turbines (WT), photovoltaics (PV), diesel gensets (DGS) and battery energy storage systems (BESS). Now that an understanding of the system is attained, a preliminary control proposal can be made, which leads to defining the BESS and DGS as grid-forming units, as long as they are placed at the same site. When both are on, the DGS will control P/f and BESS controls Q/V by droops. When the DGS is off, BESS will control both. Droops are used for the BESS to mimic DGS behaviour. PV and WT will function as grid-following units.

Each individual unit is modelled modularly in state space. State space is used as this will be the best tool with regards to control due to the ease of analysing the system in frequency and time-domain, interchangeably. The eigenvalues are checked at nominal and extreme operating points. By looking at the frequencies of the eigenvalues, these can be allocated to their respective control loop in each model. Hence when varying the operating point for V, PF and P/Q it is seen that V and P/Q have an influence on some control loops. It is checked and confirmed that these eigenvalues do not become unstable for variations to extreme operating points and the individual models are therefore stable in their operating range. A voltage sensitivity analysis is made, where it is seen that P has more influence on V than Q, and that P/Q residuals are approx. same for the load bus for all the units. This knowledge is useful for designing network level control.

Valuable insight is now given by the full model state matrix. It is found that the most influential eigenvalue is related to the PLL by the participation matrix. The PLL and the voltage control loop gain of the battery is seen to have a huge influence on stability and these device level loops are therefore tuned carefully to not enter unstable region during different operational points. The latter is seen to cause an unstable eigenvalue whenever the DGS is turned off, and is therefore retuned in order to achieve stability. This therefore shows, that the state space model can be used to retune and understand critical phenomena to help as preliminary study to prevent instability.

Finally, an example of how the model can be used to design network level control is given. The scenario is w/o the DG, as this is seen to be the most critical scenario. The device level control is investigated due to large sudden load disturbances, frequency and voltage errors are seen to appear. These are cancelled by tuning outer network level loops, where P and Q from the battery controls f and V errors, respectively. Finally, based on all the observations and procedure, a step-by-step guideline is given for design of device and network level control.

Contents

Nomenclature

Symbol	Describtion	Unit
V	Voltage	V
I	Current	A
L	Inductance	H
C	Capacitance	F
R	Resistance	Ω
X	Reactance	Ω
Z	Impedance	Ω
P	Power	W
Q	Reactive Power	VAr
S	Apparent Power	VA
f	Frequency	Hz
ω	Frequency or Speed	rad/s
PF	Power Factor	–
$p.u.$	Per Unit	–
u_k	Short circuit voltage	%
δ_n	Relative converter output voltage	–
ς_n	DC-link damping	–
P_n	Rated power	W

Index	**Description**
copper	Copper losses in transformer
T	Transformer
DC	Value referred to DC-link
s	Switching frequency
MAX	Maximum limit
id	Value behind inverter filter in d-axis
od	Inverter output in d-axis
iq	Value behind inverter filter in q-axis
oq	Inverter output in q-axis
dq	Value in dq frame
unit	Value referred to specific unit
0	Initial value
inv	value referred to inverters
line	value referred to lines
load	value referred to load
bus	value referred to buses
Q	Value referred to global Q-axis
D	Value referred to global D-axis
q	Value referred to local q-axis
d	Value referred to local d-axis
ft	Filter & transformer
p	Proportional gain
i	Integral gain
SG	Matrix referred to synchronous generator
DG	Matrix referred to full DGS
avr	Matrix referred to DGS AVR
sys	system

Abbreviation	**For**
RES	Renewable Energy Resources
DER	Distributed Energy Resources
WT	Wind turbines
PV	Photo Voltaic
ESS	Electrical Storage Systems
DG	Distributed Generation
DGS	Diesel Generator Set/Diesel Gen-set
SG	Synchronous Generator
BESS	Battery Electrical Storage Systems
ICT	Information and Communication Technology
HV	High Voltage (Above 100 kV)
MV	Medium Voltage (1-100 kV)
LV	Low Voltage (Below 1 kV)
AC	Alternating Current
DC	Direct Current
Wi-Fi	Wireless Fidelity
CSI	Current source inverter
VSI	Voltage source inverter
PI	Proportional Integral controller
MPPT	Multi Power Point Tracker
SoC	State of Charge
VRLA	Valve Regulated Lead-Acid (Battery)
CCM	Current Control Mode
VCM	Voltage Control Mode
MGCC	Microgrid Central Controller
DM	Decision Maker
NDZ	Non-detection Zone
RL	Resistive and Inductive (Load)
PCC	Point of Common Connection
DSO	Distribution System Operator
TSO	Transmission System Operator
AVR	Automatic Voltage Regulator
PSS	Power System Stabiliser
RMS	Root Mean Square
DQ	Direct/Quadrature (-axis) Global frame
dq	Direct/Quadrature (-axis) Local frame
PLL	Phase Lock Loop
SSM	State Space Model

Abbreviation	**For**
SPM	SimPower Model
EMT	Eletro Magnetic Transient
eig	Eigenvalue
EF	Eigen-Frequency

Introduction 1

Modern society is highly dependent on a stable energy supply. Following the increasing penetration of distributed energy resources (DER), such as wind turbines (WTs), photovoltaics (PVs), micro-turbines, fuel cells, battery storage ect., the conventional power system, known by centralized power generation and unidirectional power flow, is changing. These changes call for a new strategy to control the future power systems. New solutions and advanced technologies like Electrical Storage Systems (ESSs) and Information and Communication Technologies (ICTs) have brought along a concept called microgrids. An example of a new approach is seen in Denmark in the CELL project, where a novel control method of the distribution grid is implemented, as over 50 % of the total production capacity is dispersed throughout local distribution grids of 60 kV and under [Lund, 2007]. The project aims to be able to control both load feeders, generation and main circuit breakers as seen in Figure 1.1.

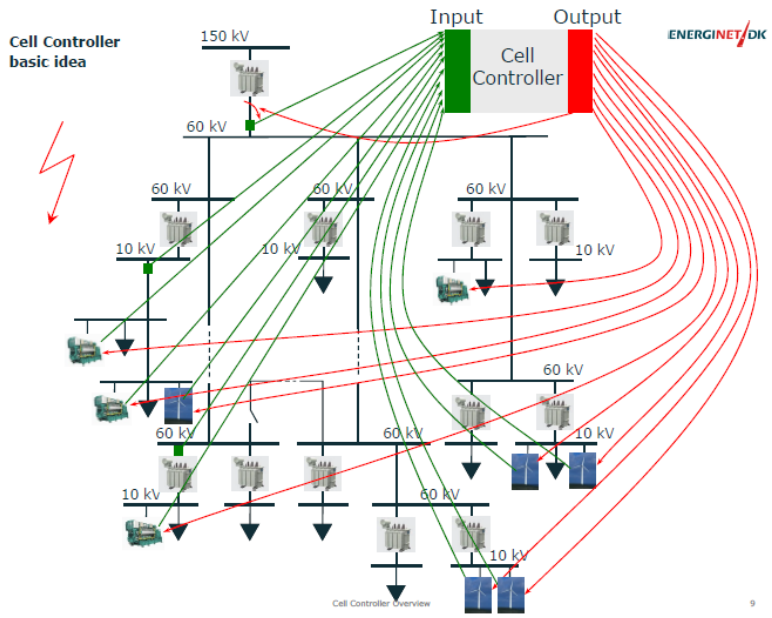

Figure 1.1: Cell controller functionalities

The main goal is to be able to control the grid in island mode whenever a disconnection to the HV grid is needed. Another goal is to make the Cell controller black-start itself to a state of controlled isolated operation.

There is no clear definition of a microgrid, however the "European technology platform of SmartGrids" defines a microgrid as a grid containing distributed generation (DG), ESS and controllable loads (such as heat pumps or electric vehicles) with the capability of working disconnected from the main power grid (islanded mode) [Platform, 2006]. When connected to the main grid the microgrid should function as a single controllable entity capable of being either a load or a small source of power, and can be used to support the main grid. Basically it is the implementation of intelligent control that distinguishes a microgrid from a regular distribution grid with DGs [Hatziargyriou, 2014].

The basic idea of the microgrid control is to balance the power demand and production locally, and by including the use of energy storage, handle high penetration of renewable technologies and optimize the utilization of these. It is also important that the grid ensures good power quality including stable voltage and frequency. Microgrids have several benefits such as [Gao, 2015]:

- Invites the possibility of using DERs, which are more scalable than large power plants

- Reduce transmission losses compared to bulk power systems, by using DERs close the the load demand
- Reducing electricity prices and carbon emissions
- Can help supply rural areas and development countries which may have grids that are likely to have power outages due to grid weakness or natural disasters. These areas may have limited access to the utility grid, hence the benefit of using a microgrid in island mode.
- Microgrids can enhance power quality for consumers and local reliability

Microgrids can be categorized in 5 different types [Hayden, 2013], namely the campus, military base, commercial/industrial, community/utility and remote isolated microgrids. The names suggest their applications.

Microgrids have already been introduced in power systems around the world, especially in Europe. As an example the Gaidouromandra, Kythnos Microgrid in Greece is an isolated grid with intelligent load control. The system contains [Hatziargyriou, 2014]:

- 12 houses
- 10 kW PV
- 53 kWh battery bank
- 5 kW diesel genset
- For monitoring and communication: 2kW PV, 32 kWh battery bank
- Overhead lines and communication cable between units
- Non critical loads such as water pumps in each house

Minor issues with humidity and loss of wireless fidelity (Wi-Fi)-signals for the communication were seen on this cite. A complex control method was applied to the cite which lead to the conclusion that such complex algorithm was not necessary for the small system [Hatziargyriou, 2014]. But the algorithm was concluded to be scalable. The main drawback was that the system communication required high costs due to the complexity of the control scheme. However, it was seen that the PVs and batteries helped utilize the renewable energy and thereby minimize the use of diesel gensets.

Another grid in Mannheim, Germany has tested the transition from grid connected to island mode. The grid is an intermeshed ring grid structure. The system consists of:

- 580 households
- Several privately owned small photovoltaic systems

- Several storage units and loads

Within this grid a big commercial load with PV, controllable loads and battery storage was used to test the transition from grid connected to island mode. A single battery was used solely for the purpose of frequency control between the transition from main grid connected to island mode. During the period of island mode the frequency increased from 50-52 Hz. Flexible loads were present in the system and a control algorithm was implemented to shed the load during critical operation such as in island mode. It was seen that the control was successful in keeping the voltage and frequency limits while still maintaining operation and seamless transition towards island mode.

A list of several pilot projects in Europe can be seen in Figure 1.2.

No	Site (responsible partner)	Country	Type of microgrid
1	Gaidouromantra on Kythnos Island (CRES)	Greece	residential/island
2	Mannheim-Wallstadt settlement (MVV)	Germany	residential
3	Bronsbergen holiday park (Continuon/EMforce)	Netherlands	residential
4	Ilhavo municipal swimming pool (EDP Distribution)	Portugal	commercial
5	Bornholm Island (DTU, OESTKRAFT)	Denmark	multi-microgrid/island
6	AGRIA farm (UKIM, BIG)	FYROM	rural – commercial
7	LABEIN test facility (LABEIN)	Spain	large-scale test facility
8	ERSE test facility (ERSE)	Italy	large-scale test facility

Figure 1.2: European pilot microgrid projects [Hatziargyriou, 2014]

Most of these grids are AC grids, however a discussion of using DC microgrids has arisen in recent studies [Guerrero et al., 2011]. This is due to the ease of control since there is no frequency control, no need for synchronization and no unbalances as stated in [Guerrero et al., 2011]. Several loads introduced in the system are also using DC. However, no regulations have been made for DC grids. DC grids has several drawbacks due to the lack of protection schemes, and in general safety standards. Furthermore, most existing DER's are developed for AC grids. For these reasons, this project will not consider DC microgrids.

It is also seen from the examples that most of these are grid connected. However, there may be many places in the world that will benefit from the option of using renewable energy sources but cannot be grid connected due to their placement and resources. Such a system can be found in developing countries, but also smaller areas where it may be beneficial to be off grid due to higher expenses related to connecting these small areas to the main grid. This motivates a research with focus

on microgrids meant for mainly or solely isolated operation, such as those in rural areas or small islands, as such areas may not have any other option than to operate in island mode.

The grid in scope will be LV and AC as this will be the commonality for these areas. Figure 1.3 shows the typical topology for such a system according to [IEC-62898-1, 2017]. The system contains some renewable DERs (WT and PV), a synchronous generator (could be small diesel gensets) and some storage. Furthermore, there are both critical and non-critical loads. The storage could be e.g. battery banks, flywheels or super capacitors, however in this report only battery electrical storage systems (BESS) will be considered. Considering the system to be a small village/community on a small island or some other remote area, critical loads could be a medical clinic or telecommunications mast while non-critical loads could be residential houses.

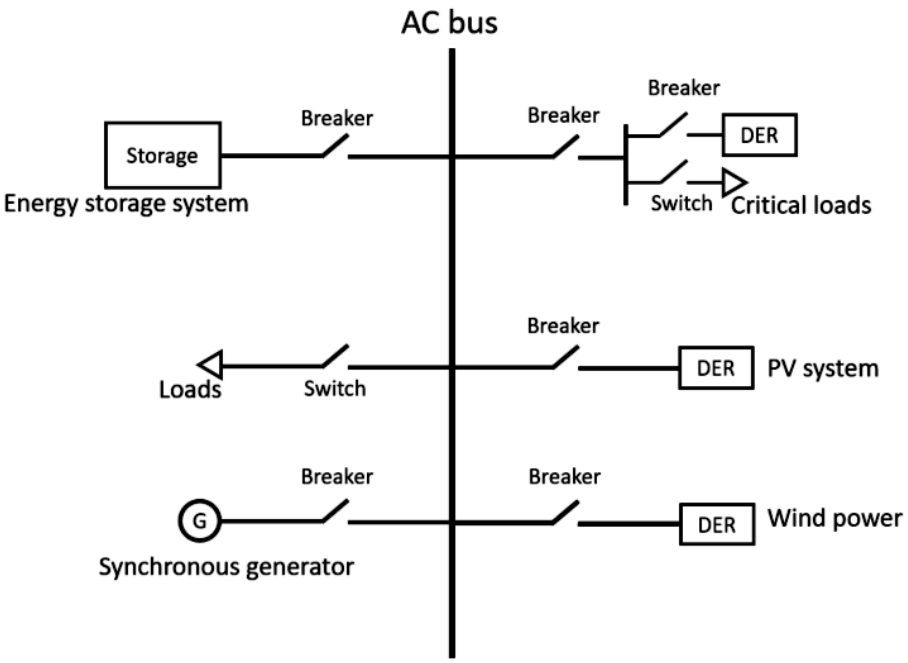

Figure 1.3: Typical topology for an isolated microgrid. [IEC-62898-1, 2017]

The core of a microgrid is the control which makes the DG's, storage and loads work together in order to achieve high quality and reliable power. Based on EPRI definitions the control architecture of a microgrid as shown in Figure 1.3 can be divided into the following layers [Maitra and Simmins, 2015]:

- Device level control - Control of individual DER units.
- Network level control - Coordination of individual DER units.
- Supervisory control - Energy management, optimal dispatch ect.

The typical functions and temporal requirements of the different control layers are shown in Table 1.1. In literature "device level control" is often called "primary control" and "network level control" is called "secondary control", these terms are however misleading as often the functions of device and network level are mixed in different ways in papers using the primary and secondary terms. Therefore, the clearly specified layers given in Table 1.1 defined by EPRI will be used in this project.

Table 1.1: Microgrid control layer functions

Control layer	Temporal requirements	Typical functions
Supervisory	Minutes	Load forecasting. Optimal dispatch. Environmental optimization.
Network level	Seconds	Correction of frequency and voltage errors. Load control. Power quality improvements
Device level	Micro- to miliseconds	Local DER control. Voltage control. Frequency control. Load sharing between DERs.

The device level control is the fast response and requires no communication as it acts based on local measurements at the individual DER units. The network level control however acts to correct steady state errors generated by the device level control and requires some interaction between the DER units. The supervisory control sends signals to the network level on a slower time-scale in order to achieve optimal dispatch.

Even though several microgrids exist in the world, it does however not seem to be the go-to solution for rural areas and development countries. This leads to the consideration of the challenges microgrids may bring which will be discussed in the following chapter.

Problem analysis 2

The previous chapter has given an introduction to the concept of microgrids and why it is relevant. This chapter will introduce the general problems regarding microgrids and what the challenges are in adopting this concept. Following this, a State of the Art review on this topic is presented, which will reveal the current trends and ideas to solve the problems.

The problems in isolated microgrids can be divided into the three different control levels, which are problems related to the upper level supervisory control, the network level control and the device level control. This chapter will focus on the problems related to device and network level control. The reason for this being that these are the fundamental controls that need to function in order to have a reliable microgrid. Having a reliable device and network level control is however cumbersome, due to the intermittent behaviour of RESs. This is especially true for isolated microgrids where there is no upstream grid that can support in periods of power mismatch between demand and production. It is therefore necessary to have a reliable and functioning device- and network level control that can stabilize the voltage and frequency of the grid. Hence, this should be accounted for first.

2.1 Problems in isolated microgrids

LV grids tend to have a high R/X ratio, compared to MV and HV grids. Cables are often used in LV grids, where the three conductors are in close proximity. The self inductance of a line is dependent on the distance of the currents return path, which due to the cable configuration is very low. The relatively thin conductors have a high resistance, which compared to the low self induction makes a high R/X ratio in LV grids. [Bergen, 1999]. This makes the control of voltage cumbersome due to the lower influence of reactive power on the voltage level. This aspect is important to consider as new control methods may be needed in order to control the voltage and frequency. Another thing that is of general concern in microgrids

is to choose one or more *grid-forming units*. This is the unit that will control the voltage and frequency of the grid. Converter based units are today usually used as *grid-following units*, meaning that they operate as current sources. A system mainly consisting of RESs, BESS and synchronous generators may have problems choosing the grid-forming unit. The problem with using the BESS or RESs as the grid-forming unit is the uncertainty of power production and power reserve. If a battery takes on V/f control it might have to be of high capacity in order to ensure stable operations when there is high or low load demand [Miller, 2017]. On the other hand, if the V/f control is done with the synchronous generator, this device might have to operate during times where it is not needed to run at rated power and hence costs will increase. These considerations need to be accounted for when defining the control of the grid [Hatziargyriou, 2014].

Another important issue is the transition from the conventional synchronous generator based grid to an inverter based grid. This transition presents new issues with regards to frequency control. In a conventional grid, the frequency is related to the rotor speed of synchronous machines. Due to the inertia from the machine, the frequency will not change instantly but will vary in a slow manner, compared to converters where the frequency is related to the converter control. In some cases, the frequency may even change in a discrete manner due to the control of converters [Miller, 2017]. It is clear, that control of converters is much faster than of synchronous machines. On the other hand, synchronous machines can provide currents in the order of 4-5 p.u. for a shorter period, which is needed in case of faults. Many converters are installed to shut down during faults and may therefore not even support the system. Given that they can operate during faults, they are only capable of supplying a current around 1.2 p.u. [Miller, 2017].

As explained in the introduction, the key element of microgrids is the ability to intelligently control the devices. This may require communication. However, there exist no general rules for communication system requirements. The microgrid operator may not want to implement fiber optics or other forms of communication lines due to economical reasons. It could therefore be necessary to look at what the system has already and how this can be used in an optimal way. Communication between devices may however be crucial in order to use a certain type of control architecture. Another issue is that the RESs may not be able to produce the amount of power needed from the device control algorithm [Gao, 2015]. The placement of the network control is also of concern. It could be necessary to place one or several units (microprocessors) that can run the control algorithm and send this information to the units [Gao, 2015].

A problem regarding the active and reactive power sharing between units arises when first of all, the active power have to be shared in an economical way, which also ensures the stability of the grid. Secondly, if the system consist of several converter based DGs, the problem arises for which one to deliver the reactive power, and how to make the control system, such that changes in the load (both reactive and active power), constantly is taken care of. In a large conventional grid, only the large units take care of this reactive power delivery. This however, does not apply in an isolated microgrid where it can be necessary for all units to share the reactive power demand among them, to ensure stability of the system.

It is clear from this, that several aspects need to be accounted for when looking at the device and network level of the microgrid. The state of the art in relation to this is therefore needed in order to understand how these problems can be solved. However, in order to understand the aspects discussed in the State of the Art review, some general theory about the microgrid and their power converter controls will be explained first.

2.2 Basics of power converter control for microgrids

As mentioned in the introduction, many DER units such as (WT, PV and BESS ect.) are power converter based and their lack of inertia makes it harder to achieve stable voltage and frequency control in a microgrid, compared to a grid with mainly synchronous generation. In recent research, there are several approaches towards designing the device and network level control in a grid with high penetration of converter based sources. In [Rocabert et al., 2012] and [Guerrero et al., 2011] the basics of how to control the power converters in a microgrid are presented. How the power converters are operated can be divided into three classifications: grid-feeding, grid-forming and grid-supporting [Rocabert et al., 2012]. The ideal representation of the different types are shown in Figure 2.1.

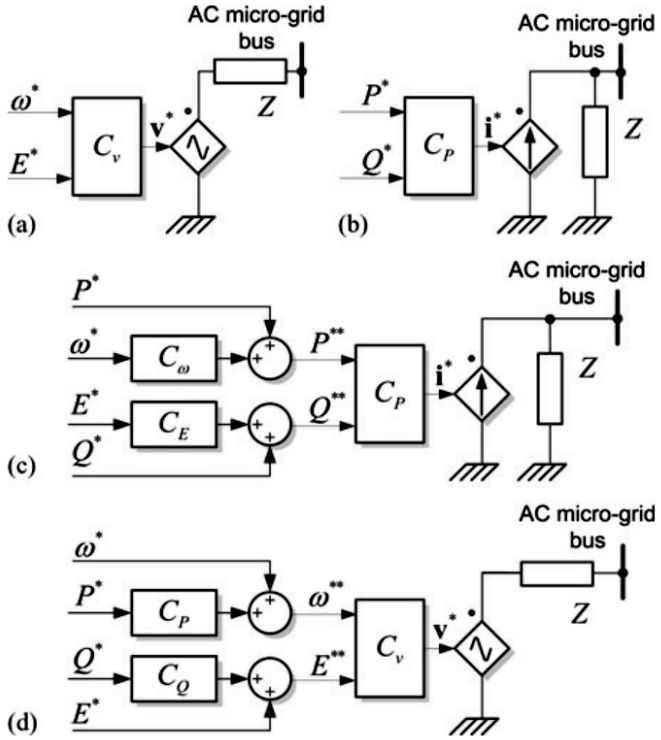

Figure 2.1: Power converter control classifications, (a) grid-forming, (b) grid-feeding, (c) grid-supporting current source, (d) grid-supporting voltage source. [Rocabert et al., 2012, P. 2]

The grid-feeding converters, Figure 2.1(b), can be represented as an ideal AC current source in parallel with high impedance and is controlled by references for the active and reactive power to be delivered to the grid, see Figure 2.2. In order for these to work there must be some other source, that sets the voltage amplitude and frequency for the grid. The P and Q references can be set either by a MPPT algorithm or controlled by the network level, in order to properly share the power generation between grid-feeding converters and help control the voltage amplitude and frequency. The grid-feeding converters are based on PI control used to adjust the output current in accordance with the P and Q references. [Rocabert et al., 2012]

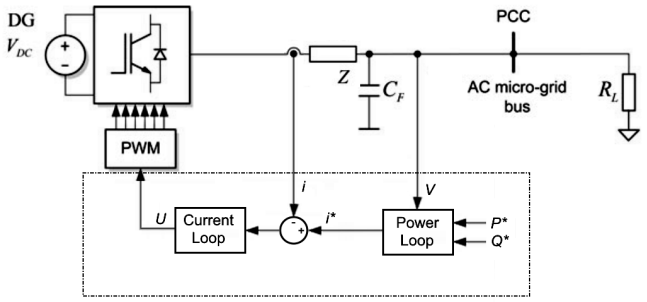

Figure 2.2: Basics control scheme of the grid-feeding power converter. [Rocabert et al., 2012, P. 3]

The grid-forming converters can be represented as an ideal AC voltage source in series with low impedance, see Figure 2.3. The grid-forming converter sets the voltage amplitude and frequency for the grid. Therefore, the voltage generated by the grid-forming converter will be the reference for the grid-feeding converters. A converter can only be operated as grid-forming in islanded mode. If the microgrid is grid connected, the main grid will set the voltage amplitude and frequency references and all power converters must be either grid-feeding or grid-supporting. The grid-forming converter has two cascaded control loops. The internal loop regulates the converter output current according to a reference set by the external voltage loop which works to regulate the output voltage. Similar to the grid-feeding, it is based on PI controllers. In order the operate several grid-forming converters in parallel, high-bandwidth communication is required [Rocabert et al., 2012]

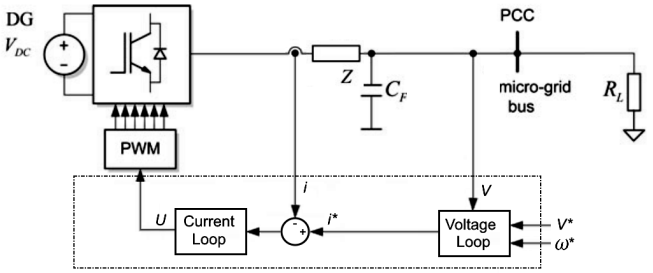

Figure 2.3: Basics control scheme of the grid-forming power converter. [Rocabert et al., 2012, P. 3]

The grid-supporting converters can be designed to work as either a voltage or current source, and should be chosen based on the overall control strategy. These converters adjust either their output current or voltage in order to keep the grid frequency and

voltage amplitude close to rated values. If operated as a current source inverter (CSI), some other source is needed to form the grid voltage. However, if operated as a voltage source inverter (VSI), this can be the grid-forming unit. The grid-supporting converters have internal control similar to the grid-feeding or forming converters based on whether they are operated as current or voltage sources, respectively. Then on top of this control, a droop control algorithm is applied. Using droop control is mainly popular for converters meant to operate as voltage sources [Guerrero et al., 2011]. In Figure 2.4, a simplified control structure for the grid-supporting VSI with droop method is shown, this structure also includes virtual impedance which is explained below.

The idea of adding droop control to VSIs is to mimic the behaviour of synchronous generators [Guerrero et al., 2011], because the droops can be considered as a virtual inertia. By using P/f and Q/V droops this type of converter can regulate the grid voltage amplitude and frequency. These converters can operate in either grid connected or islanded mode. Unlike the standard grid-forming VSIs, several of these can operate in parallel without the need for communication because the droops automatically handles the power sharing. However, using droop controlled VSIs as grid-forming will result in a small steady state error in voltage amplitude and frequency, and the network level control is required to correct this error. [Rocabert et al., 2012]

The conventional droop control method is well suited for HV and MV grids where the lines have a predominant inductive behaviour [Rocabert et al., 2012]. However, LV grids have a much different R/X ratio, it is mainly resistive, and the conventional droop method can therefore not be applied directly in LV grids, with several parallel forming units, because even a small mismatch in the grid impedance estimation will yield an inefficient power sharing between DGs [Rocabert et al., 2012].

The most common solution to this problem is adding a virtual impedance in the control loop of the power converter, first suggested in [Guerrero et al., 2004]. This virtual impedance has an effect similar to a link impedance connecting the power converter to the AC bus. By making this virtual impedance inductive the active and reactive power droops can be decoupled and proper sharing of active power can be controlled, however the method still requires precise estimation of line impedance to control to have optimal sharing. The virtual impedance changes the converter output voltage by subtracting the voltage drop over the virtual impedance from the voltage reference, this is shown in Figure 2.4 [Guerrero et al., 2011].

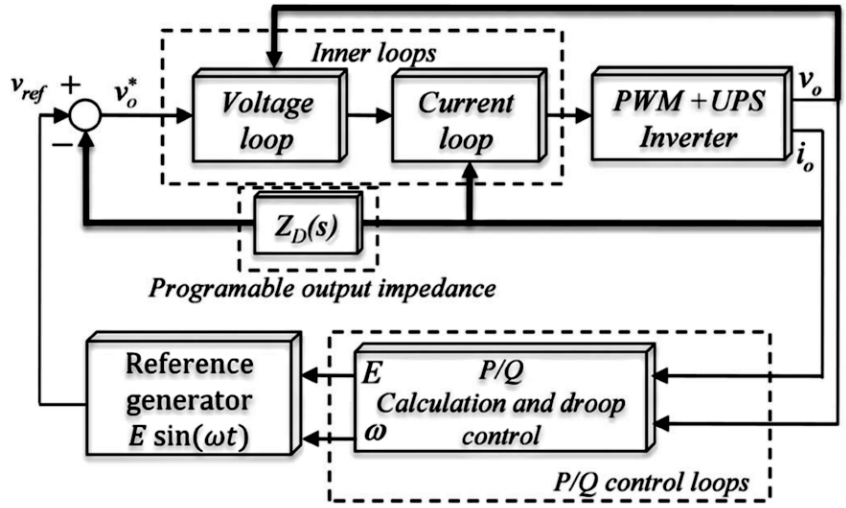

Figure 2.4: Power converter control with virtual impedance in the loop, [Guerrero et al., 2011, P. 162]

Now that some general knowledge have been acquired on microgrids and the control of converters, it is now relevant to look at the State of the Art Review, to see the current trends in isolated microgrid control.

2.3 State Of the Art Review

This section will give a systematic literature review of the current trends and ideas in forming an isolated microgrid. At first, the search method is reviewed, then the SoA criteria is listed, followed by the actual review of the literature.

2.3.1 Search Method

The search method applied to find literature in the subject of microgrids was performed using the five W's: what, words, work, where and wow. The "what" is defined as the subject "Control of Microgrid", whereas "words" refer to the definition of words used in the search for literature. The words used were mainly based on the initial review of literature and ongoing brainstorm, performed before the SoA, where keywords, near synonyms, acronyms and language were noted. "Work" is related to the search technique using boolean operators such as AND, OR and NOT, to specify the search. As an example, OR was used between "Distributed Generation" and the acronym "DG". An effort was put here, to ensure that no

relevant literature were excluded, due to spelling and different synonyms for the same subject/word. The subjects were grouped, such that e.g. "WT" OR "PV" OR "RES", were in one group. "AND" was applied between the grouped lines, and only one line was added between each specific search. In this way the amount of literature was gradually reduced from 15601 towards 95. In Figure 2.5, a screenshot from Engineering Village is shown, where the first reduction of the search is depicted.

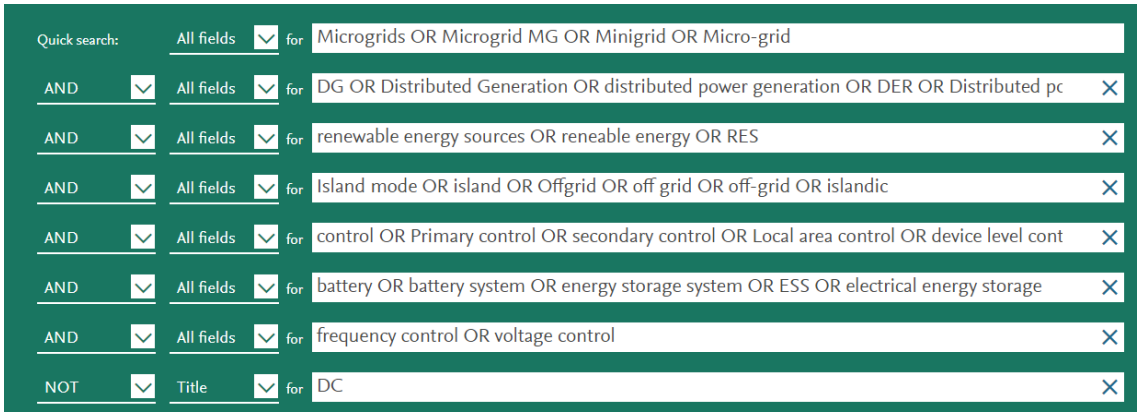

Figure 2.5: Screenshot from Engineering Village, showing the end of the first reduction of material

"Where" refers to the search engine. The search engine used was Engineering Village, who *"offers access to 12 engineering literature and patent databases providing coverage from a wide range of trusted engineering sources"* [Village]. The search was done from February 14th-18th, 2018. "WOW" refers to the evaluation of the search. The first round of evaluation was done going through material, reading abstracts, saving the relevant ones and marking all evaluated material. From here, the search was refined by trial and error, as different words and subject groups were changed, added and removed. For each search, all new material was reviewed and then marked as evaluated. In this way, the new material converged towards zero, such that the process of searching came to an end.

The entire search method was performed partly individually of all three authors, to ensure redundancy and to achieve the best coverage of the literature. The chosen literature were then sorted in "Mendeley - reference management system", to check for duplicates and to get a clear overview. The amount of literature sources were 56. From here all sources were read and discussed. Citations, year and number of "Full text reviews" were evaluated and the literature were sorted in folders and

some discarded or saved for later. From here the remaining literature were evaluated again to check if two or more had similar subjects in research or method. The newest one and/or the one with highest number of citations and/or "Full text views" was chosen as the reference used in the SoA.

2.3.2 SoA criteria

It is important to do the literature review through a defined set of criteria. These are formed based on the knowledge obtained regarding the existing problems and difficulties in forming an isolated grid. This will also help to see conformities and differences between the many papers and their methods. The following criteria and subjects will be considered:

- How do the papers solve the problem with high R/X ratio in LV grids?
- If communication is present, then what is the communication medium used? Is the communication delay considered?
- If control is present, where is this control placed? What are the requirements for the control unit? Can it be integrated in the system without costs?
- Are the capability of the DGs considered?
- Is the proposed method reproducible and is it relevant for the majority of the existing and potential microgrids?
- Are all worst case scenarios accounted for as listed below?
  - High production, low consumption.
  - Low production, high consumption.
  - Sudden large changes in production/consumption.

These points will be discussed after the review in order to see if there are any shortfalls in the methods used.

2.3.3 Review

In new research, the most commonly seen option is using one or several of the grid-supporting droop based VSIs, often with virtual impedance as grid-forming unit and the grid-feeding converters for any unit desired to work as a current source. Typically, the VSIs are used for energy storage devices and the CSIs for PV or small wind turbines [Guerrero et al., 2011]. In general, the four ways of controlling a power converter, see Section 2.2, are the basics of what is seen in new research. Several papers develop specific algorithms for the VSIs to fit their overall control structure, but the basics are the same as explained, with droop and virtual impedance. Which

power converter control to use for which DERs varies in the literature and is highly dependent on the overall control structure and how the network level control is designed. The approaches seen can be divided into three categories:

- Communication-centralized. Uses communication between DER units and the network level control is centralized
- Communication-decentralized. Again uses communication but the network level control is decentralized
- Non-communication. There is no communication between units, this way the network level control will always be decentralized. There are several approaches towards making the network level control work without communication.

In the following sections the papers found using the method explained in 2.3.1 will be reviewed. The papers have been divided into the three categories described. The basic principle of the two communication based approaches are illustrated in Figure 2.6, the supervisory control can be either centralized or decentralized though not shown in figure for simplicity.

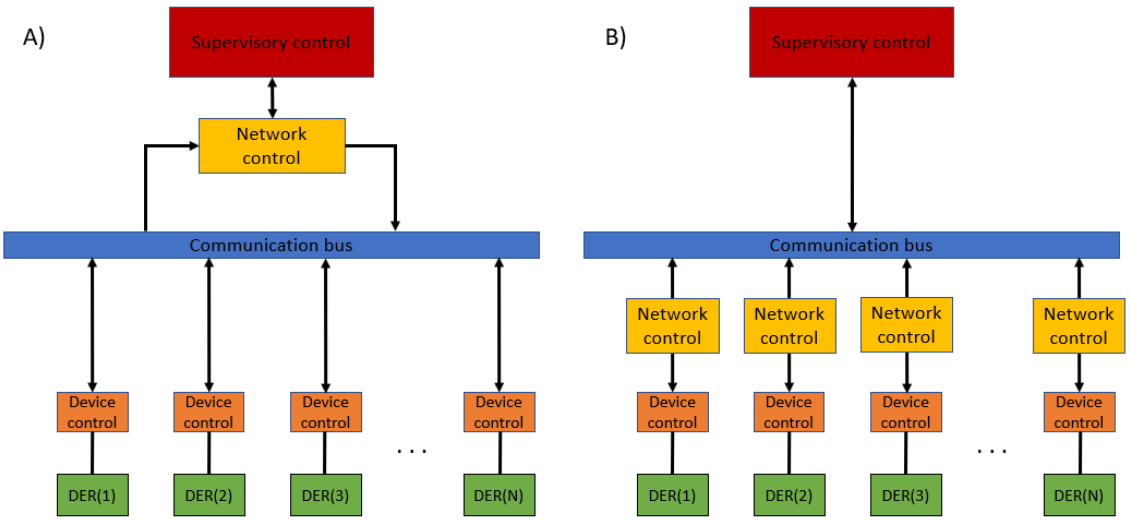

Figure 2.6: Control layers with communication, A) Network level is centralized, B) Network level is decentralized.

Communication - Centralized Architecture

The centralized control architecture for microgrids adopt the conventional large scale active power sharing method, where large synchronous generators in the power system takes care of the device level control functions in a centralized manner,

using the frequency droop control method. In microgrids however, the active power sharing method can be split into whether the frequency droop method is applied or not. The essential element in the centralized approach is the central controller which will perform network and/or supervisory control of all the units.

A non-droop control method is suggested in [Kim et al., 2016], where instead a State of Charge (SoC) based control approach is implemented. Decoupling of active power and frequency, and coupling of active power and SoC of a battery energy storage system (BESS) is proposed to eliminate frequency deviations under load changes. A relationsship between the SoC of the BESS and the active power is proposed, and frequency is set to be constant. The BESS is thereby the only unit taking care of frequency control and generation mismatch, while other units are controlled in PQ control mode, changing their PQ setpoint due to the SoC of the BESS. In case of communication failure the BESS change operation mode to power frequency droop control, while the other DGs react on load changes by sensing the frequency deviations. Mainly two problems are introduced using the BESS with SoC control, one being the inability of meeting large transient load changes, and the other being when the SoC reaches fully charged/discharged operation points, which both results in the BESS being unable to control the frequency. To overcome this the DGs must be able to support large transient load changes and be able to maintain the SoC of the BESS in allowable ranges. The latter is implemented in the local network control. For the case study a 300 ms communication delay is applied, and load change as well as RES variations are simulated.

The system presented in [Kim et al., 2016], shows good agreement with the scope of this project, as communication is considered and the presence of the battery. DG types and their capabilities are not covered and whether a diesel generator is present in the system remains unknown. There is no mention of the R/X problem.

In [Díaz et al., 2017b] a centralized coordination strategy is proposed for small migrogrids with RES, BESS' and loads, all connected to one bus. Later, a non-communication method from the same authors are presented [Díaz et al., 2017a]. The DGs consist of PV systems and WTs, and both their capabilities and fluctuating behaviours are taken into account. Simulations are made over a 24 hour window. The grid forming units are the BESS', where a droop control is implemented. The main focus is to equalize the SoC of the distributed BESS' to avoid uneven degradation of the batteries. To avoid overcharging of the BESS' an active power curtailment of the generation units, here only RES, is implemented, along with a load shedding scheme to prevent deep discharge of the batteries. The equal-

ization technique is based on droop control with predetermined droop coefficients, where a different scale-factor for each BESS is calculated. This ensures that even though the BESSs may have similar droop coefficients or different capacities, the scale-factor is changed to be able to equalize the SoC of each BESS. This makes the system able to have different charge/discharge rates dependent on which BESS have the highest/lowest SoC for a given time. The system is implemented in a lab-scale system to check how well the BESS obtains the same SoC, and afterwards keep this SoC. The generation curtailment and load shedding scheme is also tested. As the system only consists of PV and WT, there is no other way than load shedding, compared to [Karimi et al., 2017].

In [Karimi et al., 2017], BESS and a diesel generator with a synchronous generator is implemented to ensure stability when the microgrid is in island mode. The BESS takes care of the frequency control when the microgrid is disconnected from the grid, until the diesel generator is started and able to synchronize to the microgrid. In this case the diesel generator controls the frequency. Thereby the two units work as a smart integrated adaptive centralized controller. The simulations show that the control scheme is able to stabilize the frequency, after the microgrid is unintentionally disconnected.

In addition to [Díaz et al., 2017b], the authors also published [Díaz et al., 2017c], using the same grid layout, but instead focus on preserving the lifespan on the BESS, which is valve regulated lead-acid battery (VRLA) arrays. The batteries are to be charged/discharged in a two stage charge procedure, namely the limited-current charge stage and a constant-voltage charge stage. In the first stage the BESS is controlled in voltage control mode, and the BESSs can thereby act as grid-forming units. However, after reaching the second stage, the BESSs will have to change to constant-voltage charge, which can be achieved by changing the control mode to current control mode (CCM), such that the BESSs is going to be a grid-following unit. In a sceanario where all BESS' have reached the CCM, the microgrid will lack a grid-forming unit, which the authors solve by using a RES as the grid-forming unit. The RES thereby have to change to VCM and needs to be curtailed in order to have a power reserve when a load increases fast. The authors does not state at which level of SoC the transition between the two charge modes is done.

The review of literature in the subject of communication based microgrids, with centralized control showed that the BESSs can be grid-forming, but [Díaz et al., 2017c] states that due to the second charge stage, will be forced to operate as a grid-following unit if the battery is operated for optimal lifespan. [Díaz et al.,

2017c]. This introduces a lack of grid-forming unit in case of a 100 % RES based isolated migrogrid. [Karimi et al., 2017] suggests a solution with a diesel generator, which can take over as grid-forming unit with a small delay, whenever the BESSs need it.

Communication - Decentralized Architecture

As mentioned before, the centralized scheme with communication is done by having a centralized controller in the system. However, when talking about the decentralized communication, the network control is placed at each unit in the system in a distributed manner. This increases the redundancy and therefore also the reliability. Two relevant papers that corresponds to this control scheme, [Shafiee et al., 2012],[Foruzan et al., 2017], are reviewed.

The first paper [Shafiee et al., 2012] assumes that the local control has already taken place based on droop control, and the purpose of the authors is therefore to do network control e.g. compensating the voltage and frequency deviations. The network control, also called the secondary control in the paper, collects all information from the DG units such as frequency, voltage amplitude and reactive power. An algorithm using PI controllers will then produce new setpoints for the device level control to remove the steady state errors.

The system is made of two DG inverters connected in parallel to the same load, as an isolated grid. An experimental setup is also made with a nonlinear load. It is shown, that the control algorithm restores the frequency and voltage in an acceptable manner. The coordination of P and Q is done well due to the communication, as stated by the authors. Finally, the common centralized control scheme is compared to the decentralized one used in this project. The communication latency is increased to see how the two different control systems behave. It is concluded that the centralized control scheme will have difficulties with keeping the system stable, when the latency is increased above 4s. The author therefore states, that in terms of latency, the proposed control scheme will be more robust compared to the centralized one.

The paper does not specify the DGs and therefore also not the DG capabilities. The control is placed in the inverters of the DGs. The problem with R/X ratio is solved by using a virtual impedance. The paper does not comment on all worst case scenarios that are possible. Finally, it is not mentioned, what the communication link is.

In the second paper, [Foruzan et al., 2017], a distributed "primary-secondary" control strategy is proposed. This controller is placed at each DERs, as the previous paper, and aimed to properly share active and reactive power load among the units. The frequency, voltage amplitude, active and reactive power are shared through the communication link. Standard library models from PowerFactory is used to model inverters and synchronous generators. The system consists of three gas-engine-driven generators, three wind turbines, PV and energy storage.

The gensets are used to maintain a base load and they are the grid-forming units. The batteries will help during transient conditions. They also supply all reactive power during steady state conditions. PV and WT participates in voltage control and supplies power with droop control. A tertiary control layer is implemented in the units, which will control when the power from WTs and PVs are used to supply the load, based on their maximum capacity at the moment. Battery is kept at desired SoC and is used to stiffen the bus to mimic a grid-connected microgrid. The paper states, that the isolated grid will come closer to the behaviour of grid-connected case with higher capacity of batteries. It is finally concluded that the proposed algorithm works both in grid-connected and island mode.

This paper has the same shortfalls as the former paper described. It deviates by explaining the models of the DGs. It does however not mention the R/X problem.

As explained in Section 2.2, the virtual impedance method requires precise line impedance measurements, which is not feasible in a LV grid. In [Zhang et al., 2016], an adaptive consensus control method based on the virtual impedance is proposed, which compensates for the unknown line impedances and thereby makes control of reactive power and active power possible. All DER units are run as parallel VSIs with device level control based on the droop method with virtual impedance, the network level control is based on the multi agent theory and regulates the virtual impedance based on local reactive power and average reactive power from neighbouring units.

The control method is tested by simulation in a grid consisting of three DG units and two loads. The method is shown to handle loss of a DG unit and load changes. It is concluded that the method successfully eliminates reactive power sharing mismatch, and keeps equal DG output voltages in order to reduce circulating currents [Zhang et al., 2016]. The method is supposed to work without knowledge of line impedances [Zhang et al., 2016]. The paper considers communication delays, and clearly it accounts for R/X ratio in LV grids, it does however not mention the types of DGs and the capability of these.

Communication-less Architecture

The following papers describe an autonomous or decentralized communication-less control structure. The basic idea with this is to eliminate any physical communication in the system, see Figure 2.7. The main drawbacks of communication based systems, as depicted by the literature, are that the communication becomes a single point of failure and that the communication itself may not be available in the system, which then results in higher costs due to the implementation.

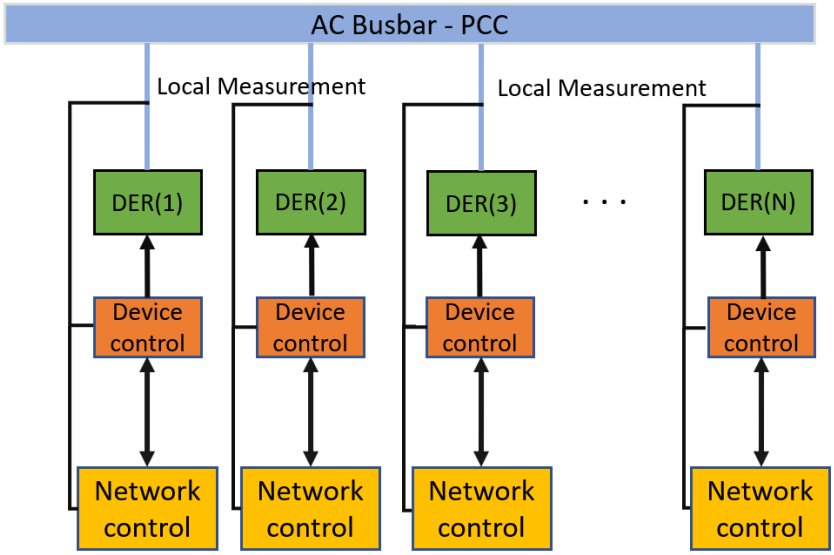

Figure 2.7: Non-communication, network level control is based on local measurement, bus-signal or state-estimators ect.

Three papers by the same authors are found, which proposes a non-communication control system [Díaz et al., 2017a], [Wu et al., 2014b], [Wu et al., 2014a]. Different approaches are depicted in all the papers. Starting with the older papers, the [Wu et al., 2014b] focuses on reactive power sharing between two DG units in an isolated microgrid, while [Wu et al., 2014a] focuses on active power control.

In [Wu et al., 2014b], Q-V droop control is claimed to be useful for VCM inverters, CCM inverters may have difficulties with applying this conventional method which has an inner current loop. The paper proposes V-Q reverse droop for CCM inverters in order to share reactive power. The CCM inverters, that most RESs are assumed to be, work with MPPT. The reactive power capability for the units depends on the active power capability. The droop coefficients for the reactive power sharing is therefore changed according to the power production from the unit. Finally, a

virtual impedance is implemented since the authors claim that the reactive power sharing will not be accurate due to the different voltage drops for each DG, depending on the connected line impedance. They assume the lines to be inductive and therefore a capacitive virtual impedance is implemented, which will compensate the line impedance loss. The system tested in real time consists of two DGs and a load. The authors conclude that the virtual impedance is necessary to achieve accurate reactive power sharing in the system, which will not result in changing the voltage beyond what is permitted in the system.

The paper does not describe the type of DG and the R/X problem is not mentioned as the paper studies a system where the lines are solely inductive.

[Wu et al., 2014a] studies an isolated AC microgrid with one ESS, two PV systems, and three distributed loads. However, in [Díaz et al., 2017a], the authors study an AC isolated microgrid with two variable RESs (PV and WT), two distributed ESSs based on banks of VRLA batteries and a single load that represents an aggregation of distributed loads. The former paper does not define the ESS type, which is however defined in the latter paper from 2017. The other difference is also that the latter paper has two batteries instead of one. Both papers use bus signalling in order to control the different units in a coordinated manner. Since [Díaz et al., 2017a] is newer and has more units similar to the system in scope of this project, this paper will be described instead of the former mentioned one.

In [Díaz et al., 2017a], each DER is controlled by its own decision maker unit. This unit contains a set of rules to be performed by each DER. The unit can be based on a deterministic finite state machine. The decision maker will control the DER by observing voltage and frequency patterns and the local measurements. The units are all connected to the same bus, which is then used as a communication bus as well. A virtual inductance is connected in series with the inverter to imitate an inductive line.

The device level control is made with droop coefficients. These are based on the rated values and the actual production level. ESSs will assume grid forming control in general while the RESs will be grid-following. Whenever the batteries reach a certain voltage regulation value, they will automatically shift to CCM. When this happens, the frequency will begin to deviate since no grid-forming unit is present. A Non-detection zone (NDZ) is defined for a frequency deviation from nominal of $\pm$ 3%. When the frequency is above this level, the DERs will change their control from CCM to VCM. The NDZ is used in order to secure that changes between the control modes only happen when the batteries are changed to CCM and not due to

normal frequency fluctuations, as stated by the author. The RESs will change their VCM to CCM whenever the power sharing exceeds the capability of the RESs.

In order for the different units to know which one is the VCM, the voltage is to be held either a little above (for ESS) or under (for RESs) the nominal, in order to let the units know who the VCM operators are. Finally load shedding is applied when the batteries are about to reach the limit of the depth of charge. This is triggered by changing the voltage in a linear manner, -15%/15s. The load will disconnect when the voltage amplitude has dropped to 10 % of nominal. When the ESS capacity become larger than 50 % the voltage will be restored in the same manner, which will trigger the load to reconnect. Charging and discharging of the two batteries are done equally, by using adjusted droops. Reactive power is only managed by grid-forming units.

When implementing the system in real time it is seen that it is not possible to ensure equal parameters for all the inverters, therefore the reactive power flow is not equally shared among the grid-forming units. The paper concludes that the following proposed system works and that the system is both scalable and expandable. The paper meets the SOA criteria from this project.

In the paper [Lou et al., 2017] a communication-less decentralized network level control is proposed based on state estimators. The method is based on a grid where all sources are inverter-based. The device level control is VSIs with droop method, which will result in deviation from nominal frequency, when the load differs from the nominal value [Lou et al., 2017]. Therefore, a network level control is proposed which reduces frequency error and adjusts power sharing between DG units. The network level control is located at each DG unit and gets its input from a state estimator which is based on a large signal model, of the entire microgrid, and local measurements. The voltage, frequency, active power and reactive power of all other DG units are estimated and based on these estimations, the network control will update settings for the device controller in order to eliminate frequency error and optimize power sharing.

The control strategy is tested by simulation in MATLAB/Simulink. The microgrid used for testing consists of three DG units connected to a common bus with line connections to two other busses each having an RL load. The lines are modelled as series RL lines with an R/X ratio of 2. The simulations show that the estimations from DG1 and DG3 converges to the actual measurement at DG2 below 0.1 sec. The method is claimed to be robust to parameter uncertainty, and is supported by making simulations where the output and line impedances have been increased by

40% compared to the values used in the large signal model, which still shows fast convergence of the state estimator. It is shown, that the controller gains have high influence on robustness and convergence speed of the estimator. It is concluded that the method is robust and effectiveness only relies on accurate modelling of MG and that it should always be possible for large microgrid systems.

This paper does not mention the types of DGs behind their inverters, and the estimation process assumes the other units are fully capable of supplying the estimated power. The paper does not investigate critical scenarios such as loss of a DG or big changes in load demand. The paper does not consider the hardware requirement of the control units. The method should be able to handle the R/X ratio of LV grids, as it is proven to be robust against parameter uncertainty.

In the paper [Wang et al., 2017] a hybrid device level control is proposed. The paper does not consider network level control and communication is therefore not mentioned, which is why it is presented in the non-communication category. The hybrid control consist of using droop based VSIs and CSIs together to form the grid compared to traditional droop method where only VSIs are considered. The CSIs uses an inverse droop and is claimed to be faster responding than VSIs, though they cannot form the grid without VSIs. The hybrid method is claimed to improve stability and dynamic performance compared to a grid with only droop based VSIs.

The method is tested in a grid consisting of two DG units connected to a PCC which has a single load connected. The load is assumed to consume only active power. The method is tested by comparing results for testing with both DGs as VSIs and with one as VSI and one as CSI. Simulations for a sudden change in load power shows the hybrid controlled system has faster settling time and less high frequency oscillations. Furthermore, hardware tests are made with two three-phase inverters "MYINV-9R144". The response to a change in droop controller gain shows that the system with two VSIs become unstable and shuts down, while the hybrid system remains stable. The hybrid system is shown to have lower overshoot and faster settling time to a load step change in the hardware experiments.

The paper does not mention the source behind the inverters, nor does it mention which line impedances were used, and whether the method is suited in LV grids are unclear. The paper gives detailed description of controller design and clearly lists parameters and the proposed device control is shown to be stable in extreme cases. However, the method does have a steady state frequency error as all other droop based device level control strategies.

In [Mondal et al., 2017] an experimental verification of decentralized control is performed in a system consisting of only diesel generator and PVs. No storage units are implemented due to investment cost reduction. The main focus is to make a stable system without real-time communication, whereas the DGs are controlled in a decentralized manner. Each DG thereby rely on the locally measured frequency and AC voltage magnitude. The PV inverters mode are VSI, such that all units in the system are grid-forming. The inverter model is presented, and a common PV cell level model is applied including the relationship between the maximum power and the PVs DC output voltage.

Then a linear relationship between the PV panel output and the AC frequency is derived based on two assumptions, one being that for all radiation levels, the maximum power point frequency is 50 Hz, and the other being that the frequency for the output open circuit voltage, for all radiation is constant.

The diesel generator is modelled using the droop control law, which for diesel generators relates the diesel engine power and the AC voltage of the generator. The functions implemented related to the local network control, is that the diesel generator only is switched on in case of when the frequency drops below the maximum power point frequency, or if the power drops below a certain level. However, it is not clear how the diesel generator receives this start-up/turn-off signals, when PV power is below/beyond the limits. The system is tested in laboratory environment, where the PVs DC link is emulated by programmable DC voltage sources. The diesel generator is emulated using a motor, generator setup. The entire system is tested in an 18 seconds time window, with constant PV, large load changes, and generator turned on/off. As mentioned, the system has no real-time communication, however it remains unknown how the diesel generator receives a turn on/off signal, from the inverters. The active and reactive power capabilities of the inverters are left out, as well as considerations about R/X ratios of the grid.

2.3.4 Discussion of the Review

In general the communication based centralized approach seems to be the most popular option in grids where all DER units are connected to the same AC bus, similar to the grid topology in scope for this project. Furthermore, the papers using centralized control often have a single grid-forming unit, though it can be used for systems with several parallel grid-forming units. The communication based decentralized approach however is more popular when the grid complexity increases and the DER units are distributed on several buses around the system, and more

popular when the grid is formed by several parallel voltage sources, because this gives better local control.

The decentralized approach is well suited for systems with several owners of DERs which might have different goals, but is control wise more complex than the centralized approach. On the other hand, the central approach is well suited for systems having a single owner/operator of all DERs and a single goal. Communication failure is more critical for the centralized approach compared to the decentralized, because the centralized have a single point, if lost, all communication will be down. The centralized approach is more susceptible to communication latency. The decentralized approach seems to be the best option for turning existing LV grids into microgrids as more and more DER units appear distributed on several buses in the system, like residential PV systems. The centralized approach however is a much simpler solution control wise and therefore looks to be well suited for building new grids, such as microgrids in rural areas, where the grid can be designed in a way that all DERs are connected to the same bus.

A general theme for the non-communication based methods is to have several grid-forming units to increase reliability if one unit fails, to control the voltage and frequency. For the non-communication method it is seen that two types of control can be made, state estimation and bus signalling. State estimation requires a large signal grid model to estimate the needed parameters for each unit. This may counteract the plug-and-play possibility as a new large signal model may be needed when changes are made in the grid. This also requires that the system has the grid parameters in order to make a large signal model. These parameters may however not be available for existing smaller systems that have been functioning for many years, due to the size and age of the system.

On the other hand bus signalling methods achieve scalability and are plug-and-play ready. It is clearly cheaper to implement this than the communication controls if the system has no existing communication medium. However, as seen by the papers, this type of control structure is only possible due to the grid layout with one common point of connection bus. For radial systems the bus signalling will be much harder to achieve as the voltage may differ from bus to bus. Another point to make is that bus signalling may be difficult to implement due to the intermittent generation. The signals must be distinctive from the regular fluctuations of voltage and frequency in order to work.

A summary of the discussed content for the three methods can be seen in Table 2.1.

Table 2.1: A summary of the discussion of the three control methods: centralized with communication, decentralized with communication and non-communication

Control Type	Commonalities	Application and advantages	Challenges
Communication - Centralized	• Storage element used as grid forming unit • RES become grid forming as backup with curtailment of power • Only one grid forming unit • Most common choice among all three methods	• System where all DGs are connected to one bus • Well suited for systems with one main goal or one grid operator • Simpler control than decentralized • More robust than non-communication, less robust than dezentralized communication	• Implementing communication • More susceptible to communication latency • One common point of failure
Communication - Dezentralized	• RES or genset used as grid forming unit • Used with several grid forming units in parallel	• Applicable for systems with DGs connected to their individual busses spread in the system • Well suited for systems with several owners of DERs with different goals • More robost than other methods • Plug-and-play capable	• More complex control than centralized • Susceptible to communication latency (but less than centralized control)
Non-communication	• Several grid forming units (e.g. several batteries or both battery and RES) • Using state estimation or bus signalling	• Only applicable for systems with one common bus connection • No extra cost for implementation of communication • Plug-and-play capable	• Harder to achieve optimal and economical dispatch • Harder to share active and reactive power • Steady state voltage and frequency errors may occur

Considering that DSOs may have an interest in optimal dispatch or economical dispatch, these aspects are harder to achieve through the non-communication based methods as the power sharing may not be completely precise. On the other hand, if the purpose is to have a grid that can operate autonomously and during times of lack of communication, bus signalling or state estimation may be a good idea, as this control can take over as a back-up whenever critical situations with no communication or external control happen.

Assessment of the SoA Criteria

Almost none of the papers described in this section, and also the disregarded ones during the literature search, are seen to fulfil the SoA criteria described in the Subsection 2.3.2. The literature that considers the R/X ratio in LV grids are seen to use virtual impedances to counteract this problem. The literature with communication rarely talks about the communication medium or latency. The same goes for the DG capability and the possible worst case scenarios. It seems like the papers introduce novel methods regularly, different approaches that can solve some parts of the problem, however the emphasis is on the novelty of the control and not the application or the practical aspects of the approach. This is both seen in the disregarded and the

presented papers. Some papers have advanced and complex mathematical functions that can control the grid, but none of these assess how this can be implemented in the grid.

Finally it is also clear, that the different methods proposed do not have a structured way of assessing the problem. The many differences in the approaches reflect a state of the art, that is more keen on introducing novel and complex ideas, rather than explaining the fundamental procedures needed in order to make a device and network level control. Vague explanations of the proposed methods also results in not being able to reproduce the same results that are achieved in some papers. A clear understanding of when the proposed method can be used seems to be lacking as well. The general procedure seen in the literature is to have a control method that is chosen from the beginning; this method is then used on the system in scope. This is counter-intuitive as the grid components, their placement and capabilities might alter the way the control should be made. It would be more practical to consider the system in hand and then analyse which control would fit such a system.

This project will therefore analyse the microgrid problems with a simpler and more practical approach. Some of the literature methods will be used, by taking some methods an mixing them to achieve a practical and simple control that works. The commonalities seen in the papers will also be used in this project. The project will strive to achieve a solution that will be in the interest of DSOs and future microgrid operators. This will be done by structuring the project in a more step-wise way, such that the procedure and methodology used in this project can be applied for other systems as well. In this way, the transparency and the relevancy will be evident.

In this chapter, problems in the microgrid were introduced and the power converter control methods were presented. Having this knowledge about how converters in the grid can be operated, the SoA was made focussing on how the problems are assessed in the literature. It can be concluded from this that several different methods of assessing stability and control of a microgrid exists. Clearly, a more generic and simple way of assessing this area of studies is needed, for which further motivates the problem statement given in the next chapter.

Problem Statement 3

From the state of the art review in the previous chapter, it is seen that several approaches have been considered by the literature authors on how to operate and control an off-grid microgrid. However, the lack of practical sense, simplicity and step-by-step guidelines in the approaches lead to the following problem statement that will form the course of this project:

How can the device and network level of a LV isolated hybrid power plant be designed in a simple and practical manner that can be used by existing and future microgrid developers?

The following sub-questions will be answered throughout this project in order to answer the problem statement above:

- What is the theory behind the functioning and capability of each DG?
- What is the relevant behaviour from the DG units that should be captured in order to do device and network level control
- What are some fundamental rules that can and should be applied in the microgrid, that can handle the problems seen in the SoA, in a simple manner?
- How can the microgrid system be modelled in a modular manner to capture both the capabilities of the power electronic units and the behaviour of the power system?
- What are the capabilities and/or limits of the models used in this project?
- How does the proposed control design approach differ in relation to the ones discussed in the SoA?
- How does the system and control behave in critical scenarios such as:
  - High production, low consumption
  - Low production, high consumption
  - Sudden large changes in production/consumption

3.1 Problem Scoping

Given the time to conduct this project, a clear outline of the scope is necessary.

As given by the problem statement, the focus will be on the device and network level control. This is in the $ms - s$ time frame. It is therefore out of scope of this project to look at supervisory control, which will consider load forecasting, optimal dispatch and environmental optimization.

This results in not looking into e.g. the state of charge control of the battery which will happen in a minute time frame. As the focus of the project is more on giving a step-wise guide on how to asses off-grid hybrid power plant problems, it is also not necessary to propose the specific communication medium that should be used, as the communication medium will be specific for different objectives. Some general assumptions will therefore be made in order to evaluate the system in scope of this project, it is however up to the specific microgrid owner to handle, how this will be done in their system. Further assessment of this is given in Section 4.5.

This project will focus on stability studies at ms to s level. Therefore, only small disturbance voltage and frequency stability will be assessed. Transient analysis are out of scope of the project, so that short circuit studies etc. are not analysed for the units. This time frame is valid for showing the capability of the device level control and the possibilities of network level control to eliminate steady state errors in frequency and voltage.

The type of system could be placed anywhere in the world, as long as it is operated in island mode. The rules for regulation of frequency and voltage are not present for such isolated microgrids, therefore these requirements will be set be the project writers, inspired by Danish grid codes.

Sizing of the load and generation units will be out of scope of this project. The sizing will be given from a techno-economic study [Petersen and Iov, 2018], which has made a thorough study for these types of systems. The specific type of BESS system is not considered, and hence the lifetime and optimal operation of this is not considered.

3.2 Problem Solving Procedure

Firstly, the system has to be characterized. This includes a description of how the individual units in the system work. Here, it has to be described which parts of

each units that are essential for device and network level control. This will be done in System Characterization, Chapter 4.

A discussion is then needed as to what the goal of this microgrid is. This is relevant as it will shape the way the design and analysis of the system will be made. To some extent this discussion will reveal how the microgrid will operate in the specified time frame, and how this will be done in a practical way. Based on these points, and the critical scenarios that can occur in the system along with capabilities of the units, a general idea for the proposed control methodology will be given. This is done in System Characterization, Section 4.5.

Based on this knowledge, it is now known how to design the units and the grid. Small-signal analysis will be made, this will be done by state space models. The reason for doing it with such models in time domain and not impedance-based models, is that the state space models can easily be translated to transfer functions and hence frequency domain. The impedance models can only be done in frequency domain. Furthermore, the time domain state space models allow the user to analyse internal states and do eigenvalue analysis, which gives valuable information about the stability of the system.

The relevant dynamics of the units will be included in order to depict accurate results in simulations with regards to device and network level control. All the models are done in Matlab/Simulink environment and they are done in a modular manner, as this is most practical for a system that is subject to changes. The modular approach will also make the individual analysis of each component easier and the effects of this component will be evident in comparison to making the whole system at once, and thereby not knowing what will influence what. The models will be verified by a comparison with known dynamic models in Simulink or a Matlab script. Furthermore, the models should be analysed to see if they are stable, in different operating points, before collecting the entire system. The models will be presented, verified and the stability of each one will be assessed in Chapter 5, Small-Signal Stability.

Having the verified models of each unit, it is now important to look at how this grid behaves, when the models are connected to the grid model. This will give insight to if further tuning of the individual models is needed and which sensitive parameters that exists in the system. The knowledge that can be attained from this study is very insightful when considering how the higher level controls should be made in order to keep the system stable. This is done by looking at the eigenvalues of the entire system matrix, and evaluating the participation matrix, to locate the

eigenvalues. This insight is also one of the reasons why the state space model is made. The analysis will be performed in Chapter 6 - Complete System Stability and Sensitivity Analysis.

The system will then be tested, using a dynamic model of the microgrid. This test is performed to be able to see which control loops that should be implemented in the Network Level Control (NLC), assuming that the Device Level Control (DLC) is insufficient. The control loops can then be designed from transfer functions derived directly from the state space model. The control loops can then be implemented to check how the NLC can assist the DLC. This will be done in Chapter 7 -Network Control Design and Tests.

Based on the experience from all this, a guideline will be given, which will be directed towards people working in the field of microgrids in island mode. More specific a guideline on how to approach any specific system and make a reliable device level control and how to asses the network level control, is given. This is given in Chapter 8 - Guideline for Control in Isolated Microgrids.

3.3 Success Criteria

The project will revolve around answering the sub-questions given in the Problem Statement, meanwhile the success criteria is defined as follows, "Creating a simple guideline to make an isolated microgrid DLC and NLC, where the focus is on stability and where the control issues can be assessed, using state space models".

System Characterization 4

The system in scope has to be analysed carefully in order to asses the control that should be implemented. This requires a thorough examination of the equipment in the system, its capabilities and also a discussion of the goals that needs to be reached in the system. All this will be done in this chapter. Based on this, an outline of the proposed control will be given.

Regardless of the goals and the specific system in scope, an examination of the system is needed firstly. The microgrid in scope of this project is seen in Figure 4.1. It includes generation from photovoltaics (PV), wind turbines (WT), diesel generator set (DGS), battery energy storage (BESS) and aggregated loads.

This microgrid system is chosen, as it is representative of future and current off grid microgrids, that are placed in rural areas with the implementation of renewable generation sources. Such areas will have loads such as residents, a school, agriculture, a commercial load etc. As mentioned in the previous chapters, the trend is towards using wind turbines, photovoltaic and storage elements. However, existing rural areas might have a DGS already and this units usage should be minimized, as the other technologies are integrated in the system. On the other hand it might be beneficial to install a DGS even though the microgrid is build from the bottom. The reason for this is that RES cannot deliver power, when the source is not there. Any system therefore needs a backup that is not dependent on external intermittent sources, in this case it is the DGS. It might be possible in the future to replace this with another unit that runs on e.g biofuel, nevertheless a backup is needed.

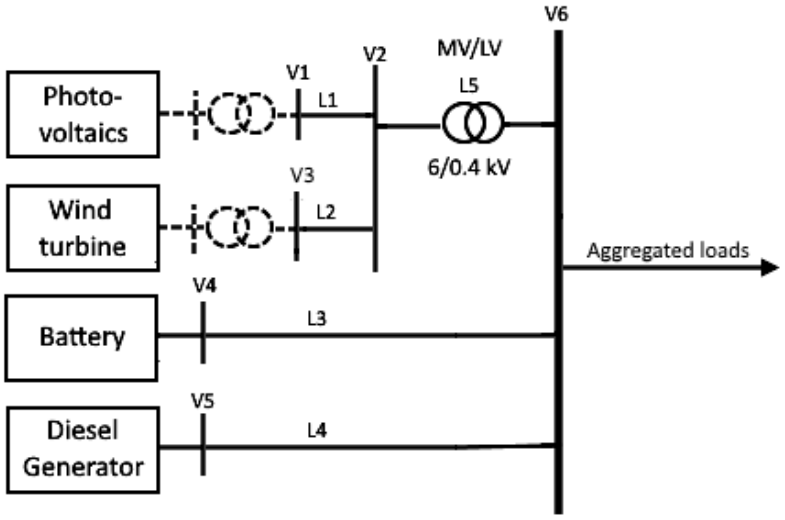

Figure 4.1: The microgrid in scope of this project.

The sizing of the components, as seen in Table 4.1, is given by a thorough techno-economic study from [Petersen and Iov, 2018], as this is out of scope of the project.

Table 4.1: Sizing of the components and the loads, given by a techno-economic assesment [Petersen and Iov, 2018].

PV	40 kW
WTG	80 kW
BESS	160 kWh/ 90 kW
DGS	90 kW
Peak Load Demand	88 kW
Daily energy consumption	appr. 850 kWh

From Figure 4.1 it is seen that the system is a 400V LV system, however the WTs and PVs are connected to 6kV lines and the voltage is stepped down by a MV/LV transformer. These units may be placed further away than the DGS and BESS, as the utilization of the resource and the space needed to implement them in the system, will have an influence. The line data is found from Nexan Cables, for the 6.6 kV cables, and NKT for the 400 V cables. The transformer data (L5) is found from the existing models in PowerFactory, which is a 150 kVA, 10/0.4 kV transformer. This transformer will be capable of handling maximum power production from the WTs and PVs. Transformers are characterized by their rated power S_T, copper

losses P_{copper} and the short circuit voltage u_k. The equivalent series impedance of the transformer is calculated as seen from Equations 4.1. The values are depicted in Table 4.2. The problem with using a 10/0.4kV transformer instead of the 6/0.4 kV one is that the short circuit voltage may vary, dependent on the specific transformer, between the values 4-8 %. A value of 6% is therefore used. The PV and WT transformers are found similarly using PowerFactory.

$$Z_T = \frac{V_T^2}{S_T} \cdot u_k \tag{4.1}$$

$$R_T = \frac{V_T^2}{S_T^2} \cdot P_{copper} \tag{4.2}$$

$$X_T = \sqrt{Z_T^2 - R_T^2} \tag{4.3}$$

Table 4.2: Data for the lines and transformer in the microgrid.
Transformer stats refered to HV side.

Line	**R/l (Ω /km)**	**L/l (mH/km)**	**l (km)**
L1 6.6kV (3x25)	0.927	0.397	3
L2 6.6kV (3x25)	0.927	0.397	3
L3 400V (3x95)	0.420	0.207	0.1
L4 400V (3x95)	0.420	0.207	0.1
L5 6/0.4kV 150kVA Transformer	4.608	53	N/A
WT 6/0.4kV 100kVA Transformer	6.120	65.8	N/A
PV 6/0.4kV 40kVA Transformer	20.25	94.74	N/A

The next sections will describe the units in the system and their capabilities.

4.1 Diesel Generator Set

The diesel generator set or diesel genset (DGS), is basically two units mechanically connected, namely the diesel engine and a generator. The type of generator is chosen to be a synchronous generator, as it is the most common type of generator. The synchronous generator is normally implemented with a Automatic Voltage Regulator (AVR), which controls the terminal voltage of the generator, by adjusting the field voltage of the generator according to a reference voltage from the grid. In the AVR, the exciter and Power System Stabiliser (PSS) is included. Thereby, a DGS can be seen as three different systems in one unit, diesel engine as the prime mover with governor, the synchronous generator, and the AVR, as shown in Figure 4.2.

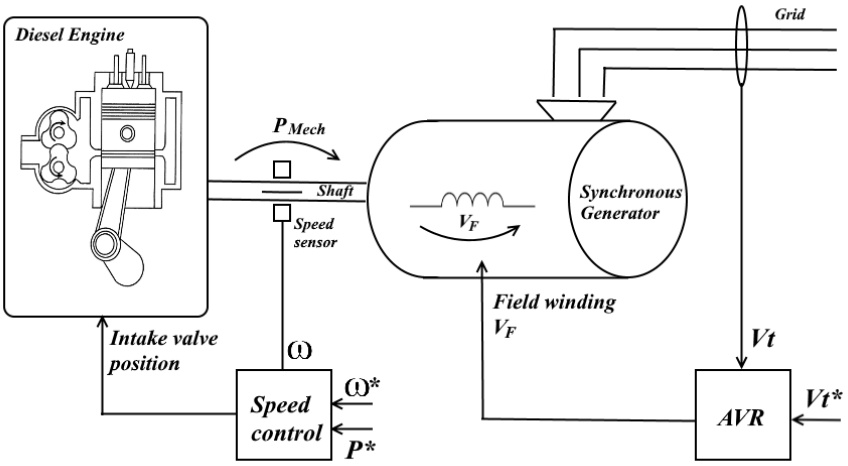

Figure 4.2: Structure of the diesel generator set.

The DGSs total size is 90 kW, and have been chosen to be split in two parallel 45 kW DGSs, to increase the redundancy of the total network and in order to operate one unit at a time, such that there exist two efficient operating points, in the range from 0-90 kW, instead of one. Therefore, a datasheet for a DGS of size 48 kW (60 KVA) and a datasheet for a synchronous generator of size 49.6 kW (62 KVA) has been used to find all necessary parameters. It is assumed that since the synchronous generators datasheet, could be the one found in the total DGS datasheet, then these values are correlated. The parameters are listed in Table A.1 and Table A.2 in Appendix A, along with the references for the datasheets. The minimum requirements for reactive power capability, as stated in the Danish grid codes, is included in Appendix A.

AVR

Based on the size of the DGS, it is assumed that a fast response time of the AVR can be applied, for which a Type 1S as referred to [Anderson and Abdel-Aziz, 1977] or ST1A as referred to [Kundur, 1994] is chosen. This type of excitation system is simple and includes PSS signals, such that it is possible to include this later, if necessary. The STA1 is a fast system, and thereby the exciter response time is usually neglected and only an amplifier response time T_A is considered. The parameters applied to the model are obtained from [Anderson and Abdel-Aziz, 1977], and are listed in Table A.3 in Appendix A, where K_F and K_A are the gains of the feedback and amplifier, respectively. T_F is the response time of the feedback.

4.2 Photovoltaics

The PV plant is considered to be functioning as the generic topology proposed in [Teodorescu et al., 2011], see Figure 4.3. The grid connected DC-AC inverter controls the DC link voltage (V_{DC}) and the reactive power output Q, while the boost converter handles the MPPT function. Based on the scope of this project, is to desired to find a plant model (DG units, device level controls and grid), which can be used for this study to design the network level control. Therefore only the grid side converter needs to be considered, in order to properly capture the dynamics of the PV plant affecting the grid stability [Gkountaras, 2017].

The output LCL filter can be considered, as a single inductor representing both filter and transformer inductance. Because of high X/R ratio, the resistance can be neglected. Furthermore, the filter capacitor will have a value around 10 μF and it will therefore only have an effect in the higher frequency dynamics, which is out of scope. Therefore it will also be neglected [Adamezyk, 2012].

The switching frequency of the grid side converter is considered to be, 5kHz which is a standard value for low voltage converters in the 10-1000kW scale [Gkountaras, 2017].

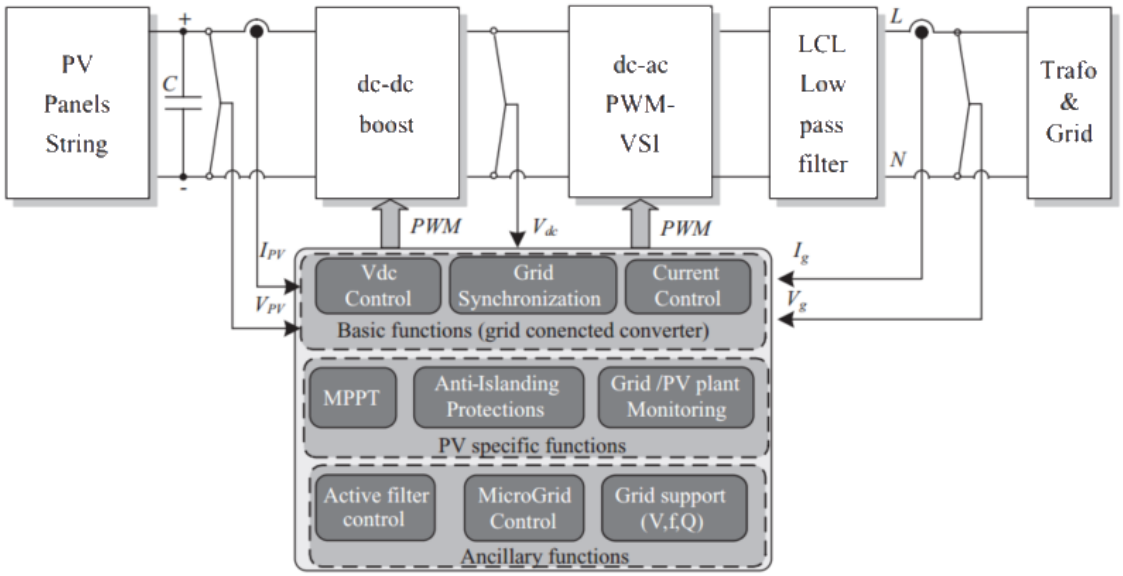

Figure 4.3: Generic PV control structure, [Teodorescu et al., 2011, P. 29].

The DC link voltage V_{DC} is set to be 1000V, which is in the middle of a typical range

of 800-1200V. The DC link capacitor C_{DC} is found using equation (5.8) [Karlsson, 2002, P. 39], where $\omega_{lp} = 2\pi 25 = 157 rad/s$, $\varsigma_n = 1/\sqrt{2}$, $\delta_n = 0.05$ and P_n is the rated power.

$$C_{DC} = \frac{P_n}{V_{DC}^2} \cdot \frac{2\varsigma_n^2}{\omega_{lp}} \cdot \frac{1}{(1-\delta_n)\delta_n} \tag{4.4}$$

The output filter inductor is found using equation (4.5) [Farrokhabadi et al., 2017]. ΔI_{max} is set to be 2% of the rated current, and f_s is in rad/s.

$$\Delta I_{max} = \frac{V_{DC}/3}{L_f 4 f_s} \tag{4.5}$$

The specifications used to model the PV plant are given in Table A.4 in Appendix A. An example from a datasheet is given for the reactive power capabilities in Appendix A.

4.3 Wind Turbines

The wind turbines have a total power rating of 80kW, and are considered as one unit, even though the wind plant might consist of several smaller turbines. The turbines are considered to be type 4, which is the typical topology in the 10-1000kW range. In a type 4 turbine (full power back-to-back converter) the grid side converter handles the DC link voltage and reactive power control, while the turbine rectifier controls the active power [Teodorescu et al., 2011], see Figure 4.4.

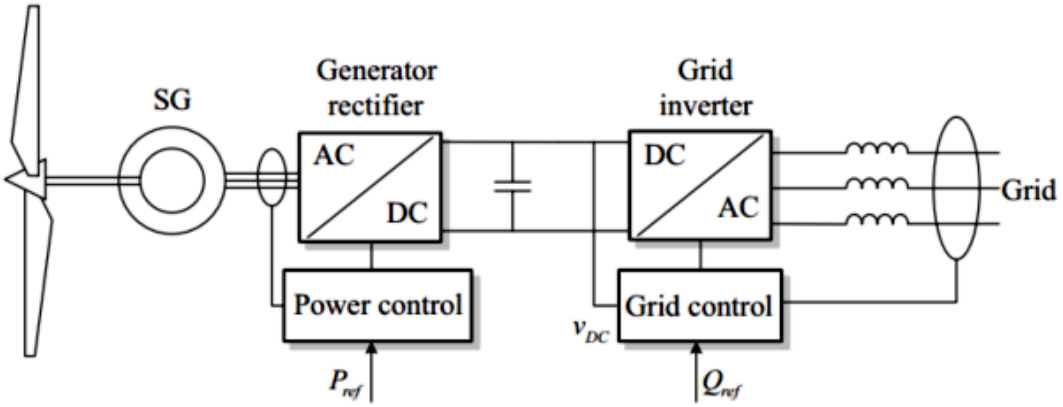

Figure 4.4: Type 4 WT control structure, [Teodorescu et al., 2011, P. 137]

Similarly to the PV plant, only the grid side converter needs to be considered, when the objective is to analyse the dynamics related to grid stability and network control design. The DC link capacitor and output filter inductor is found using equations 4.4 and 4.5, respectively. The specifications used to model the WT unit are given in Table A.5 in Appendix A. The minimum requirements for reactive power capability, as stated in the Danish grid codes, is included in Appendix A.

4.4 Battery Energy Storage System

The general control structure of a BESS ment for microgrids is explained in [Farrokhabadi et al., 2017]. Unlike the PV and WT structures, the grid side converter does not control the DC link in a BESS. Instead, the grid side converter controls either voltage and frequency or active and reactive power, dependent on whether the BESS is desired to function as a grid-following or grid-forming unit. The battery buck-boost converter controls the DC link, see Figure 4.5.

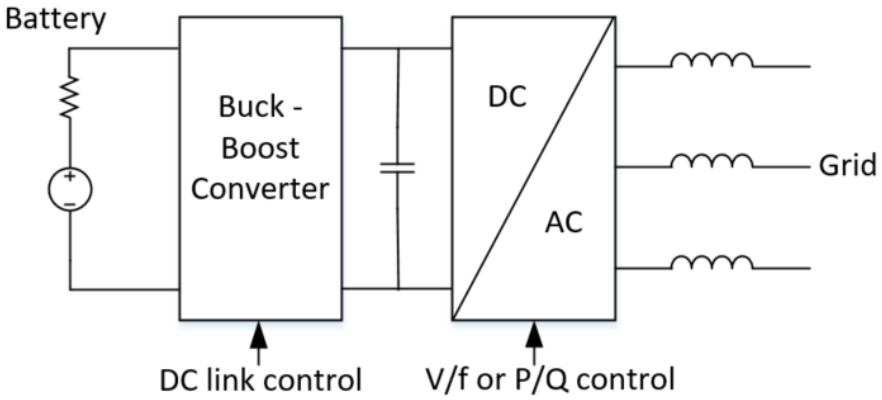

Figure 4.5: BESS control structure.

Again only the grid side converter needs to be considered, and the battery, buck-boost converter and DC link can therefore be approximated as a voltage source [Farrokhabadi et al., 2017]. The output filter inductor is found using equation (4.5).

The specifications used to model the BESS are given in Table A.6 in Appendix A. Because only the operation of the grid side converter is important, the specific type of battery is not considered. The minimum requirements for reactive power capability, as stated in the Danish grid codes, is included in Appendix A. However these states that the BESS is not required to deliver reactive power, when the active power output is 0. Throughout this project, it is however assumed that this is possible, as it is found that PV-inverters which has similar characteristics as BESS, has full reactive power capabilities, as stated in Appendix A.

4.5 Proposed control method

Before moving on to the next chapter, where the models of each unit will be made, it is necessary to consider the control methodology, which may influence how the individual models are made. This is the next step to be considered after characterizing the grid in scope of the project. Another reason for having this procedure is to look at the specific system in scope and then consider the control strategy which is something that is not seen in the SoA. Rather, it is seen that a specific control strategy is used regardless of the system characteristics.

The end goal of this section is therefore to propose a control method, which can be achieved by the following procedure:

(A) Outline the main goal of the microgrid.
(B) Discuss the capability of each unit from a microgrid control aspect.
(C) Outline the critical scenarios that should be accounted for in such a system.
(D) Discuss which control approach should be used in order to asses the previous points.

(A) The main goal:
The goal of the microgrid needs to be outlined clearly since this will influence the control strategy. As discussed in the beginning of this chapter, this microgrid is a good representation of isolated grids in rural areas that may be made in the future and existing grids. A general and common goal would therefore be to ensure stability during all possible production and load level scenarios. These scenarios will be defined later in step **(C)**. This goal will ensure that the microgrid works no matter what, and the possibility of blackout will be low. This will be the goal of the control in this project and is stated as follows:

The main goal of the microgrid control is to ensure stability during all possible production and demand scenarios in a practical and simple manner and utilizing the renewable generation the most.

This is a prerequisite for a functioning grid and can therefore be seen as a general goal that most microgrid owners should have. Other goals, such as optimal dispatch, economical dispatch etc. may be obtained by a higher level of control.

(B) The Unit Capabilities:
The latter mentioned goal will require a system including a grid-forming unit. This step is therefore to discuss which units in the system, that can be used with this function. The PV and WT will have an MPPT and since the goal suggests utilizing the renewable generation the most, it is deemed necessary to use these units as grid-following units instead. These units potential as a grid-forming unit is also degraded due to their intermittent nature. Instead, using them as a grid-following unit and thereby CSI will help utilize more of the renewable energy.

The DGS can be used as the grid-forming unit, however as the goal in **(A)** requires using RES's the most, using the DGS as the grid-forming unit will be counter-intuitive. Hence, it is not plausible to use this unit as the only grid-forming unit.

From Section 2.3 it is clear, that the most commonly used device is the storage unit of the system. However, scenarios may occur, where this unit will not have enough stored power to keep the balance in the system. Hence, relying only on the BESS may cause scenarios with instability. This is something that needs to be assessed in

(D).

From this discussion it is clear, that none of the units can operate as a standalone grid-forming unit. The most prominent ones are the storage unit and the DGS. Some control strategy is therefore needed in order to be able to use these units as the grid-forming unit. This will be discussed in **(D)**.

(C) Critical Scenarios:
The critical scenarios in the microgrid need to be considered, as the control method should account for such scenarios. This is something that is missing in the SoA in Section 2.3 for some of the literature. Critical scenarios are typically given by the extreme cases with regards to production and load consumption. However, having a storage unit in the system creates another variable. This is depicted in Figure 4.6 where the extreme cases are shown in the lower part of the figure.

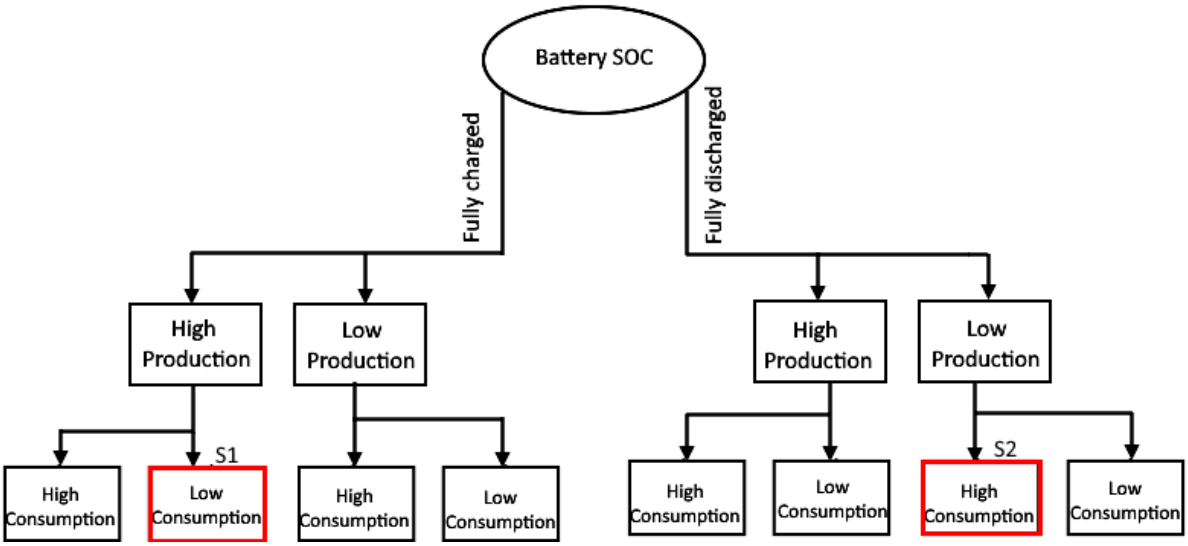

Figure 4.6: The extreme scenarios that can take place in this specific microgrid system.

There are in total 8 extreme cases. However, two of them, marked with red, are considered the most severe ones. If the control of the units can account for these two scenarios, the others can be handled as well. The first severe scenario is when the BESS is fully charged, the production from the units are high and the load is low. This will create an excess amount of power flow in the system due to the island mode. Consequences of this will e.g be high voltage rises, which may lead to damage of major equipments (insulation failure). This scenario is from now on called S1. The other severe scenario, from now on called S2, is when the BESS is discharged,

the production is low and the consumption is high which may lead to e.g voltage dips. These scenarios must be accounted for when proposing a control method.

(D) Proposed control method:
From **(B)** it is clear that the BESS should be used as the grid-forming unit. However, considering scenario S2 from **(C)**, control of V and f will fail in this scenario. As discussed before, in case of an existing rural grid, a reliable source such as the DGS will be available. In the other case where the microgrid is build from the bottom, such a source is necessary to ensure power as a backup. So in most cases this unit will be available for rural isolated microgrids. Then one way to counteract scenario S2 would be to place the BESS and the DGS at the same site and have fast communication between them. In this way, the DGS will be used only for backup purposes, such as when there is no generation from the WT and PV, the load is high and the BESS is becoming fully discharged. Scenario S2 can be counteracted, by starting the DGS before the BESS discharges, and in this way both charge the BESS and supply the necessary power to the load.

A problem arises then as two units will now try to keep the voltage and frequency of the grid. This will require accurate tuning of their individual control coefficients. This can however be solved by placing the units at the same site, which is the reason why this is suggested. The required speed of measurements and signals that are valid in this system are shown in Figure 4.7. It is seen that by fast communication, the BESS can deactivate its frequency control and receive the actual frequency from the DGS and thereby follow this value. In this way, the two units will not counteract each other and the stability of the system can be remained. Such control is simple and practical in comparison to e.g. communication-less control, which would require complex algorithms. This is a novel method to act on the problems with two parallel grid-forming units and BESS charge/discharging which is not seen in the SoA section. Considering the network level control, this would then be placed at this site, with the reliable generation unit and the BESS.

The other scenario S1 is where the BESS is fully charged, production is high and the consumption is low. Assuming that there is no dump load, two things can happen, one being that the BESS reaches its charging limit, the voltage rises and may lead to blackout. The second is that the power from the WT and PV is curtailed. In order to do curtailment these units need a signal that will suggest this action. As seen from Figure 4.7, the placement of the PVs and WTs are not as flexible as the BESS and it is therefore not possible to assume fast communication to these units from the BESS/DGS site. However, fast communication is not needed if the

curtailment signal is sent when the BESS reaches e.g. 80% SoC. In this way, some slower communication method e.g. Wi-Fi can be used to send this signal to the units, which still makes the control remain simple.

4.5.1 Summary

In order to summarise, the specific device level control required, to follow the proposed control method, will here be stated clearly.

When "on" the DGS will be the grid-forming unit, and therefore controlled using standard governor and fast excitation for this size of generator. Therefore, the device level control inputs will be power reference, speed reference and terminal voltage reference.

The control of the inverter based units, will be stated related to the definitions presented in Section 2.2 and defined in [Rocabert et al., 2012].

As explained the PV and WT should be grid-following units with the possibility of power curtailment. Their device level control will therefore be based on the grid-feeding power converter, and the control inputs will be active and reactive power references.

The BESS should be the grid-forming unit when DGS is off, and when DGS is on, the BESS will follow frequency reference from DGS, but still control the voltage at its bus. As explained in Section 2.1 it is problematic that fully inverter based grids does not have any inertia, and it is desired that the frequency response to power changes should be the same with and without DGS. Therefore the BESS will have P/f droop control as this emulates "virtual" inertia. Furthermore, it does not make sense to have inverse droops when a diesel genset is present. Therefore, BESS voltage control will be based on a Q/V droop. The BESS control will therefore be based on the grid-supporting VSI, which can function as grid-forming unit [Rocabert et al., 2012]. The BESS device level control will therefore have inputs voltage reference, frequency reference and active and reactive power references.

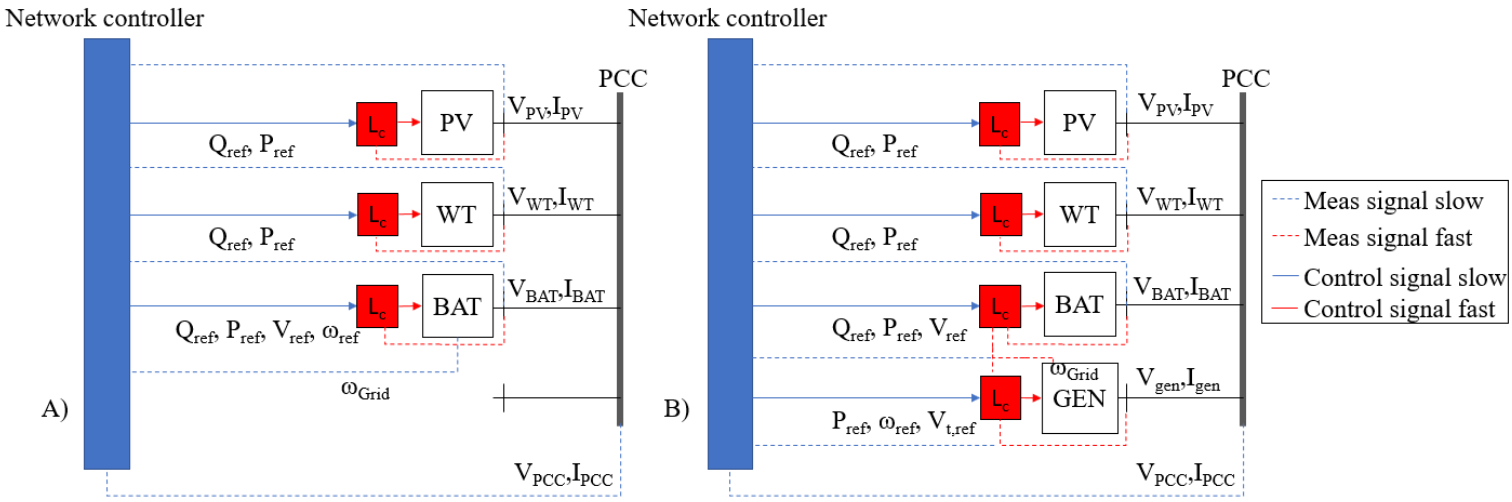

Figure 4.7: The device and network level control capabilities and required speed of measured and control signals. L_c is the local control. A) When the DGS is off, B) When the DGS is on. The slow signals are in the second range, while the fast signals are in micro-milliseconds.

The full control structure with both DGS on/off is illustrated in Figure 4.7. This sums up a control method that can be used to satisfy the microgrid goal, regards the unit capabilities in the system and can take care of the critical scenarios that may happen in the system. It is now possible to make the models based on these principles.

The chapter introduced the system components, including the size and grid layout. The sizing of the units and loads and main grid layout, was defined from [Petersen and Iov, 2018], whereas from here the cables, transformers and the specific types of components was selected by the authors. This was done having the practical implementation as well as the control structure in mind, such that the units will have capabilities not counteracting the main goal of the project. Moreover, a control method was proposed based on the capabilities of the units. This strategy will be the foundation for the design of the small-signal models in the following chapter.

Small-Signal Stability 5

After the system in scope has been described, it is relevant to describe the design of the system. This is done in this chapter, where the small-signal equations for the system are derived and a state-space model is made modularly of each component in the system. The state space models are verified and then analysed for stability at several critical operational points. Voltage sensitivity analysis is done, to tune the droops properly in the models and to understand the system better. Finally, the employment of the models for other studies is discussed.

This project will focus on small signal analysis of the system, as stated in the Scoping of the project. Due to the non-linear behaviour of the power system, linearisation can be made by assuming small signal behaviour. However, this requires an operating point which will not vary. This is given in power systems by considering the variables in dq-frame, tracking the voltage phasors, such that the variables become DC values and small signal linearisation is permitted. Furthermore, decoupling of active and reactive power control can be accomplished by transforming such systems into dq frame.

As explained in the Problem Solving Procedure Section 3.2, the small-signal stability will be done using state space models. Impedance-based models are only utilized in frequency domain, whereas the time domain state space models can be transformed into transfer functions and thereby frequency domain as well. Hence, several aspects can be included by doing state space models. Impedance-based models cannot be used for phasor-based modelling, it is however more straightforward to achieve models in the linear form. However, the state space models will give information on the states, the internal stability and eigenvalue analysis can be done, which will give valuable information about the system stability. For these reasons, the state space approach is chosen in this project.

The whole microgrid system will be modelled modularly to utilize the ease of changing the models if necessary, later in the project. This is highly suggested, as the system equipment may change in real life. The whole system will be modelled as

shown in Figure 5.1. It is depicted, that the generator models will provide the DQ currents, the load model will generate the DQ load current and the grid model will provide the DQ voltages at each bus in the system.

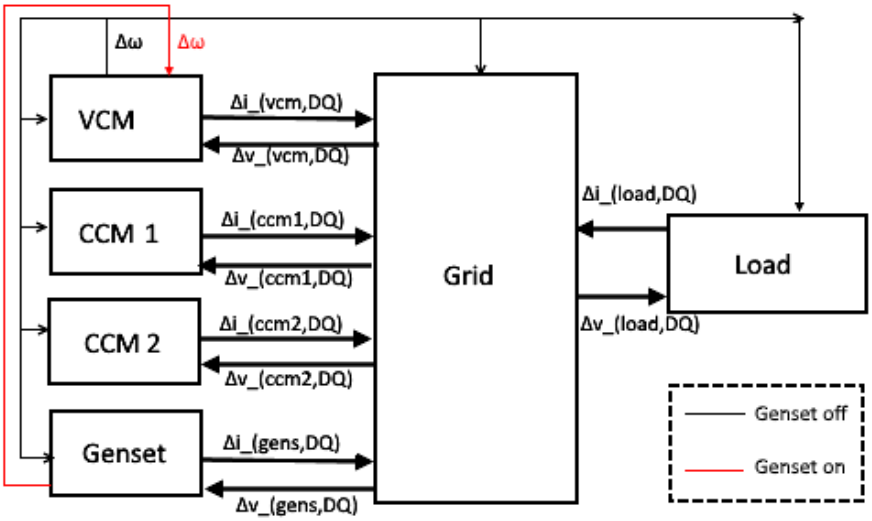

Figure 5.1: The modular state space model of the microgrid, with inputs and outputs.

When modelling in dq frame, each unit will be running in its own local frame, while the grid is running in a global frame, therefore current outputs of each unit needs to be transformed to the global frame [Wang et al., 2017]. The angle difference between the two frames is denoted δ, this is shown in Figure 5.2 for the example of referring a CCM unit to the global frame.

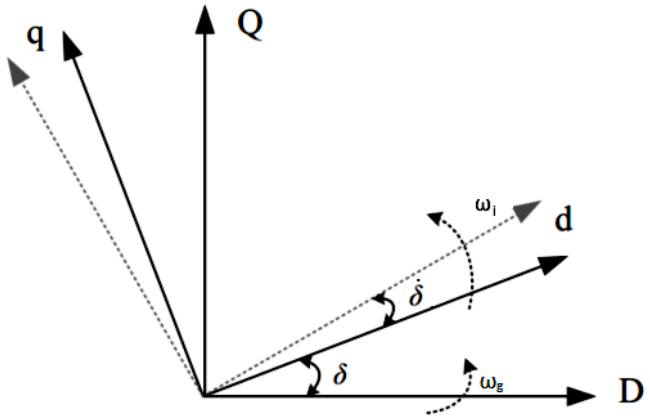

Figure 5.2: Capital letters are global frame, and small letters local frame. Global frame rotating with ω_g and local frame rotating with ω_i.

The battery, operated in VCM mode, will set the common reference frame, which all the other components are referred to. This is done by using the transformation technique shown in equations 5.1. Whenever the DGS is turned on, this unit will provide the battery with the frequency and will therefore set the common reference frame. Capital letters for DQ is used to denote the common reference frame axis. The common reference rotating angular speed is ω_g and the individual angles of the units with respect to the common reference frame are δ_i.

$$[f_{DQ}] = [T_i] * [f_{dq}] \tag{5.1}$$

$$[T_i] = \begin{bmatrix} cos(\delta_i) & -sin(\delta_i) \\ sin(\delta_i) & cos(\delta_i) \end{bmatrix}$$

It should be noted that a state space model of the grid is included in this project. As seen from the SoA Section 2.3, some papers do not include this aspect of the power system, rather they analyse the converter controls only. This will not depict the actual behaviour of the whole system, and therefore the state space model of the grid and load is included as well.

The model is made in p.u. and the output currents of individual units therefore need to be converted to the correct power base. The power base change is done according to Equation (5.2).

$$I_{global} = I_{unit} \cdot \frac{P_{base,unit}}{P_{base,global}} \tag{5.2}$$

5.1 Modelling

5.1.1 Wind Turbine and PV plant

As seen from the SoA Section 2.3, most of the papers do not consider the DC link, which may however have an influence on the control as the DC link is controlled by the grid side converter, for both battery and PV. It is therefore included in this project as this will give a more precise model for network level control design. The PV plant and WT unit can both be represented by their grid side converter, which handles DC link and reactive power control. The full model to be used is shown in Figure 5.3 including the control structure.

The "machine" side converter is represented by a voltage controlled current source, which adjusts the current dependent on the DC voltage in order to deliver the specified active power. The WT and PV are supposed to function as PQ controlled units seen from the network level control. However, an instant change in active power would not be realistic, therefore a filter is implemented between the power reference and the actual power to be delivered by the current source. This filter represents the time response of either PV or WT and their "machine" side converters. The power to be delivered by the current source is limited by the actual available power. The time response is 1s for the WT and 100ms for the PV [R&D, 2011] [Wang et al., 2016]. The converter is considered to be ideal and since the switching frequency is 5kHz, the internal converter states can be neglected, as it is much faster than the scope of this project. Therefore, the output voltage, is considered to be equal to the voltage reference.

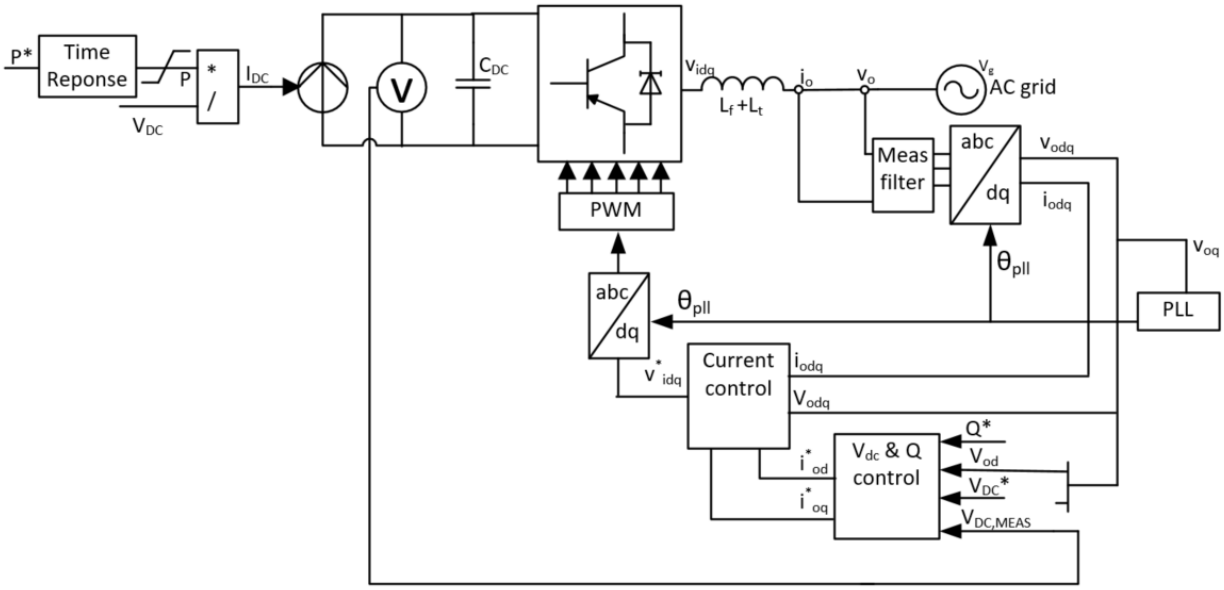

Figure 5.3: WT and PV grid side converter and control structure.

The control consists of an inner loop (current controllers) and outer loops which controls V_{DC} and the reactive power Q. A PLL is used to track the frequency of the grid. Finally, a low pass filter is included to represent the response of real voltage and current transducers. In the following section, the mathematical description of the system used to derive the state space model will be presented, the model is derived in the dq-frame rotating with speed ω_g.

State equations

The current source representing the "machine" side converter is controlled by V_{DC} in order to give a constant power, the current delivered is given by Equation (5.3).

$$I_{DC} = \frac{P}{V_{DC}} \tag{5.3}$$

The output filter is described by equation (5.4), where ω_g is the grid frequency:

$$\begin{aligned} \dot{i}_{od} &= \frac{1}{L_{ft}}(v_{id} - v_{od}) + \omega_g i_{oq} \\ \dot{i}_{oq} &= \frac{1}{L_{ft}}(v_{iq} - v_{oq}) - \omega_g i_{od} \end{aligned} \tag{5.4}$$

The low pass filter representing voltage and current transducers are described by Equation (5.5), where X is the output of the transducer and x is the input, actual

voltage or current. In this way any voltage or current denoted with capital V or I is a measured value outputted by the transducer. The transducer bandwidth is 10kHz and 30kHz for voltage and current transducers respectively [SA].

$$X = \frac{\omega_{mv,i}}{s + \omega_{mv,i}} x <=> \dot{X} = \omega_{mv,i} x - \omega_{mv,i} X \tag{5.5}$$

In dq-frame the active and reactive power is given by Equation (5.6).

$$\begin{aligned} p_o &= \tfrac{3}{2}(v_{od} i_{od} + v_{oq} i_{oq}) \\ q_o &= \tfrac{3}{2}(v_{oq} i_{od} - v_{od} i_{oq}) \end{aligned} \tag{5.6}$$

The actual active power delivered by the source is given by Equation (5.7), where T_{unit} represents the time response of either PV or WT.

$$\dot{P} = \frac{1}{T_{unit}} P^* - \frac{1}{T_{unit}} P \tag{5.7}$$

By neglecting losses in the converter, the power balance of the DC link is given by Equation (5.8).

$$\dot{V}_{DC} = \frac{P}{C_{DC} V_{DC}} - \frac{p_o}{C_{DC} V_{DC}} \tag{5.8}$$

The structures of PLL, current control, V_{DC} and Q control are shown in Figure 5.4

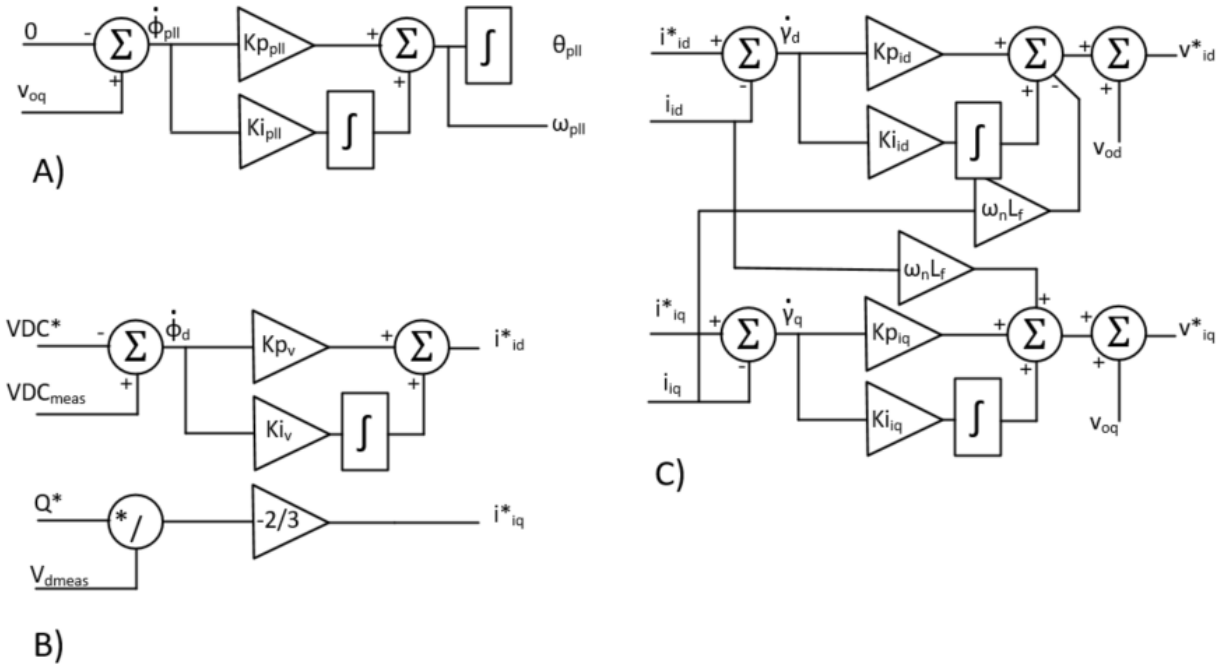

Figure 5.4: Control structure of A) PLL, B) V_{DC} & Q control, C) inner current controllers.

The phase locked loop (PLL) Figure 5.4 A), is tracking the frequency of the grid, by constantly setting V_{oq} to zero, meaning the d axis is aligned with the voltage phasor. The PLL is described by Equations (5.9), (5.10) and (5.11). The specific PLL structure used here is a "synchronous reference frame" (SRF)-PLL, which can handle high bandwidth [Teodorescu et al., 2011, P. 182].

$$\dot{\phi}_{pll} = V_{oq} \tag{5.9}$$

$$\omega_{PLL} = Kp_{PLL}\dot{\phi}_{PLL} + Ki_{PLL}\phi_{PLL} \tag{5.10}$$

$$\dot{\theta}_{PLL} = \omega_{PLL} \tag{5.11}$$

The change in angle between the global and local frames is described by Equation (5.12).

$$\dot{\delta} = \omega_{pll} - \omega_g \tag{5.12}$$

In Figure 5.4 B), the V_{DC} and Q controllers are shown. The V_{DC} is described by Equation (5.13). Because the PLL adjusts $V_{oq} = 0$ the active power output depends only on v_{od} and i_{od}. Therefore, the V_{DC} control gives the reference i^*_{od} because the capacitor balance is only affected by changes in active power. Similarly, the Q control is based on the assumption that the PLL has settled, meaning $v_{oq} = 0$, and therefore the output reactive power is only dependent on v_{od} and i_{oq}. The Q control is described by Equation (5.14). The latter equation only consider the V_{od} assuming that the q-axis voltage is zero. During disturbances this may however take on a different value from zero. Since the current loops are much faster than the PLL, this change will not be significant and visible on the voltage, therefore, Equation (5.14) is a valid approximation.

$$\begin{aligned} \dot{\phi}_d &= V_{DC,meas} - {V_{DC}}^* \\ {i_{od}}^* &= Kp_v\dot{\phi}_d + Ki_v\phi_d \end{aligned} \tag{5.13}$$

$${i_{oq}}^* = \frac{Q*}{-\frac{3}{2}V_{od}} \tag{5.14}$$

The inner current controllers are shown in Figure 5.4 C), they are designed as described in [Zhou et al., 2015] in order to fully decouple the d and q axis. The current controller is described by Equation (5.15). As mention before, the output of the converter V_{idq} is assumed to be equal to the reference V^*_{idq}, because the converter acts much faster than the current control loops [Gkountaras, 2017].

$$\begin{aligned} \dot{\gamma}_d &= {i_{id}}^* - I_{id} \\ \dot{\gamma}_q &= {i_{iq}}^* - I_{iq} \\ {v_{id}}^* &= Kp_{id}\dot{\gamma}_d + Ki_{id}\gamma_d - \omega_n L_f I_{iq} + V_{od} \\ {v_{iq}}^* &= Kp_{iq}\dot{\gamma}_q + Ki_{iq}\gamma_q + \omega_n L_f I_{id} + V_{oq} \end{aligned} \tag{5.15}$$

All of the above Equation combined are used to define a state space model of the system, the voltage v_{gdq} is an input coming from the grid model and is therefore equal to v_{odq} after reference frame transformation. The state space model has the following states, inputs and outputs:

$$x = [\delta\ \phi_d\ \gamma_d\ \gamma_q\ i_{od}\ i_{oq}\ \phi_{pll}\ P \\ V_{DC}\ I_{od}\ I_{oq}\ V_{od}\ V_{oq}]$$

$$u = [P^*\ Q^*\ {V_{DC}}^*\ v_{gd}^{global}\ v_{gq}^{global}\ \omega_g]$$

$$y = [i_{od}^{global}\ i_{oq}^{global}]$$

The model is then linearised around an equilibrium point (x_0, u_0) according to the procedure described in [Kundur, 1994, P. 700-704]. The A, B and C matrixes of the linearised state space model is given in Appendix B, it is also shown how to initialize the model in the appendix.

5.1.2 BESS

As explained in Chapter 4 the BESS can be modelled as its grid side converter, with a voltage source representing the DC link, buck-boost converter and battery. The battery grid side converter with control structure is shown in Figure 5.5.

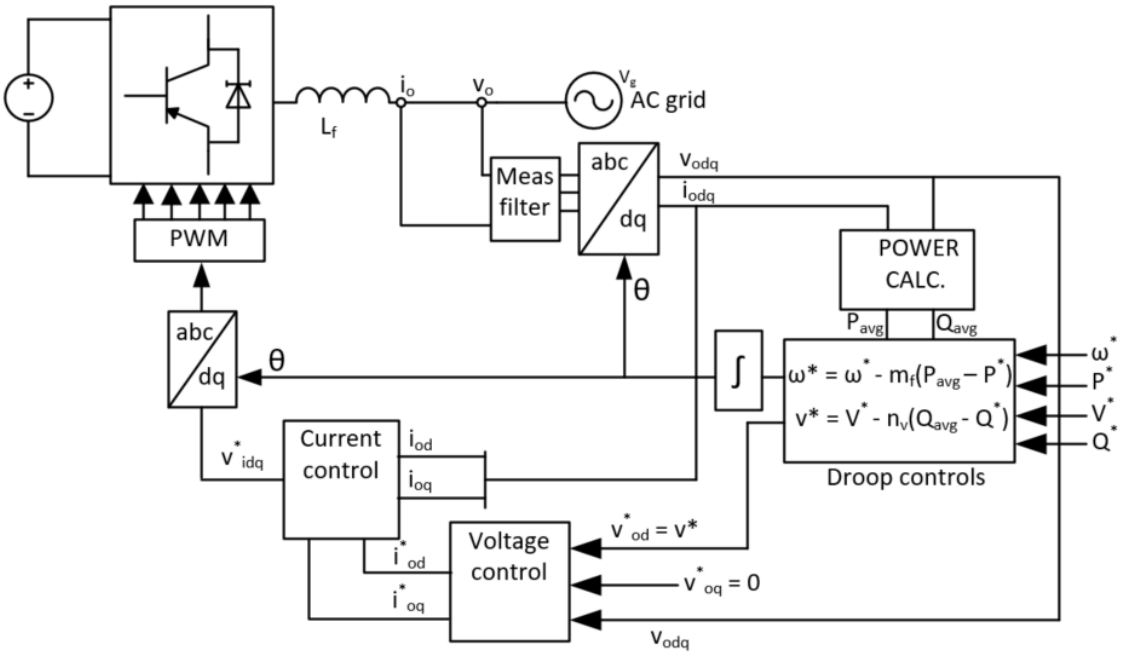

Figure 5.5: Battery grid side converter and control structure.

The control consists of the following control layers: inner current controllers, voltage controller and finally droops, setting the reference for V_d and ω dependent on the changes in reactive and active power respectively. The mathematical description of the system used to derive the state space model is described in the following section. As explained in section 4.5 the BESS and the genset will be the grid-forming units. When the genset is not running, the BESS controls the grid frequency with the P/f droop, while when the genset is running, the BESS is following the genset speed using high bandwidth communication and so the P/f droop is inactive when the genset is running.

State Equations

The output filter, measurement filter and current controllers are similar to the PV and WT model, and is again described by Equations: (5.4), (5.5) and (5.15).

The power calculations are for the battery done using the measured voltage and currents, while it in the PV and WT model was done using the actual values. Furthermore the average P and Q are found using a low pass filter. The power calculations are performed according to Equation (5.16). The cut-off frequency of the low pass filter ω_c should be much less than the fundamental grid frequency [Mueller, 2014].

$$\begin{aligned} p &= \tfrac{3}{2}(V_{od}I_{od} + V_{oq}I_{oq}) \\ q &= \tfrac{3}{2}(V_{oq}I_{od} - V_{od}I_{oq}) \\ \dot{P}_{avg} &= \omega_c p - \omega_c P_{avg} \\ \dot{Q}_{avg} &= \omega_c q - \omega_c Q_{avg} \end{aligned} \tag{5.16}$$

The droops used to control voltage and frequency is given by Equation (5.17). Because the battery is the grid-forming unit $\omega_g = \omega^*$ and $\delta = 0$, meaning that the battery dq-frame is aligned with the global reference frame.

$$\begin{aligned} \omega^* &= \omega^* - m_f(P_{avg} - P^*) \\ v^* &= V^* - n_v(Q_{avg} - Q^*) \end{aligned} \tag{5.17}$$

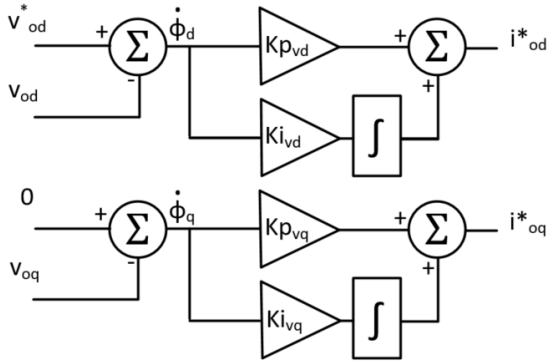

Figure 5.6: Battery converter voltage controllers.

The structure of the voltage controllers are shown in Figure 5.6, and described by Equation (5.18).

$$\begin{aligned} \dot{\phi}_d &= v^* - V_{od} \\ \dot{\phi}_q &= -V_{oq} \\ {i_{od}}^* &= Kp_{vd}\dot{\phi}_d + Ki_{vd}\phi_d \\ {i_{oq}}^* &= Kp_{vq}\dot{\phi}_q + Ki_{vq}\phi_q \end{aligned} \tag{5.18}$$

All of the above Equations are used to define a state space model of the system, with the following states, inputs and outputs:

$$\begin{aligned} x = [&P_{avg}\ Q_{avg}\ \phi_d\ \phi_q\ \gamma_d\ \gamma_q \\ &i_{od}\ i_{oq}\ V_{od}\ V_{oq}\ I_{od}\ I_{oq}] \end{aligned}$$

$$u = [\omega^*\ P^*\ Q^*\ V^*\ v_{gd}^{global}\ v_{gq}^{global}\ \omega_g]$$

$$y = [\omega^*\ i_{od}^{global}\ i_{oq}^{global}]$$

The model is then linearised around equilibrium point (x_0, u_0) according to the procedure described in [Kundur, 1994, P. 700-704]. The A, B and C matrixes of the linearised state space model are given in Appendix B, it is also shown how to initialize the model in the appendix.

5.1.3 Diesel Generator Set

Diesel engine modelling

The Diesel Generator Set (DGS) is split in three models as presented in Chapter 4. The first model is the diesel engine, where the delays of a general diesel engine is included. The first delay presented is the fuel actuator delay T_a, which takes into account the time for the psychical valve to change position, such that more or less fuel can be added. The input for the engine is the change in power, controlled by the governor which is included with a proportional and an integral droop gain.

The proportional gain is the inverse of the droop coefficient R, which is 5% such that a 5% change in speed/frequency corresponds to the valve changing position from closed to fully opened or that the output is going from 0-100%. The integral gain ensures that the steady state error is removed. Furthermore, the load reference can be set such that it is possible to change the operating point of the DGS according to a demand. After the actuator delay, a combustion delay T_d and an ignition delay T_c is included to fully describe the dynamics of a diesel engine. The continuous time block diagram is shown in figure 5.7. [Tameghe et al., 2015] [Kundur, 1994]

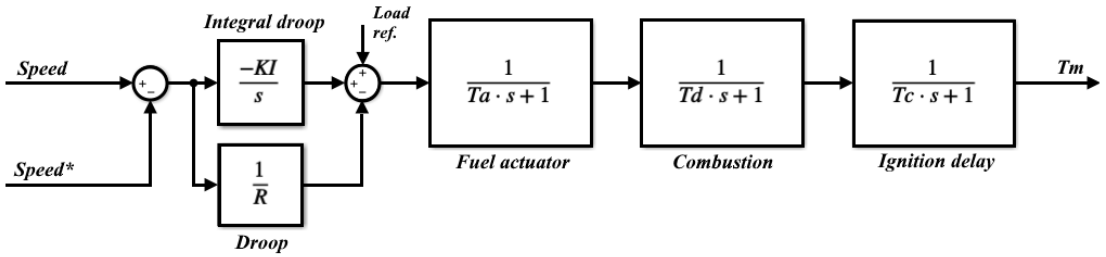

Figure 5.7: Diesel engine block diagram.

The state space model can be derived from the block diagram, by separating each integrator from its feedback, and thereby defining each state to the right of the integrator. Following this method the state equations can be derived as in equations 5.19 -5.22.

$$\dot{X}_1 = (X_2 - X_1) \cdot \frac{1}{T_c} \tag{5.19}$$

$$\dot{X}_2 = (X_3 - X_2) \cdot \frac{1}{T_d} \tag{5.20}$$

$$\dot{X}_3 = (X_4 + P^* - (\omega - \omega^*) \cdot \frac{1}{R} - X_3) \cdot \frac{1}{T_a} \tag{5.21}$$

$$\dot{X}_4 = (\omega^* - \omega) \cdot K_I \tag{5.22}$$

The corresponding matrices, A and B, can be obtained as in equation 5.23. The C matrix outputs the state X_1, which is equal to the power output of the engine.

$$\dot{X}_{DE} = \begin{bmatrix} \frac{-1}{T_c} & \frac{1}{T_c} & 0 & 0 \\ 0 & \frac{-1}{T_d} & \frac{1}{T_d} & 0 \\ 0 & 0 & \frac{-1}{T_a} & \frac{1}{T_a} \\ 0 & 0 & 0 & 0 \end{bmatrix} \cdot \begin{bmatrix} X_1 \\ X_2 \\ X_3 \\ X_4 \end{bmatrix} + \begin{bmatrix} 0 & 0 & 0 \\ 0 & 0 & 0 \\ \frac{-1}{R \cdot T_a} & \frac{1}{R \cdot T_a} & \frac{-1}{T_a} \\ -K_I & K_I & 0 \end{bmatrix} \cdot \begin{bmatrix} \omega \\ \omega^* \\ P^* \end{bmatrix} \tag{5.23}$$

$$= A_{DE} \cdot x + B_{DE} \cdot u,\ y = 1 \cdot X_4 = C_{DE} \cdot X_4$$

The output of the diesel engine can be either seen as a change in power or a change in torque, since the equations are derived in per unit values and due to the fact that the relationship between power and torque is proportional to the speed of the shaft, which at nominal speed is equal to 1. This output is one of the inputs to the synchronous generator. [Kundur, 1994]

Synchronous generator and AVR modelling

The state space modelling of the synchronous generator is based on [Anderson and Abdel-Aziz, 1977], where a $7x7$ $0dq$ state space model for a synchronous generator for stability studies is derived and linearised. The dynamic model includes the stator and rotor flux linkage equations. The non-linear terms appear due to the stator equations dependence on the speed of the rotor, and a linearisation is thereby needed. The linearised matrices are shown in equations 5.24 to 5.27, however one state, δ_r which is the rotor angle, has been removed since it has no influence on the other states. v is the inputs to the model, where v_d and v_q is the input from the grid model, after reference frame transformation, the field voltage v_F is the output from the AVR model and v_D and v_Q are the internal rotor voltages which is equal to zero. The last input is the power/torque T_m from the diesel engine model.

$$v = -Kx - M\dot{x}\ [pu] \tag{5.24}$$

$$v = \begin{bmatrix} v_d \\ -v_F \\ v_D = 0 \\ v_q \\ v_Q = 0 \\ T_m \end{bmatrix},\ x = \begin{bmatrix} i_d \\ i_F \\ i_D \\ i_q \\ i_Q \\ \omega \end{bmatrix},\ \dot{x} = \begin{bmatrix} \dot{i}_d \\ \dot{i}_F \\ \dot{i}_D \\ \dot{i}_q \\ \dot{i}_Q \\ \dot{\omega} \end{bmatrix} \tag{5.25}$$

$$K = \begin{bmatrix} r & 0 & 0 & \omega_0 L_q & \omega_0 k_{MQ} & \lambda_{q0} \\ 0 & r_F & 0 & 0 & 0 & 0 \\ 0 & 0 & r_D & 0 & 0 & 0 \\ -\omega_0 L_d & -\omega_0 k_{MF} & -\omega_0 K_{MD} & r & 0 & -\lambda_{d0} \\ 0 & 0 & 0 & 0 & r_Q & 0 \\ \frac{\lambda_{q0} - L_d i_{q0}}{3} & \frac{-k_{MF} i_{q0}}{3} & \frac{-k_{MD} i_{q0}}{3} & \frac{-\lambda_{d0} + L_q i_{d0}}{3} & \frac{-k_{MQ} i_{d0}}{3} & -D \end{bmatrix} \tag{5.26}$$

$$M = \begin{bmatrix} L_d & K_{MF} & K_{MD} & 0 & 0 & 0 \\ K_{MF} & L_F & M_R & 0 & 0 & 0 \\ K_{MD} & M_R & L_D & 0 & 0 & 0 \\ 0 & 0 & 0 & L_q & k_{MQ} & 0 \\ 0 & 0 & 0 & k_{MQ} & L_Q & 0 \\ 0 & 0 & 0 & 0 & 0 & -\tau_j \end{bmatrix} \tag{5.27}$$

The inputs are thereby the grid voltages, however, in [Anderson and Abdel-Aziz, 1977], the state space model is derived using parks transformation, to a $0dq$ frame, where the d-axis is aligned with the magnetic flux and leads the q-axis by 90 deg., the stator EMF is therefore aligned with the q-axis, whereas the previous models derived are based on $dq0$ frame where the q-axis is leading the d-axis by 90 deg. and the voltages are aligned with the d-axis. Therefore, it is necessary to change the model from, frame used in [Anderson and Abdel-Aziz, 1977], to the global dq-frame, as shown in Figure 5.8. The figure shows the change from $dq0$ (black lines) to $0dq$ (red line).

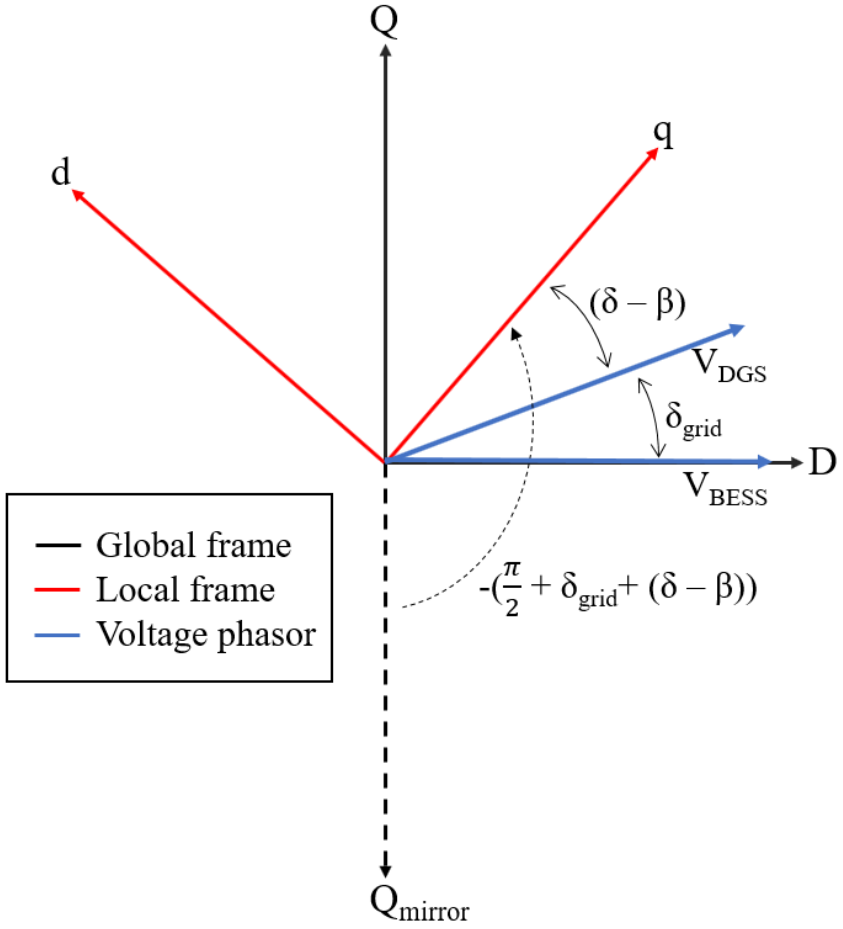

Figure 5.8: The red line indicates the location of the q-axis, in a 0dq-frame, and the black lines indicates the location of the global dq0-frame.

The following transformation 5.28 has been applied to change the input from the grid, V_{d-grid} and V_{q-grid} to the voltage inputs to the model, v_d and v_q. The transformation matrix shifts the Q-axis to Q_{mirror} and then rotates it by -$(\pi/2 + (\delta - \beta) + \delta_{grid})$.

$$P_{dq-qd} = \sqrt{3} \begin{bmatrix} cos(-\pi/2 - (\delta - \beta) - \delta_{grid}) & -sin(-\pi/2 - (\delta - \beta) - \delta_{grid}) \\ -sin(-\pi/2 - (\delta - \beta) - \delta_{grid}) & -cos(-\pi/2 - (\delta - \beta) - \delta_{grid}) \end{bmatrix} \tag{5.28}$$

Where the angle $\delta - \beta$ is the angle between the phase voltage V_a and the q-axis as explained in [Anderson and Abdel-Aziz, 1977, P. 150-160]. δ_{grid} is the initial voltage angle between the bus voltage at the BESS and the DGS. The $\sqrt{3}$ factor is because

of the specific choice of transformation used in [Anderson and Abdel-Aziz, 1977]. The d-q voltage applied to the synchronous generator is thereby found using 5.29.

$$\begin{bmatrix} v_d \\ v_q \end{bmatrix} = P_{dq-qd} \cdot \begin{bmatrix} v_{d-grid} \\ v_{q-grid} \end{bmatrix} \tag{5.29}$$

The C matrix of this system will output states from the synchronous generator. It is however only i_d, i_q and the speed ω that is needed. Again, the output currents need to be changed to fit the grid model. This is done using the inverse of 5.28, as shown in Equations 5.30.

$$\begin{bmatrix} i_{d-grid} \\ i_{q-grid} \end{bmatrix} = P_{dq-qd}^{-1} \cdot \begin{bmatrix} i_d \\ i_q \end{bmatrix} \tag{5.30}$$

To obtain the matrices A and B, Equation 5.24, is used and the $\dot{x}$ is isolated to give Equation 5.31.

$$\dot{x} = -M^{-1} \cdot K \cdot x - M^{-1} v = A_{SG} \cdot x + B_{SG} \cdot u \tag{5.31}$$

The calculation of initial conditions, and the derivation of constants applied in matrix K and M, can be found in Appendix B.4.

AVR

For the AVR, a simple model with an amplifier and a feedback has been used. The purpose of the AVR is to regulate the output voltage to a given reference. The inputs to the model are PSS signal V_S, the reference V_t^* and the actual voltage terminal/grid voltage V_c. The output is the field voltage v_F, which is the input to the synchronous generator. The model is shown in Figure 5.9.

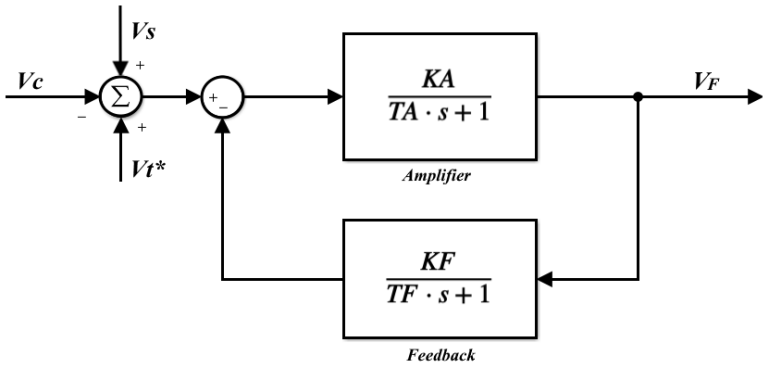

Figure 5.9: AVR block diagram.

In order to derive the state space representation the method control canonical form is used, which has the drawback that only the input and output have physical meaning, but the states are unknown [Phillips and Parr, 2010]. However, since the internal states are irrelevant the method is applied for simplicity. The state space representation is shown in Equation 5.32.

$$\dot{x} = \begin{bmatrix} 0 & 1 \\ -a_1 & -a_2 \end{bmatrix} x + \begin{bmatrix} 0 & 0 & 0 \\ 1 & -1 & 1 \end{bmatrix} \begin{bmatrix} V_t^* \\ V_c \\ V_s \end{bmatrix} = A_{AVR} \cdot x + B_{AVR} \cdot u \tag{5.32}$$

$$y = \begin{bmatrix} b_2 & b_1 \end{bmatrix} \cdot x = C_{AVR} \cdot x \tag{5.33}$$

The constants a_1, a_2 b_1 b_2 are calculated as in 5.34, following the control canonical form [Phillips and Parr, 2010].

$$a_1 = \frac{T_A + T_F + K_F \cdot K_A}{T_A \cdot T_F},\ a_2 = \frac{1}{T_A \cdot T_F} \tag{5.34}$$

$$\tag{5.35}$$

$$b_1 = \frac{K_A}{T_A},\ b_2 = \frac{K_A}{T_A \cdot T_F} \tag{5.36}$$

At last the three models is assembled, such that the only output is the currents in dq-frame fed to the grid model, and the only inputs is the grid voltages in dq-frame, which is given by the grid model. The assembling of the the three models can be found in appendix B.4.

5.1.4 Grid and Load

The grid and load model is derived in this section. It is seen from Section 2.3 that most of the studies do not consider the dynamics from the power system grid. These models are however needed, in order to reflect how the changes from the generation units will impact the network voltages. The state equations will be given, as referred to the common reference frame.

An example of the grid and load mode is shown in Figure 5.10. The grid cables and loads are modelled by their inductance and resistance. There are several ways to model the loads in a power system, the simple approaches being constant PQ, constant I and constant Z. It is an ongoing discussion on, how an aggregated load should be modelled to include the exact dynamic behaviours, especially in this time where several non-linear loads are introduced into the systems [Yamashita et al., 2011]. In this project a constant Z load is considered in order to streamline how the state space models for the grid and load are derived. A community will consist of many different load types. Hence, it is not possible to apply a specific load model. A Z load is seen sufficient for this study, since the specific load response is out of scope.

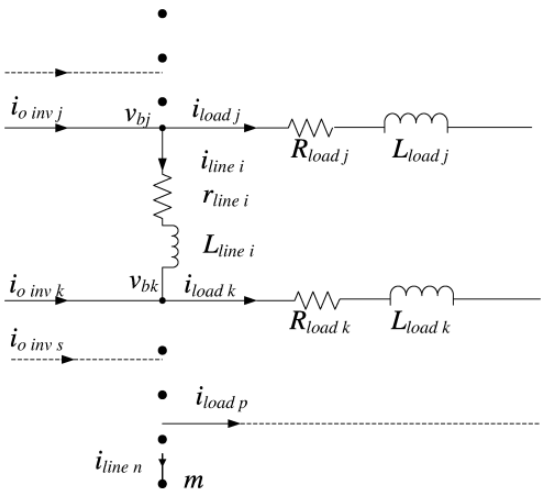

Figure 5.10: The grid model including the resistance and inductance of the cables [Pogaku et al., 2007].

From KVL, the dynamic equations will follow, as given in Equation 5.37 and 5.38.

$$v_{busD,j} - v_{busD,k} = L_{linei} \cdot \frac{\partial i_{lineDi}}{\partial t} - \omega L_{linei} i_{lineQi} + R_{linei} \cdot i_{lineDi} \tag{5.37}$$

$$v_{busQ,j} - v_{busQ,k} = L_{linei} \cdot \frac{\partial i_{lineQi}}{\partial t} - \omega L_{linei} i_{lineDi} + R_{linei} \cdot i_{lineQi} \tag{5.38}$$

The equations are rearranged to have the derivative terms on the left hand side, as seen from Equation 5.39 and 5.40.

$$\frac{\partial i_{lineDi}}{\partial t} = \omega i_{lineQi} - \frac{R_{linei}}{L_{linei}} \cdot i_{lineDi} + \frac{1}{L_{linei}} v_{busD,j} - \frac{1}{L_{linei}} v_{busD,k} \tag{5.39}$$

$$\frac{\partial i_{lineQi}}{\partial t} = -\omega i_{lineDi} - \frac{R_{linei}}{L_{linei}} \cdot i_{lineQi} + \frac{1}{L_{linei}} v_{busQ,j} - \frac{1}{L_{linei}} v_{busQ,k} \tag{5.40}$$

The same procedure is applied to the loads. The dynamic equation is given in equation 5.41 and 5.42 along with the rearranged equations in 5.43 and 5.44.

$$v_{busD,i} = L_{loadi} \cdot \frac{\partial i_{loadDi}}{\partial t} - \omega L_{loadi} i_{loadQi} + R_{loadi} \cdot i_{loadDi} \tag{5.41}$$

$$v_{busQ,i} = L_{loadi} \cdot \frac{\partial i_{loadQi}}{\partial t} - \omega L_{loadi} i_{loadDi} + R_{loadi} \cdot i_{loadQi} \tag{5.42}$$

$$\frac{\partial i_{loadDi}}{\partial t} = \omega i_{loadQi} - \frac{R_{loadi}}{L} \cdot i_{loadDi} + \frac{1}{L} v_{loadD,i} \tag{5.43}$$

$$\frac{\partial i_{loadQi}}{\partial t} = -\omega i_{loadDi} - \frac{R_{loadi}}{L} \cdot i_{loadQi} + \frac{1}{L} v_{loadQ,i} \tag{5.44}$$

Finally the state space linearised model is derived by linearising around an equilibrium point, and the following expressions are derived; Equation 5.45, for the grid model and the Equation 5.46 for the load model.

$$[\Delta \dot{i}_{lineDQ}]_{10x1} = A_{grid_{10x10}}[\Delta i_{lineDQ}]_{10x1} + B_{1grid_{10x12}}[\Delta v_{busDQ}]_{12x1} + B_{2grid_{10x1}}[\Delta \omega]_{1x1} \tag{5.45}$$

$$[\Delta \dot{i}_{loadDQ}]_{2x1} = A_{load_{2x2}}[\Delta i_{loadDQ}]_{2x1} + B_{1load_{2x12}}[\Delta v_{busDQ}]_{12x1} + B_{2load_{2x1}}[\Delta \omega]_{1x1} \tag{5.46}$$

The actual matrices can be found in Appendix B.

Calculating the bus voltages

In order to calculate the currents, a fictitious resistor r_n of a high value is connected between each bus and ground. A high value is chosen to reduce the influence on the dynamic stability of the system. The voltages in dq-frame can be calculated as follows:

$$v_{Di} = r_n \cdot (i_{genDi} - i_{loadDi} + i_{lineDi,j}) \tag{5.47}$$

$$v_{Qi} = r_n \cdot (i_{genQi} - i_{loadQi} + i_{lineQi,j}) \tag{5.48}$$

i_{geni} are the currents from the generation units. Linearising and transforming to state space form results in the following equations:

$$[\Delta v_{DQ}] = R_n \cdot (M_{GEN}[\Delta i_{genDQ}] + M_{LOAD}[\Delta i_{loadDQ}] + M_{GRID}[\Delta i_{lineDQ}]) \tag{5.49}$$

R_n is a diagonal matrix, of size 12x12 with r_n on the diagonal. M_{gen} is a mapping matrix, that maps the ith generation unit to the jth bus. It is a 12x8 matrix, where e.g element $M_{gen}(i, j)$ is denoted with 1, and all the other entries are zero in this row. M_{load} is a 12x2 matrix, which maps the loads to their respective bus with a -1. Finally, M_{grid} maps the connecting lines to their respective buses. A -1 or 1 is used for line currents that are leaving or entering the bus node, respectively.

5.2 Controller Design

In this section, response criteria for the outer control loops of the DER units are defined. It is further described how the controller gains have been selected.

WT and PV

The control should meet the following criteria:

Control Parameter	Overshoot	Settling time
V_{dc} subject to ΔP	<2%	<100 ms
Q subject to $\Delta Q*$	<2%	<10ms

The inner current controllers are tuned using Equation (5.50), given in [Zhou et al., 2015] where it is stated that ω_{ic} should be 4% of the switching frequency. By tuning with SISOTOOL in Simulink, 4.5% is found to give the best response, where f_s is

5kHz.

$$\begin{aligned} \omega_{ic} &= 0.045 \cdot 2\pi f_s \\ Kp_{idq} &= \omega_{ic} L_{ft} \\ Ki_{idq} &= \omega_{ic} Kp_{idq} 0.1 \end{aligned} \tag{5.50}$$

The Q control described by Equation (5.14), is simply the relation between voltage and current, and no tuning is required. The DC link control is tuned similarly to the inner current controllers using Equation (5.51), except now the capacitor is the plant instead of the inductor [Gkountaras, 2017, P. 49]. Again by using SISOTOOL, it is found that ω_{dc} should be 2% of f_s.

$$\begin{aligned} \omega_{DC} &= 0.02 \cdot 2\pi f_s \\ Kp_v &= \omega_{DC} C_{DC} \\ Ki_v &= \omega_{DC} Kp_v 0.1 \end{aligned} \tag{5.51}$$

The PI controller of the PLL is designed using the guidelines given in [Sezi, 2010]. The method is simple and yields fast convergence and no overshoot. The controller gains are found using equation (5.52), where M = 64 is the typical number of samples per measurement cycle [Sezi, 2010, P. 4]. This control design yields a settling of 2.35ms which is proven to give a stable response in [Sezi, 2010], in good agreedment with [Teodorescu et al., 2011].

$$\begin{aligned} c &= \frac{2\pi}{M} \\ Kp_{PLL} &= \frac{0.5}{c} \\ Ki_{PLL} &= 0.1c \end{aligned} \tag{5.52}$$

BESS

The inner current control loops are tuned the same way as for the PV and WT model, using Equation (5.50). The outer voltage controllers are tuned as explained below. The control should meet the criteria:

Control Parameter	Overshoot	Settling time
v_{od} subject to ΔV	<2%	<10 ms

The voltage controllers are tuned, to find the proper relation to the current controller gains using SISOTOOL. The best response is found using the relation given in Equation (5.53).

$$\begin{aligned} Kp_{vdq} &= Kp_{idq} \cdot 1.5 \\ Ki_{vdq} &= Ki_{idq} \cdot 300 \end{aligned} \tag{5.53}$$

The droop gains of the BESS m_f and n_v should be selected dependent on the specific grid where the BESS is to be implemented. The Q/V droop gain n_v is selected using the voltage sensitivity analysis presented in Section 5.4.1.

The results presented in Appendix C, are made using the BESS bus as slack bus, and it is therefore not included in the sensitivity analysis. However, if instead the DGS is selected as slack bus, the results for the BESS bus is exactly the same as the presented results for the DGS, because the cables going from BESS and DGS to the common bus have the same length. Therefore entrance (9,9) in Figures C.2 and C.3 shows how much a change in Q from the BESS changes the voltage at the BESS bus. It is seen that the value is 0.0071 for high production and 0.0083 for low production. Therefore n_v is selected to be 0.0075.

The P/f droop gain m_f is only active when the DGS is not running. Because other equipment in the grid is dependent on the frequency response, eg. relays, it is desired to have the same response whether the DGS is running or not. Therefore the gain m_f is set to 0.05 matching the droop coefficient R (5%.) of the DGS as explained in Section 5.1.3.

Diesel Generator Set

The DGS has mainly two tuning points, one being the AVR where the voltage response is tuned, and the other being the governor in the diesel engine model. For the AVR, typical values from [Anderson and Abdel-Aziz, 1977], has been applied, which can be found in Appendix D.4. The criteria for voltage response is defined using the recommendations from [DEFU, 2011], where the average voltage level over a time interval of 10 minutes should be less than ±10%.. This is applied for the upper limit, and defined to be 10 seconds, to ensure that the recommendation is respected. For the lower limit, the response should be slower than for the BESS, to avoid hunting effect, as they regulate buses in close proximity voltages. The lower limit is set to be 10 times slower than for the BESS. Considering overshoot, the same criteria is applied as for the BESS.

Control Parameter	Overshoot	Settling time maximum	Settling time minimum
v_{od} subject to ΔV	<2%	<10 s	>100 ms

For the governor, the integral gain KI can be regulated, to adjust the settling time of the rotor speed, and thereby the net frequency. Again a typical value from a governor in [Kundur, 1994], has been applied. To ensure that the frequency response is acceptable, the recommendations in [DEFU, 2011] is applied, where the average frequency over a 10 second interval deviates by a maximum of ±1%. Well aware that this is the recommendation for the main grid, and therefore not 100% applicable for isolated microgrids, the maximum response time is set to 1 second, with a maximum overshoot of 4%.

Control Parameter	Overshoot	Settling time
f subject to ΔV	<4%	<1 s

5.3 Model Verification

The verification of each model will be done by a comparison with either EMT models in SimScape (Simulink) or with a Matlab script. The procedure in this section is to define some test cases that will be used to justify the verification of the model. Some data are compared and a deviation is depicted in graphs. In general this deviation can be calculated as

$$\%Deviation = \frac{x_{EMT} - x_{SS}}{x_{EMT}} \cdot 100 \tag{5.54}$$

where x_{EMT} and x_{SS} are the parameters in the EMT and state space model, respectively.

The test cases are chosen to range from one extreme to another extreme operating point. Meaning testing both large and small change and both high and low power. These test cases will therefore justify a verification of the models, because if they are valid in the extreme points they will also be in between.

5.3.1 WT and PV

In this subsection the state space model (SSM) is verified by comparison with a model made in Simscape -> PowerSystems (SPM). All model parameters used for both the state space and PowerSystems model are given in Appendix D.

Furthermore, the results presented in this section, will be used to verify that the control meets the criteria defined in Section 5.2. As explained in Appendix D the state space model is running in p.u. values, while the EMT model is running in absolute time, and the results from the state space model is moved to absolute time in order to compare.

When doing these comparisons the filter representing the machine side converter have been neglected, because it is desired to see how the DC link behaves to an instant change in power. If the model acts as desired in this case, it will also do so when the filter is included, meaning the power changes will happen much slower. The control is made in p.u. for both models. Four test cases have been defined for comparison of the responses:

- Test 1: V_{DC} response to $\Delta P = 0.1 \rightarrow 0.11$p.u. starting at PF $= 0.9$
- Test 2: V_{DC} response to $\Delta P = 0.1 \rightarrow 1$p.u. starting at PF $= 0.9$
- Test 3: Q response to $\Delta Q^* = 0.01$p.u. starting at $P_0 = 1$p.u. & PF $= 0.9$
- Test 4: Q response to $\Delta Q^* = 0.1$p.u. starting at $P_0 = 1$p.u. & PF $= 0.9$

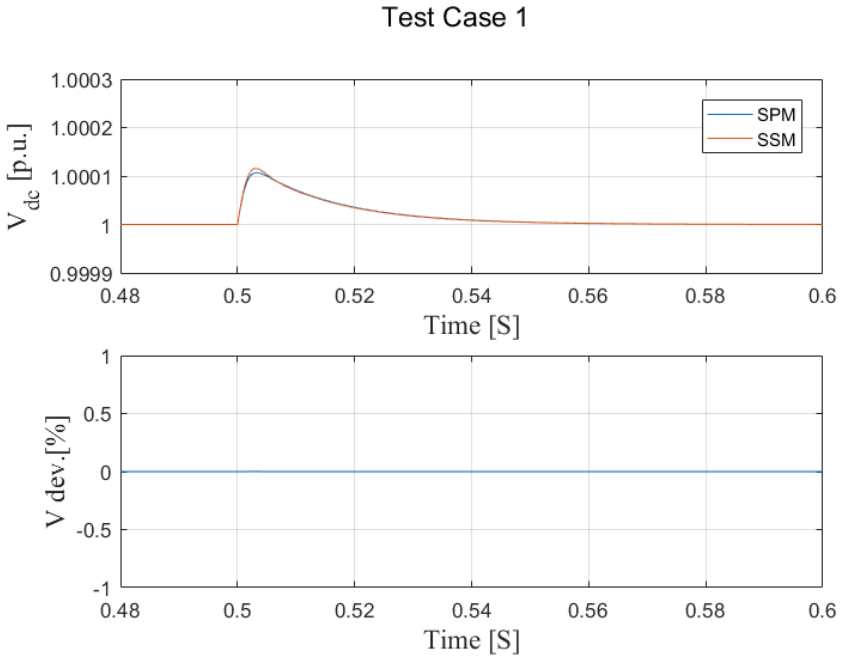

Figure 5.11: Response of DC link voltage to a small change in active power output from the current source.

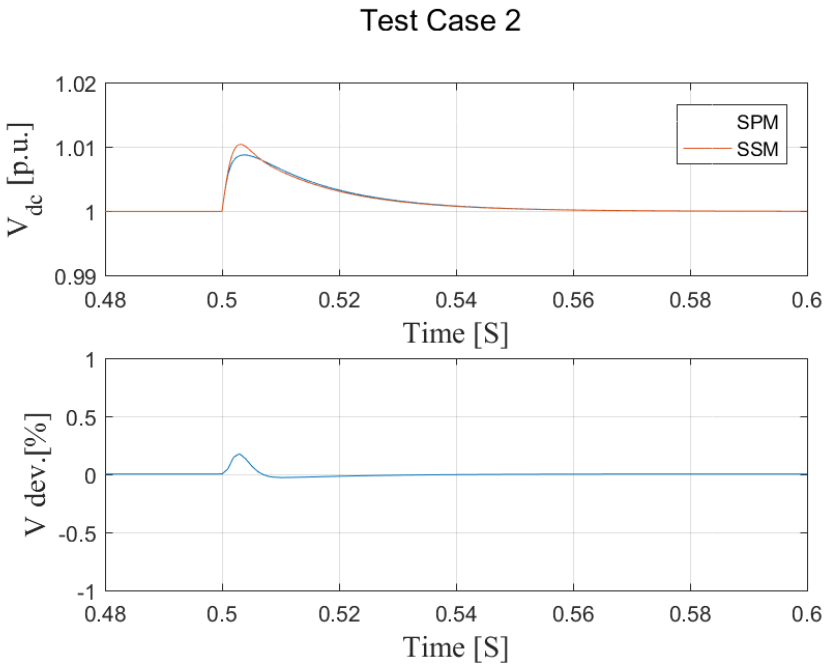

Figure 5.12: Response of DC link voltage to a large change in active power output from the current source.

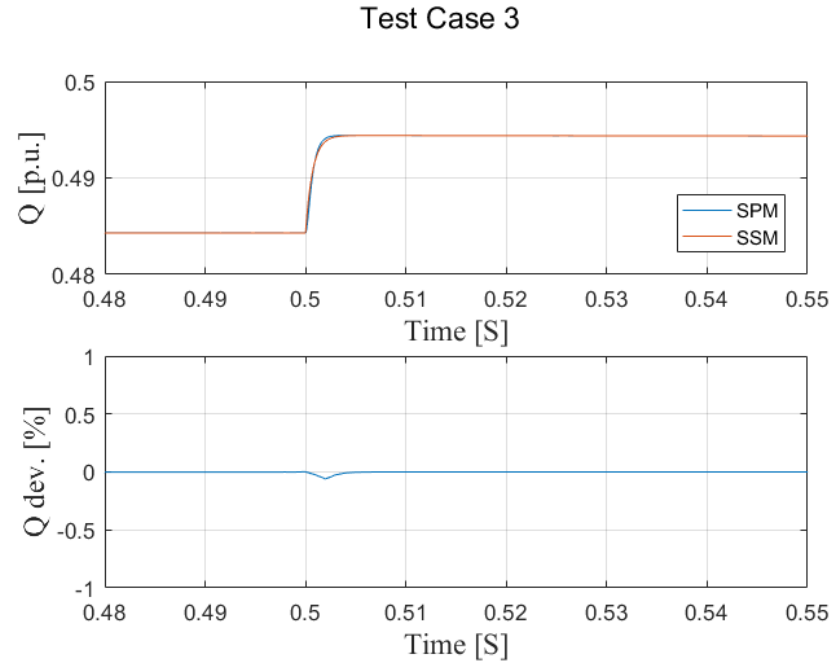

Figure 5.13: Response of the reactive power output, to a small change in reference.

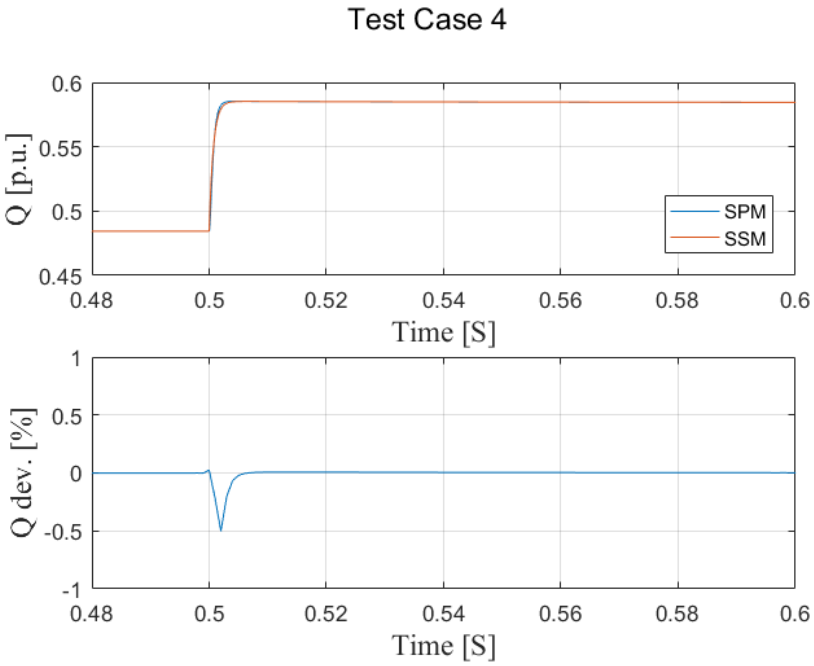

Figure 5.14: Response of the reactive power output, to a large change in reference.

Table 5.1: Comparison of state space model and simpower model for PV & WT.

	Settling time [ms]	Final Value [p.u.]	Maximum Deviation [%]
	t_{set}	V_{final}	$V_{deviation}$
Test 1	60	1	0.0008
Test 2	60	1	0.1736
	t_{set}	Q_{final}	$Q_{deviation}$
Test 3	3	0.4943	0.0603
Test 4	3	0.5843	0.5030

Results of the described test cases are shown in Figures 5.11, 5.12, 5.13, 5.14 and compared in Table 5.1.

Test 1 and 2 shows the behaviour of the DC link to power change. The highest deviation is found in test 2. The deviation peaks at the same time as V_{dc} because the SSM have a higher overshoot than the SPM. The peak deviation is 0.1736 % and is reduced to a negligible value again within 10ms. In both tests the settling time is 60ms and the voltage change from nominal to peak corresponds to 1.2% of

the change in power, meaning the the control meets the criteria of 100ms settling time and 2% overshoot.

Test 3 and 4 shows the reactive power output response to a change in reference. The deviation has a peak during the rise of Q, and the highest deviation is found in test 4 to be 0.503%, similar to test 1 and 2 the deviation is reduced to zero again in a time below 10ms. In both tests the settling time is 3ms and the Q overshoot is approximately 0.95%, which is within the limits of the controller design criteria.

The maximum deviation between the state space and EMT model is found in the last test to be 0.5%. The peaks in deviation is found during the transients and are reduced to a negligible value again within a few ms. Furthermore, the models have the same settling time. This project is not concerned with fast transients and the models are to be used for designing network level control working in the second range. Therefore, these small deviations found during the transient response can be ignored. Hence, the state space model is considered verified and valid for the analysis in scope.

5.3.2 BESS

In this subsection the state space model (SSM), is verified by comparison with a model made in Simscape -> PowerSystems (SPM). All model parameters used for both state space and PowerSystems model are given in Appendix D. Furthermore, the results presented in this section, will be used to verify that the control meets the criteria defined in Section 5.2. As explained in Appendix D the state space model is running in p.u. values while the EMT model is running in real time, and the results from the state space model is moved to real time in order to compare. Both models are doing the control in p.u. The model is connected to a simple RL load, and the response in v_{od} and ω^* is compared for step changes in voltage reference V^* at different loads. Four test cases have been defined for comparison of the responses:

- Test 1: $\Delta V^* = 0.01$p.u. and load $P_0 = 1$p.u. & PF $= 0.9$
- Test 2: $\Delta V^* = 0.01$p.u. and load $P_0 = 0.1$p.u. & PF $= 0.9$
- Test 3: $\Delta V^* = 0.1$p.u. and load $P_0 = 1$p.u. & PF $= 0.9$
- Test 4: $\Delta V^* = 0.1$p.u. and load $P_0 = 0.1$p.u. & PF $= 0.9$

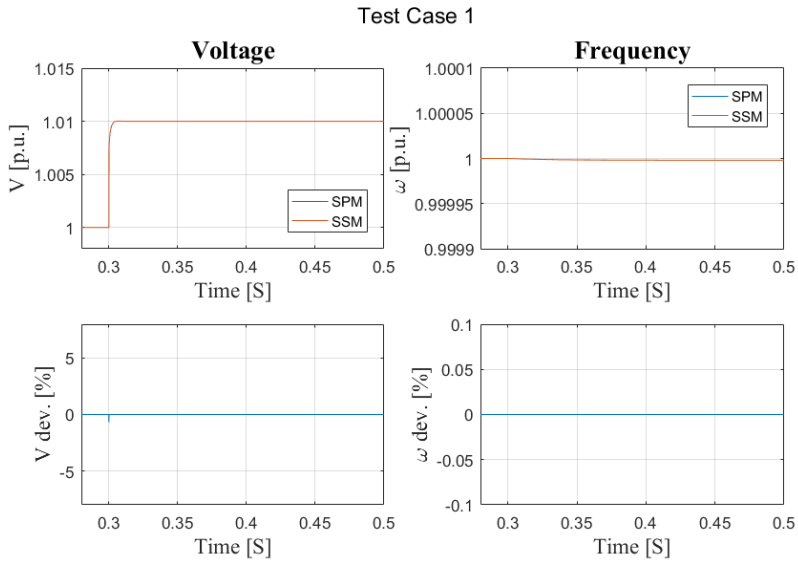

Figure 5.15: Response of voltage and frequency to, small voltage change and large load.

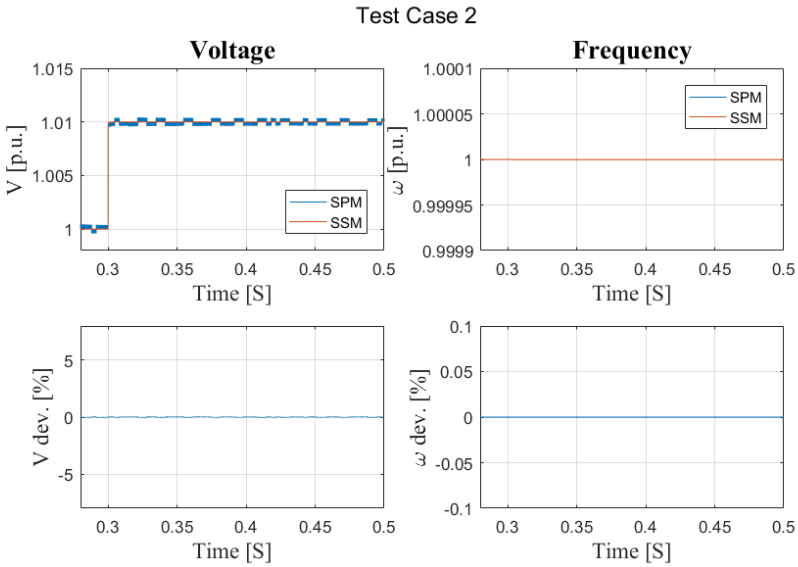

Figure 5.16: Response of voltage and frequency to, small voltage change and small load.

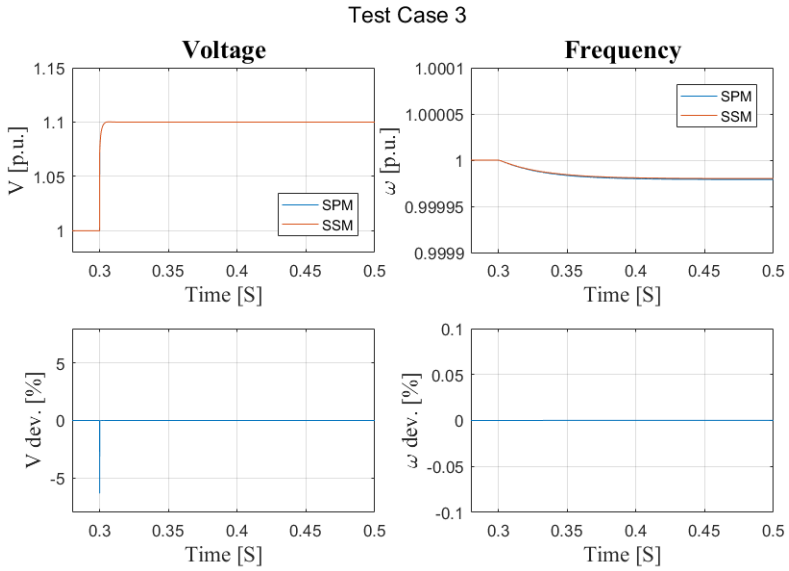

Figure 5.17: Response of voltage and frequency to, large voltage change and large load.

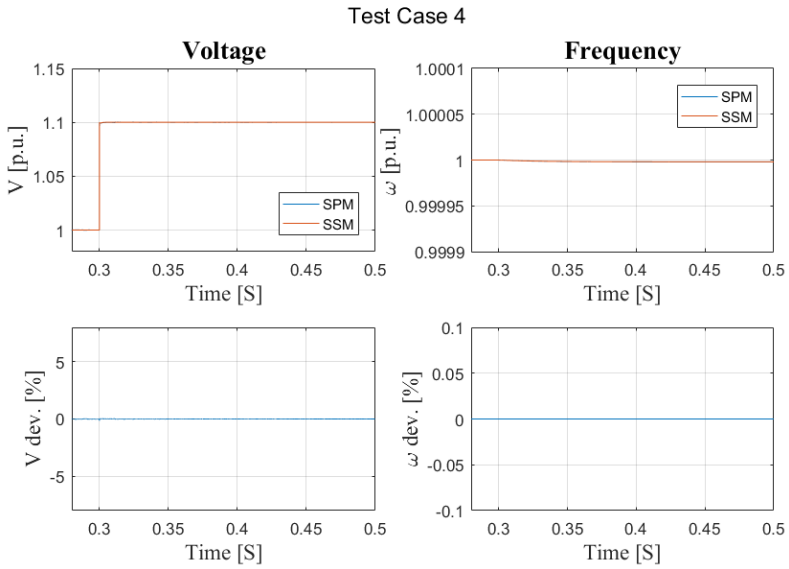

Figure 5.18: Response of voltage and frequency to, large voltage change and small load.

Table 5.2: Comparison of state space model and simpower model for BESS.

	Settling time [ms]	Final Voltage Value [p.u.]	Maximum Voltage Deviation [%]	Maximum Frequency Deviation [%]
	t_{set}	V_{final}	$V_{deviation}$	$f_{deviation}$
Test 1	5	1.0100	0.6726	0.0000
Test 2	0.01	1.0100	0.0409	0.0000
Test 3	5	1.100	6.343	0.0001
Test 4	0.01	1.100	0.1454	0.0000

Results of the described test cases are shown in Figures 5.15, 5.16, 5.17, 5.18 and compared in Table 5.2. The tests shows the behaviour of the grid-forming battery model to a change in voltage reference. The change in voltage reference also makes a small change in the power delivered, as the unit is connected to a constant impedance load. Because of the P/f droop this also results in a small change in frequency. However the change in frequency is only visible in test 3 where the deviation still is below 1% and it can therefore be neglected. It is seen the settling time is dependent on the size of load, where high load results in the slowest settling time, however at rated power the settling time is 5ms meaning the control meets the criteria. In all tests the voltage overshoot is 0.18%, again within the limits of the controller design criteria.

The maximum deviation between the state space and EMT model is found in the third test to be 6.3%. The peaks in deviation are found during the transients and are reduced to a negligible value again within less than a 1 ms. As for the case with WT and PV, this project is not concerned with fast transients and the models are to be used for designing network level control working in the second range. Therefore, these small deviations found during the transient response can be ignored. Hence, the state space model is considered verified, and valid for the analysis in scope.

5.3.3 Diesel Genset

For the verification of the diesel genset, a model from MATLAB simulink -> Simscape -> Power Systems of a synchronous machine has been used. The model is connected to the same AVR and governor as the state space model, such that the response is comparable. All values applied to the two models can be found in Appendix D.4. The genset is tested using a simple load, such that the AVR has a voltage feedback. The models are verified in four test cases, similar to the BESS, checking the frequency and voltage response due to a change in the reference voltage

amplitude. Both models is in p.u., and as for the BESS, the state space model is in p.u. time, while the simscape model is in seconds, for which moving the state space model time to absolute time, is necessary. The four test cases have been defined to check the model at full load 100%, and 30% loading, both at $PF = 0.9$ lagging. The base power for the generator is $45kW$, such that full load for the test cases corresponds to $P = 1$ or in complex notation $S = 45kW + j \cdot 21.8kVAr$ corresponding to $1 + j \cdot 0.48p.u.$ The change in reference voltage amplitude is made for a change of 1% and 10% for both loading scenarios to see the response of a small and a large change in reference. The four cases are listed below.

- Test 1: $\Delta V^* = 0.01$p.u. and load $P_0 = 1$p.u. & PF $= 0.9$
- Test 2: $\Delta V^* = 0.01$p.u. and load $P_0 = 0.1$p.u. & PF $= 0.9$
- Test 3: $\Delta V^* = 0.1$p.u. and load $P_0 = 1$p.u. & PF $= 0.9$
- Test 4: $\Delta V^* = 0.1$p.u. and load $P_0 = 0.1$p.u. & PF $= 0.9$

The upper part of the following graphs 5.19 to 5.22 shows the change in frequency and change in voltage magnitude, for the two models, while the lower part shows the deviation between models. Finally the deviation is listed in a table and discussed.

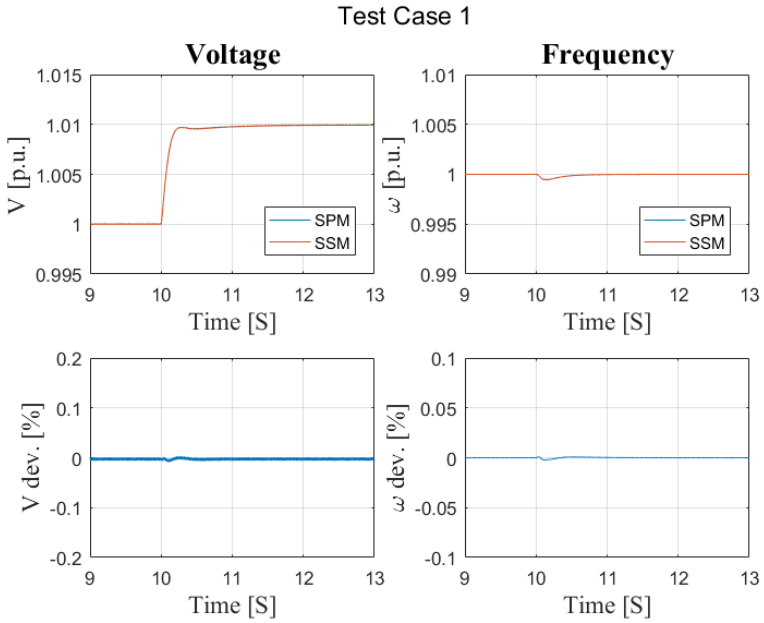

Figure 5.19: Test 1: Response of terminal voltage and frequency to a small change reference voltage.

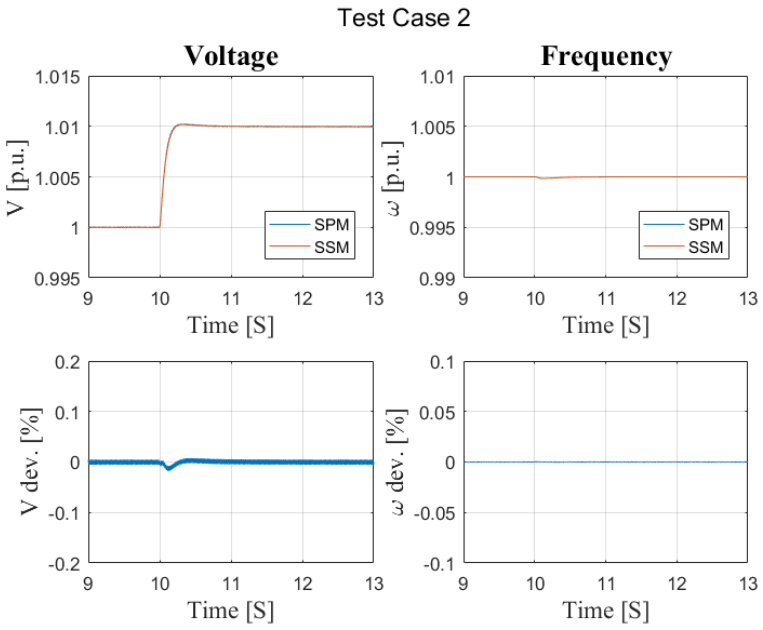

Figure 5.20: Test 2: Response of terminal voltage and frequency to a small change reference voltage.

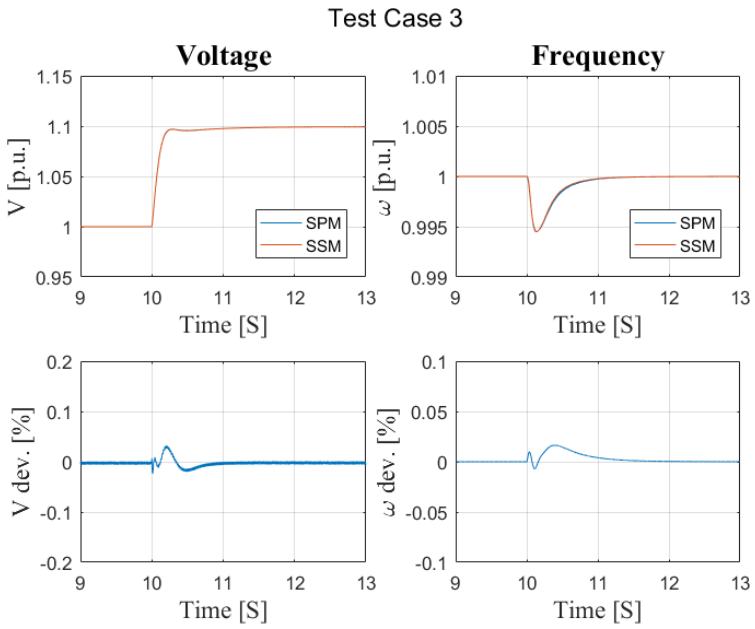

Figure 5.21: Test 3: Response of terminal voltage and frequency to a large change reference voltage.

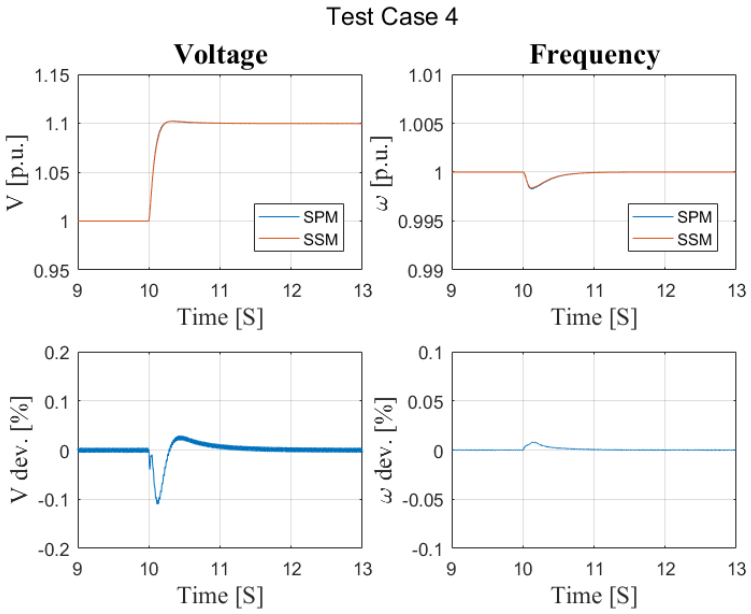

Figure 5.22: Test 4: Response of terminal voltage and frequency to a large change reference voltage.

Table 5.3: Comparison of state space model and simpower model.

	Settling time [ms]	Final Voltage Value [p.u.]	Maximum Voltage Deviation [%]	Maximum Frequency Deviation [%]
	t_{set}	V_{final}	$V_{deviation}$	$f_{deviation}$
Test 1	210	1.0099	0.0086	0.0023
Test 2	210	1.0099	0.0175	0.0006
Test 3	210	1.0993	0.032	0.0163
Test 4	210	1.0997	0.1105	0.0082

In Test Case 1 and 2, a small change of $0.01p.u$ is applied to the reference voltage at $t = 10s$. At the left side of Figure 5.19 and 5.20, the voltage response is shown. The settling time is found to be around 210 ms for both cases, while the settling value is 1.0099, as listed in table 5.3. The small steady state error can be explained by the model of the AVR, as this have no integral gain to eliminate the steady state error. However, this is still seen as acceptable, since the voltage at a generating unit is set higher to compensate for any line losses towards the main substation. The settling time of 210 ms, is quite fast for a non-converter based production unit, however the size of the genset is relatively small, and therefore also the inertia,

which can explain the fast behaviour. The maximum voltage deviation between the two models is negligible. The change in voltage magnitude introduces a change in power, whereas the frequency is affected as shown in 5.19 and 5.20, and it is shown that the models are able to remove the frequency error completely. The two models maximum frequency deviation is 0.0023% in Test Case 1 and even lower for Test Case 2, which again is negligible.

For Test Case 2, the same tendency is seen as for Test Case 1, but with lower peak values. This indicates that the model of the genset can handle small changes at low load. A slightly larger voltage deviation of 0.0175% can be found in Test Case 2, which indicates that one model acts slightly different at low load. Overall the state space model is verified to be working properly for small changes in the voltage reference.

For Test Case 3 and 4, the reference voltage is changed by 0.1 *p.u.*, to test how the models respond to a large change in reference voltage. Compared to the previous two cases, the settling time is unchanged, and the voltage overshoot is below 1% The voltage settles at 1.0993 *p.u.* for case 3 and at 1.0997 *p.u.* at case 4, which again is due to the lack of integral control in the AVR. A larger overshoot in frequency is found in Test Case 3 and 4 which is a result of the larger step in voltage, demanding a larger power change, and thereby a larger frequency deviation, compared to Test Case 1 and 2. Especially at full load (Test Case 3), the frequency is deviating. However, for all the test cases the frequency is deviating by less than 0.6 % from unity and is for all cases settling back at 1 *p.u.*. The change in frequency can affect the overall stability in the system, and further tuning may be necessary, however further investigations is continued in Chapter 6.

As seen in Table 5.3 the largest deviation of 0.11% can be found at Test 4, where the reference is stepped up by $0.1p.u$ with the generator at low load. Still this deviation is very low and the model is seen as verified for larger changes in voltage reference.

Since the state space model has proven to be able to eliminate the frequency error after a change in power, the need for showing changes in power reference or load, has been left out.

5.3.4 Grid and Load

The verification of the grid and load state space model is done using a load flow script made in Matlab. The numerical solver used is the Newton-Rhapson method. The load flow is solved to get an initial equilibrium point, which is used in the state

space model. It should be noted that the slack bus in the load flow is bus 4, which is where the battery is placed. Hence, $\angle V_4$=0 from the load flow and cannot be used for the percentage deviation. The load is $P_{load} = 65kW$ and $PF_{load} = 0.95$. All generating units have a $PF = 0.97$.

To verify the model, the procedure will be as follows:

- Test 1: All generation units (except slack bus) generate 0.1 times their rated active power at $PF = 0.97$
- Test 2: All generation units (except slack bus) generate 1 times their rated active power at $PF = 0.97$
- Test 3: All generation units (except slack bus and PV) generate 0.1 times their rated active power at $PF = 0.97$, PV generate 1 times times its rated active power at $PF = 0.97$
- Test 4: All generation units (except slack bus and genset) generate 0.1 times times their rated active power at $PF = 0.97$, genset generate 1 times their rated active power at $PF = 0.97$

The change in voltage from the load flow and the state space model is compared and the deviation is shown in Figure 5.23 for Test 1. This test shows the scenario where the production level from all units, except the slack bus, is low compared to the load. The calculated generation currents from the load flow at the equilibrium point are given as input to the model. It is therefore expected that the state space model outputs voltages equal to the equilibrium point.

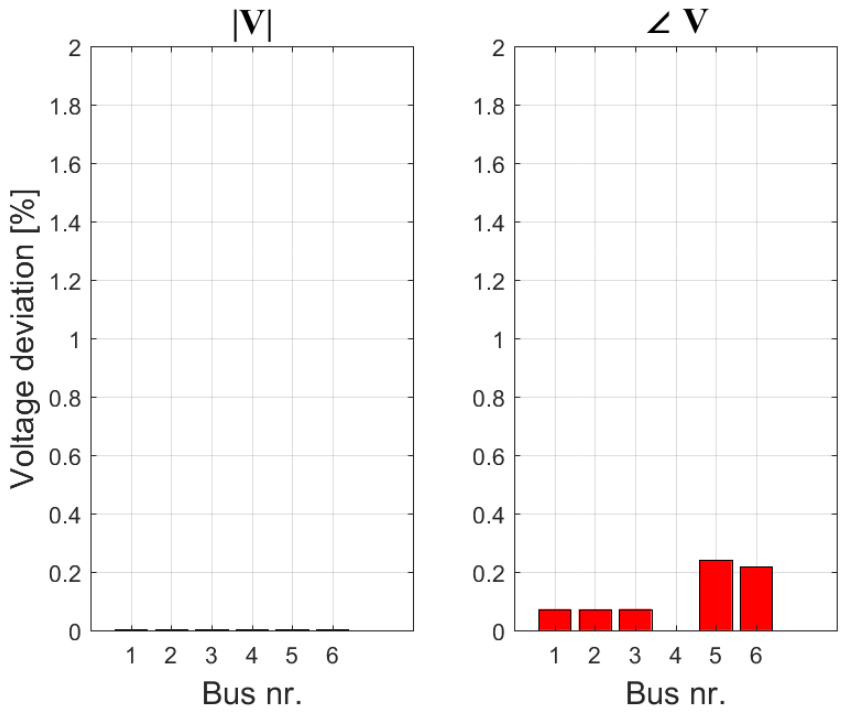

Figure 5.23: Test 1: The percentage deviation between the state space model and the load flow solver voltages.

It can be seen from Figure 5.23 that the voltage angles have a higher deviation from the load flow, which is a tendency seen in the other tests as well. The voltage amplitude deviations are insignificant (10^{-3}) and can therefore not be seen. The highest deviation between the load flow and the state space model in voltage angle is 0.24 % (V_5), which is deemed acceptable. For the angles it can also be observed that the LV buses have a higher deviation. One reason for this could be, that the load is modelled as constant PQ-load, whereas in the state space model, it is a constant Z-load. This might give a small deviation, which can be noticed as in Figure 5.23. Furthermore, the load flow converge based on the criteria set up, this may also have an influence on the higher order decimals.

Results from Test 2 is seen in Figure 5.24. This test illustrates the scenario where the generation from all units, except the slack bus, is high compared to the load.

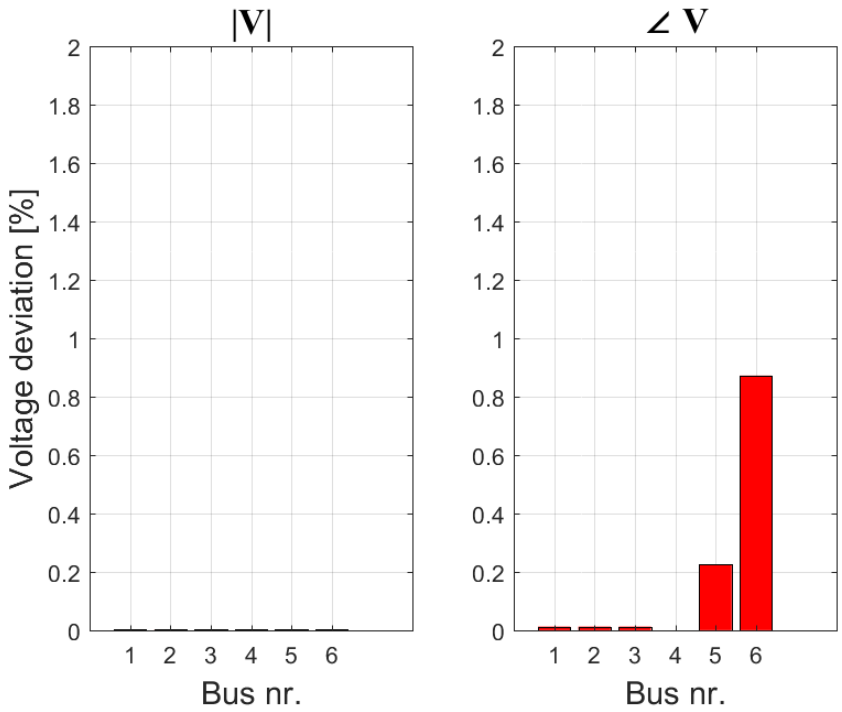

Figure 5.24: Test 2: The deviation between the state space model and the load flow solver voltages.

The same tendency is showcased in this test, as the deviation is low for $|V|$, the $\angle V$ have a higher deviation than $|V|$ and the $\angle V$ at the LV side have a higher deviation in general. The reason for the mismatch was assessed for Test 1, however in this case it is higher, the highest deviation being 0.88 % for bus V_6. The absolute values are given in Table 5.4 for the load bus.

Table 5.4: Test 2: State space and load flow voltage magnitude and angle for bus V_6

Param.	Load Flow	State Space
$\|V_6\|$	1.0596	1.0596
$\angle V_6$	-0.104 deg	-0.141 deg

It is clear, that the deviation is seen on the angle the most. However, the angle for the voltages are so small, that this will have an insignificant impact on the voltages. It is therefore assumed, that the state space model is still representable for the actual grid voltages, and the deviations on the $\angle V$s can be disregarded.

Figure 5.25 and 5.26 show the results for Test 3 and Test 4, respectively. The former

is used to test a scenario, where there is a higher production from on the HV side. The results are similar to Test 1 and will therefore not be discussed further. The latter is representing a scenario, where the production level is higher from the LV side. The test is similar to Test 2, and again a high deviation is seen for bus V_5 and V_6 in the angle. However, as discussed for Test 2, the angles are small and will therefore not impact the voltage magnitude. The communality between Test 2 and 4 indicates, that whenever a high production is present from the diesel genset, a higher deviation is seen for the voltage angles at the last two buses. In other words, whenever the flow of power on the LV side is high, the mismatch between modelling with a constant PQ- or Z-load increases.

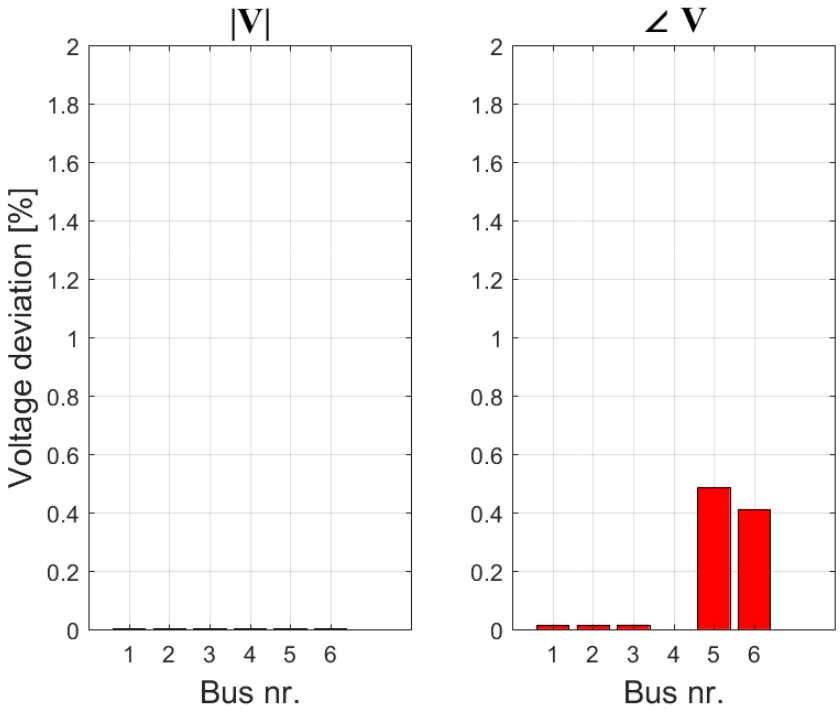

Figure 5.25: Test 3: The deviation between the state space model and the load flow solver voltages.

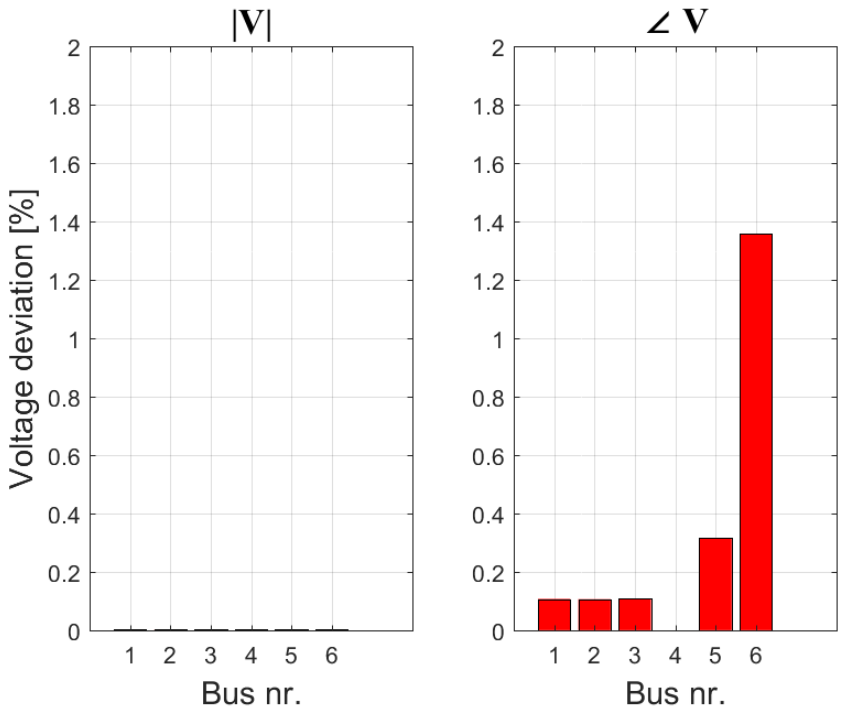

Figure 5.26: Test 4: The deviation between the state space model and the load flow solver voltages.

In general it can be assumed that this state space representation can be used to accurately depict the actual static behaviour of grid and load and will therefore be used in the analysis of the whole system.

5.4 Analysis of Individual Models

The individual models will now be analysed using the theory explained in Appendix C about stability analysis, participation and voltage sensitivity. One of the main reasons to make the system in a modular manner is to analyse and predict how the individual models will behave solely, as this information may be difficult to analyse when looking at the total system.

Firstly, the voltage sensitivity matrix will be found. From this matrix it is possible to see critical buses and influence of P and Q on the voltage. This will help in understanding if care should be taken towards certain critical buses and how the voltage can be controlled with droops. Secondly, a stability analysis will be made

with the focus of analysing the components eigenvalues to see if any of them are positive or are subject to large changes.

5.4.1 Sensitivity analysis

As seen from the theory explained in Appendix C the sensitivity matrix of the system can be found by inverting the Jacobian matrix, which is already available from the load flow script. The sensitivity matrix will tell how much the voltage magnitude and angle will change with a unit step change in P and Q. These values are called residuals. It is of general interest to look at the load bus (Bus 6) as this bus connects both the generating units and the loads. The following tests will be made to see how the values change according to the given equilibrium point.

- Test 1: Nominal production from units with PF=0.97 - High production relative to the load.
- Test 2: 0.1 of nominal production from units with PF=0.97 - Low production relative to the load.

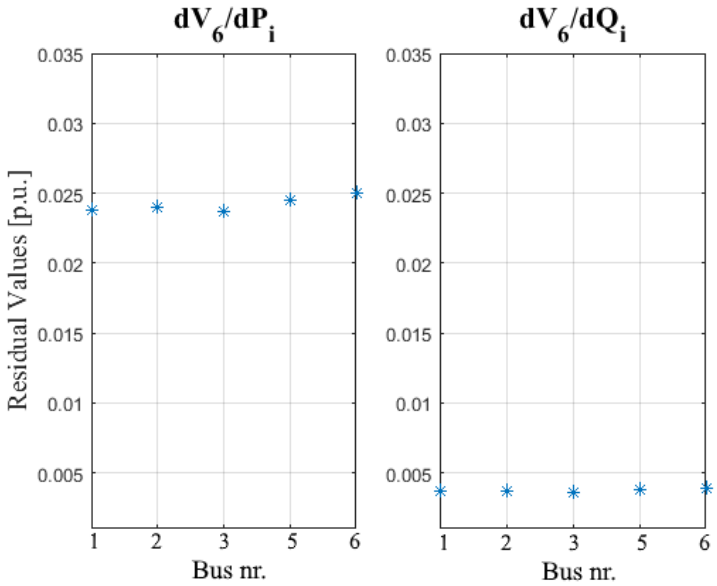

Figure 5.27: Test 1: The residual values for voltage at bus 6 for a step change in P (left) and Q (right).

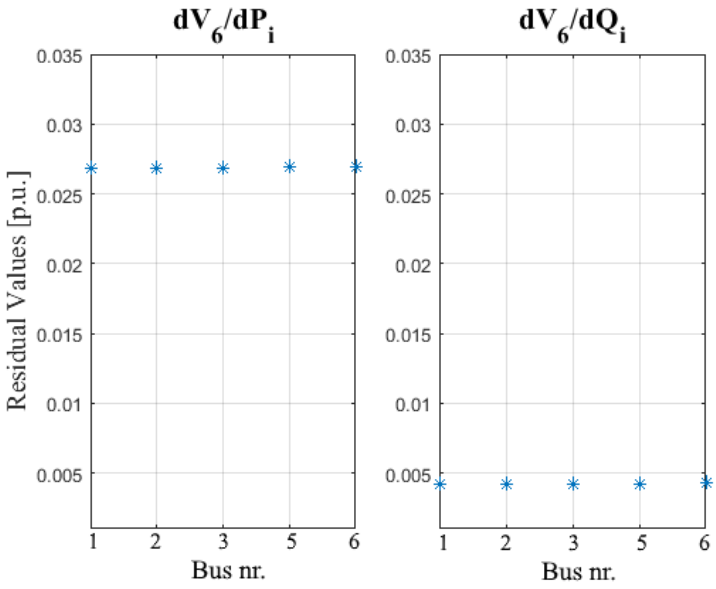

Figure 5.28: Test 2: The residual values for voltage at bus 6 for a step change in P (left) and Q (right).

The influence of a step change in the generating units for P and Q at bus 6 is depicted in Figure 5.27 and Figure 5.28 for Test 1 and 2, respectively. The sensitivity matrix for Test 1 and 2 are given in Appendix C.

Firstly, the two Test scenarios are compared. It is clear that the values do not change much between the tests. It can therefore be assumed that the values will be in this range during most operations in the power system.

Looking at the difference between S_{VP} and S_{VQ}, it is clear that this is a power system with high R/X ratio. This results in the voltage being more susceptible to P flow rather than Q, which has to be considered when tuning droops. This knowledge will also affect the system control methodology as it now may be cumbersome to distinguish the voltage and frequency control.

When comparing the individual buses to each other it is clear, that each unit has almost the same influence on bus 6. This suggests that the WTs and PVs can help stabilize the voltage at this bus as well as the battery and the diesel generator. The highest influence is seen from the load itself, which is expected as this "unit" is closest to bus 6.

Based on this analysis it can be concluded, that in case it is desired to use grid feeding units such as PV and WT to assist voltage control, at the network control

level, it is their P set point that should be regulated and not their Q, as normally seen in MV grids where WT's are used to assist voltage.

5.4.2 Stability Analysis

The stability analysis is performed in order to find critical eigenvalues (eig) for each production unit in the system. The critical eigs denoted λ_{Crit} are defined in 2 different groups:

- Group 1: eigs being positive for a given operational point
- Group 2: eigs with large variation from one operating point to another.

Group 1 eigs are defined to ensure that no unstable operation points appear, in any given possible operation point. A positive eigenvalue represents an unstable system, as explained in Appendix C.

Group 2 eigs are defined to understand how different operational points may influence the eigenvalues. If a large change is seen, it should be identified if this change may lead to unstable operational points.

The analysis is split up in two parts. Part one is where the eigs of Group 1 are found, which is done by calculating the eigs for each unit at their nominal operating point. Part two defines eigs of both Group 1 and 2, by producing eigs at extreme operating point. The extreme operating points are defined in part two.

It should be noted that because the state space models are designed in p.u. time, therefore eigenvalues are also related to this time frame. To get the actual natural frequency [rad/s] of an eigenvalue, it must be multiplied with $\omega_{base} = 2\pi 50$.

In order to relate eigenvalues to specific control loops, the pole due to a controller can be approximated by closing the loop of the given controller, with a gain of 1 as plant. The pole of this transfer function will be close to the eigenvalue of the given controller. Even though the actual plant is not a gain of 1, the position of the closed loop pole, will be primarily effected by the PI controller, hence this will give an indication of the eig value. The eigenvalues related to measurement filters will have a frequency close to the cut-off frequency of the filter.

Part 1

The eigs are calculated at each units nominal operating point along with the Natural Frequency (ω_n), Damping Ratio (ζ) and Time Constant τ, presented in Appendix

C.3. The eigs can now be checked for positive real values, and any positive eig is marked in the Table. An example of such table is seen in Table 5.5 for the DGS.

From this test it is seen that no eigs have positive real parts and therefore none of them are marked in the Tables in C.3. However, the battery has two eigenvalues with real parts equal to 0. As explained in C, such as system can only be checked for stability by Lyaponov's Second method. This is checked, and it is thereby concluded that all the systems are stable at the nominal operating point. Furthermore, the damping ratios and the natural frequencies of each eigenvalue can be seen. A very low value for the damping ratio is not desired, as this will lead to longer oscillatory responses. In this project, a value above $\zeta > 0.4$ is deemed accepted, which all the units follow at their nominal point [Phillips and Parr, 2011]. This value is chosen based on the generally accepted open loop phase margins of $Phasemargin > 40\,\text{deg}$ and the translation $PhaseMargin = 100 \cdot \zeta$ [Phillips and Parr, 2011].

Table 5.5: Eigenvalue (in increasing order), natural frequency, damping ratio and time constant of the diesel genset system matrix at equilibrium point with nominal power and PF=0.9

λ_{no}	λ	$f_n[p.u.]$	$f_n[Hz]$	ζ	τ	Origin
λ_1	-15.92+0.000i	2.533	795.45	1	$0.2000e^{-3}$	T_A (GOV)
λ_2	-5.258+0.000i	0.8369	262.9	1	$0.6054e^{-3}$	AVR
λ_3	-0.6583+0.8905i	0.1763	55.37	0.5945	$4.835e^{-3}$	SG
λ_4	-0.6583-0.8905i	0.1763	55.37	0.5945	$4.835e^{-3}$	SG
λ_5	-0.8359+0.000i	0.1330	41.80	1	$3.808e^{-3}$	K_I (GOV)
λ_6	-0.2833+0.1056i	$48.12e^{-3}$	15.12	0.9371	$11.23e^{-3}$	SG
λ_7	-0.2833-0.1056i	$48.12e^{-3}$	15.12	0.9371	$11.23e^{-3}$	SG
λ_8	-0.07794+0.1279i	$23.83e^{-3}$	7.490	0.5205	$40.84e^{-3}$	GOV
λ_9	-0.07794-0.1279i	$23.83e^{-3}$	7.490	0.5205	$40.84e^{-3}$	GOV
λ_{10}	-0.05962+0.000i	$9.488e^{-3}$	2.981	1	$53.39e^{-3}$	SG
λ_{11}	-0.01358+0.000i	$2.160e^{-3}$	0.6786	1	$234.5e^{-3}$	SG
λ_{12}	$-0.1927e^{-3}$+0.000i	$30.67e^{-6}$	$9.635e^{-3}$	1	16.52	AVR

Part 2

Mainly three parameters may vary under operation for the units, namely the active power P, the power factor PF and the voltage magnitude $|V|$. Each parameter is varied between a high and low operational point, according to Table 5.6. This range can be changed according to the given rules of the microgrid.

Table 5.6: Extreme operation points

	High / 1	Low / 0
P	1 p.u.	0.1 p.u.
PF	1	0.707
$\|V\|$	1.15 p.u.	0.85 p.u.

The high and low values can be chosen to be specific for each unit, depending on the ranges of power, power factor and voltage. However, for simplicity, the extreme cases are tested here. The high and low value of the voltage magnitude is set at a value, where the unit should be able to operate under normal conditions. The network level controller should be able to ensure that the units are within this range.

All high/low combinations can be achieved by making a table of the possible combinations as in Table 5.7. This defines the 8 possible scenarios.

Table 5.7: Combined extreme scenarios

Cases –>	C1	C2	C3	C4	C5	C6	C7	C8
P	1	1	1	1	0	0	0	0
PF	1	1	0	0	1	1	0	0
$\|V\|$	1	0	1	0	1	0	1	0

Now that the 8 cases have been defined, the next step is to calculate the eigs to start the analysis. The tables thereby easily reveal if the eigs are at a stable point. This information will reveal if it is necessary to retune some gains or if some operating conditions should be avoided. The 8 cases are not shown here, but were seen to result in negative real part eigenvalues. From this it is concluded, that the units are stable in their operating ranges.

Now the differences between the 8 cases are investigated. This is done by a comparison of two cases, where only one parameter changes.The natural frequencies of the eigevalues (EF) are compared in the two cases. This is done to see how the frequencies change when a parameter (V, PF or PQ) is changed from high to low or from low to high. The comparisons made, are listed below.

- C1 and C2 - $|V|$ is changed.
- C1 and C3 - PF is changed.
- C1 and C5 - P is changed.
- C7 and C8 - $|V|$ is changed.

- C6 and C8 - PF is changed.
- C4 and C8 - P is changed.
- C5 and C6 - $|V|$ is changed.
- C5 and C7 - PF is changed.
- C2 and C6 - P is changed.
- C3 and C4 - $|V|$ is changed.
- C2 and C4 - PF is changed.
- C3 and C7 - P is changed.

In total 16 tables are made, each table presenting the four units and their EF changes between the two cases. A collection of the most interesting three tables can be found in Appendix C.3. The last 13 tables are not presented as the same change (or less) is observed compared to the ones depicted in C.3.

Marking the critical values

As concluded before, none of the eigs become unstable in the extreme operating points, thereby no eigs are defined in Group 1.

Table 5.8 depicts the general tendencies seen from the analysis of comparing two cases, where only one parameter is changed. All Group 2 eigenvalues are marked with red.

Table 5.8: The percentage change of the eigs (in the same order as above) when subject to V, PF and P changes. The colour red indicates the critical changes (Group 2)

eig no.	C1-C2: V Sweep (%-change)				C1-C5 P Sweep (%-change)			
	Battery	Genset	WT	PV	Battery	Genset	WT	PV
λ_1	0	0	0	0	0	0	0	0
λ_2	0	0	0	0	0	0	0	0
λ_3	0	0,49	0	0	0	0,14	0	0
λ_4	0	0,49	-0,31	-0,31	0	0,14	0	0
λ_5	0	1,93	36,47	36,47	0	-0,02	0	0
λ_6	0	0,01	0	0	0	-1,08	0	0
λ_7	0	1,15	15,8	15,77	0	-1,08	0	0
λ_8	0	1,15	15,8	15,77	0	6,73	0	0
λ_9	0	1,93	-4,2	-4,17	0	6,73	0	0
λ_{10}	0	-22,55	0	0	0	-55,25	0	0
λ_{11}	0	12,31	0	0	0	27,36	0	0
λ_{12}	0	0	0	0	0	0	0	0
λ_{13}	-	-	-0,01	-0,01	-	-	0	0

From this analysis it is generally seen, that the eigenvalues do not change due to the change of PF, hence it is not shown in Table 5.8. In case of P change it is seen, that the EFs change for the diesel generator only. This is expected as the dynamics of the genset changes with its operational point, where operation at the nominal point will yield the highest efficiency. Finally, all units except the battery is seen to be affected by a voltage change. The voltage will inevitably effect the eigenvalues of the units in the system as some control loops are dependent on the measured voltage. This should also be seen in the battery, however the voltage control loops of the battery is open loop whenever the battery is not connected to an external grid. Hence, no change is seen when analysing the battery model solely.

The frequency of λ_5, λ_7 and λ_8 for the WT and PV are seen to change by up to 26.32%, as the voltage is changed, hence they are categorized as Group 2. Furthermore, λ_10 and λ_11 for the diesel genset are changed by up to 22.55% when the voltage is changed, and up to 55.25% when the power is changed. These eigenvalues are therefore also in Group 2.

Analysis of the critical values

The eigs λ_5, λ_7 and λ_8 for the WT and PV are found to change when the voltage is changed. Therefore, a sweep is made in Figure 5.29, which shows that the eigs are stable in the entire range, and the eigenvalues are moving away from the imaginary axis, which indicates stable operation. λ_7 and λ_8 are seen to increase their imaginary values, this may result in lower damping ratios, however the change is not large enough to be concerned. The reason for the change of λ_5 is located to be dependent on state δ which is related to the park transformation, where δ is the angle between the reference voltage at the BESS and the voltage at the WT or PV. The eig pair λ_7 and λ_8 are found to be related to the output filter of the units, which is dependent on the point of linearisation, where again the voltage magnitude is included.

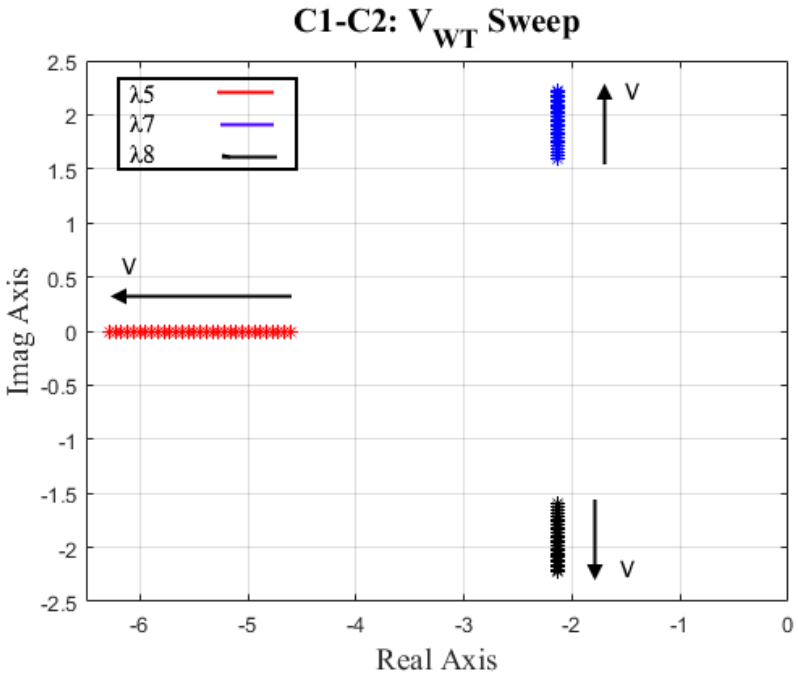

Figure 5.29: Pole-zero mapping of the critical eigs of WT for changes in voltage

For the diesel genset, λ_{10} and λ_{11} changes due to voltage and power changes. The sweeps for voltage and power are shown in Figures 5.30 and 5.30, respectively. It is seen, that the unit will be stable for all operation points between the two extremes. However, it is found that the two eigs are related to the diesel engine which takes care of the power set point as well as the frequency, hence the eigs are affected when the power is changed between the two extremes. The voltage affects the current output of the machine and therefore also the torque/power produced by the synchronous

generator, which is fed to the diesel engine. The change of the eigs are therefore in good agreement with the behaviour of the genset.

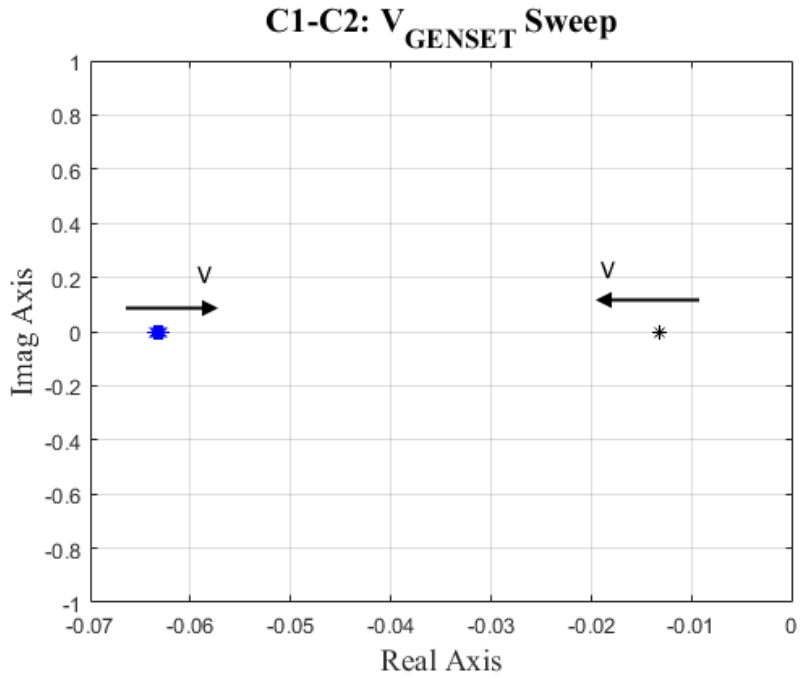

Figure 5.30: Pole-zero mapping of the critical eigs of genset for changes in voltage.

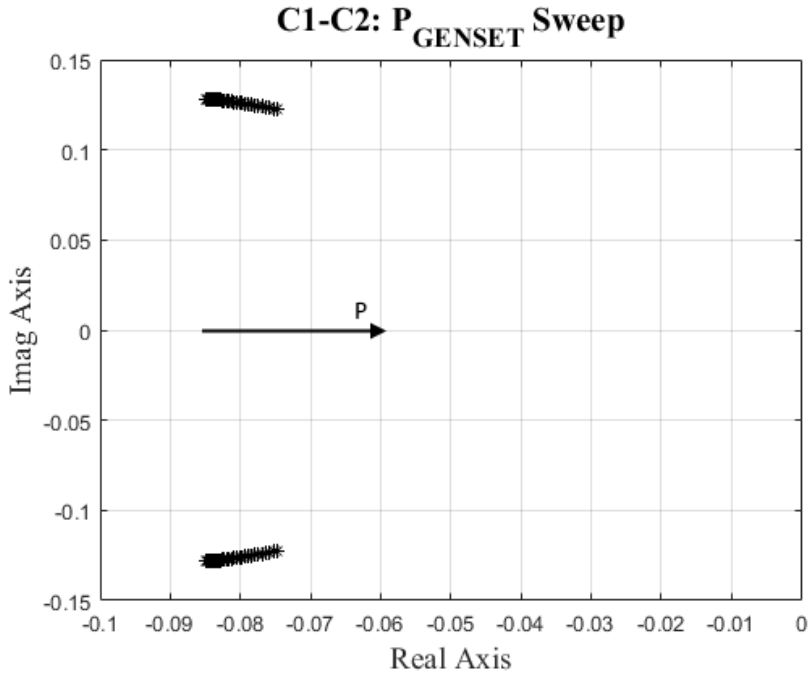

Figure 5.31: Pole-zero mapping of the critical eigs of genset for changes in P.

No instability problems, related to eigs of Group 1, are found during this analysis, however if a case with a positive eig had occurred, a sweep towards the unstable point could have been performed to find the point at which the unit becomes unstable. Thereby, the parameters influencing the state could be found and adjusted in order to ensure stable operation in all scenarios.

5.5 Model Adequacy

The models have been derived to be able to perform a stability analysis. However, other capabilities and limitations of the models will be discussed here.

Capabilities

- The WT, PV and BESS models can be used for tuning controllers, to accommodate different scenarios, or grid codes, since current and voltage control loops have been implemented for these units.
- The rotor side of the DGS has been modelled, and any studies where the behaviour of the dq-rotor currents/voltages due to grid disturbances in power or voltage can be performed using this model.

- The DC-voltage link control has been modelled for the PV and WT, and studies regarding impacts from the grid on the DC-link can be performed using these models.
- The fully combined model bandwidth will be limited by the reference frame transformation, which will not be correct to changes faster than the settling of the PLL. Therefore the model bandwidth is 425 Hz.

Limitations

- The models are derived in dq-frame assuming the phases to be in balance. Any unbalance between phases can not be assessed using the models.
- Investigations regarding higher frequency components, such as harmonic studies can not be performed, considering the model bandwidth and the fact that switching of the converters are not modelled and no grid capacitances have been included.
- Large disturbance studies such as fault analysis can not be performed using the models, since each model is a small-signal model, which is only accurate for small disturbances.
- The WT model does not include the dynamics of the pitch control and shaft, and any study investigating this behaviour can not be performed.
- The PV is derived excluding the DC-converter MPPT algorithms, and thereby the behaviour of this can not be examined.
- The BESS model is derived without modelling any SoC control, cells or battery management system. Studies regarding the cell-level behaviour of a battery can thereby not be performed.
- The models are applicable to asses both voltage and frequency stability in microgrids.

The models were derived and linearised to yield specific state space models. Each model has been verified, to ensure that the models work as intended. Thereby the stability and sensitivity analysis could be made. This analysis showed that each model of the production units were stable, in their entire working range. Voltage and P/Q were seen to alter some eigenvalues, however not to cause instability. The sensitivity analysis of the grid showed that the grid voltages were sensitive to changes in active power more than reactive power, as for a LV grid. Furthermore, all units were seen to have approximately the same residue values, hence they have almost the same influence on the load bus. Having this stated, the total model can be assembled, to check if instabilities occurs when the models work as a whole.

Complete System - Stability & Sensitivity Analysis

6

Now that it has been concluded that each production unit is stable in the entire operating range, the next step is to analyse the entire microgrid. This is done to be able to design and tune the network level controller and to check for unstable operation points. To do this, the different models namely PV, WT, BESS, Diesel Generator Set (DGS) and grid model must be collected for which is done in Section 6.1. Two different models are assembled, one with the DGS as the grid-forming unit, and one without the DGS, where the BESS is the grid-forming unit. The analysis of the microgrid stability is performed in Section 6.2, where the two systems are checked for unstable operation points, and the critical eigs are located and analysed. This will show which influence different device level control parameters have on the total system, and these can be retuned if necessary.

6.1 Microgrid Model Assembling

The two complete systems are now found by considering the inputs and outputs of the distinct state space models. From Figure 5.1 it is noted, that the production units output the generated currents , which is to be used as one vector in the grid model. Hence, the generating units should be combined into one model. This will result in an A-matrix including all states from the 4 production unit models. The following A-matrix is defined for the case where the DGS is turned on:

$$A_{GEN} = \begin{bmatrix} A_{PV} & 0 & 0 & 0 \\ 0 & A_{WT} & 0 & 0 \\ 0 & 0 & A_{BESS} & 0 \\ 0 & 0 & 0 & A_{DGS} \end{bmatrix} \tag{6.1}$$

The PV is connected at bus 1, the WT at bus 3, BESS at bus 4, and the DGS at bus 5 as shown in Figure 4.1. Thereby, the B-matrix takes the form shown in Equation 6.4, where the B matrices from each unit only contains the columns related to inputs V_d and V_q, and B_ω contains the column related to frequency from the individual models.

$$B_{GEN} = \begin{bmatrix} B_{PV}^{13x2} & 0^{2x2} & . & . & . & 0^{2x2} & B_{\omega,PV}^{13x2} \\ . & . & B_{WT}^{13x2} & 0 & . & . & B_{\omega,WT}^{13x2} \\ . & . & 0 & B_{BESS}^{12x2} & 0 & . & B_{\omega,BESS}^{12x2} \\ 0^{2x2} & . & . & 0 & B_{DGS}^{12x2} & 0^{2x2} & 0^{2x2} \end{bmatrix} \tag{6.2}$$

For the microgrid model where the BESS is the grid-forming unit, meaning that in stead of following the DGSs frequency, it follows a reference frequency of 1 $p.u.$ the matrices A and B are defined as follows:

$$A_{GEN} = \begin{bmatrix} A_{PV} & 0 & 0 \\ 0 & A_{WT} & 0 \\ 0 & 0 & A_{BESS} \end{bmatrix} \tag{6.3}$$

$$B_{GEN} = \begin{bmatrix} B_{PV}^{13x2} & 0^{1x2} & . & . & 0^{1x4} & B_{\omega,PV}^{13x1} \\ . & . & B_{WT}^{13x2} & . & . & B_{\omega,WT}^{13x1} \\ 0^{1x2} & . & 0^{1x2} & B_{BESS}^{12x2} & 0^{1x4} & B_{\omega,BESS}^{12x1} \end{bmatrix} \tag{6.4}$$

Now the complete model for the two microgrid models can be derived along with the state matrix, which is to be analysed for stability purposes. This is done by defining the system states x_{sys}, the input u_{sys} and the output y_{sys} as:

$$\Delta\dot{x}_{sys} = \begin{bmatrix} \Delta\dot{x}_{genDQ} \\ \Delta\dot{x}_{lineDQ} \\ \Delta\dot{x}_{loadDQ} \end{bmatrix}, \Delta u_{sys} = \begin{bmatrix} \Delta v_{busDQ} \\ \Delta\omega \end{bmatrix}, \Delta y = \Delta v_{busDQ}$$

The input to the system is:

$$\Delta u_{sys} = \begin{bmatrix} \Delta v_{D1} & \Delta v_{Q1} & \Delta v_{D2} & \Delta v_{Q2} & . & . & . & \Delta v_{D6} & \Delta v_{Q6} & \Delta \omega \end{bmatrix} \tag{6.5}$$

Hence the state space representation can be given by:

$$\Delta \dot{x}_{sys} = \begin{bmatrix} A_{GEN} & 0 & 0 \\ 0 & A_{GRID} & 0 \\ 0 & 0 & A_{LOAD} \end{bmatrix} \Delta x_{sys} + \begin{bmatrix} B_{GEN} \\ B_{GRID} \\ B_{LOAD} \end{bmatrix} \Delta u_{sys} \tag{6.6}$$

where GEN is the generation unit matrices from Equation 6.3, $LOAD$ is the load model matrices and $GRID$ is the grid model matrices. It is known that voltages are calculated by the mapping matrices, which can be inserted in the above equation, such that:

$$\Delta \dot{x}_{sys} = \begin{bmatrix} A_{GEN} & 0 & 0 \\ 0 & A_{GRID} & 0 \\ 0 & 0 & A_{LOAD} \end{bmatrix} \Delta x_{sys} + \begin{bmatrix} B_{GEN} \\ B_{GRID} \\ B_{LOAD} \end{bmatrix} \begin{bmatrix} R_n \cdot M_{GEN} C_{GEN} & R_n \cdot M_{GRID} & R_n \cdot M_{LOAD} \\ & M_\omega & \end{bmatrix} \Delta x_{sys} \tag{6.7}$$

Where M_ω maps the common frequency $\Delta\omega$ from the states. With DGS M_ω is given as:

$$M_\omega = \begin{bmatrix} 0^{1x43} & 1 & 0^{1x18} \end{bmatrix} \tag{6.8}$$

Without DGS M_ω is given as:

$$M_\omega = \begin{bmatrix} 0^{1x26} & c_{1,1} & 0^{1x23} \end{bmatrix} \tag{6.9}$$

Where $c_{1,1}$ is found in the BESS C matrix given in Appendix B.

Rearranging this matrix gives the resulting state matrix of the entire system.

$$A_{mg} = \left[\begin{bmatrix} A_{GEN} & 0 & 0 \\ 0 & A_{GRID} & 0 \\ 0 & 0 & A_{LOAD} \end{bmatrix} + \begin{bmatrix} B_{GEN} \\ B_{GRID} \\ B_{LOAD} \end{bmatrix} \begin{bmatrix} R_n \cdot M_{GEN} C_{GEN} & R_n \cdot M_{GRID} & R_n \cdot M_{LOAD} \\ & M_\omega & \end{bmatrix} \right] \tag{6.10}$$

For the case with DGS, the B matrix of the full system is defined in Equation (6.11) where B_{ref} contains the columns of individual models B matrix related to control

reference inputs.

$$B_{mg} = \begin{bmatrix} B_{ref,PV}^{12x2} & 0 & 0 & 0 \\ 0 & B_{ref,WT}^{12x2} & 0 & 0 \\ 0 & 0 & B_{ref,BESS}^{12x4} & 0 \\ 0 & 0 & 0 & B_{ref,DGS}^{12x4} \\ 0^{12x2} & 0^{12x2} & 0^{12x4} & 0^{12x4} \end{bmatrix} \tag{6.11}$$

For the case without DGS, the B matrix of the full system is defined in Equation (6.12), where $D_{\omega,BESS}$ is given in Equation (6.13) and $d_{1,1}$ and $d_{1,2}$ is given in Appendix B.

$$B_{mg} = \left[\begin{bmatrix} B_{ref,PV}^{12x2} & 0 & 0 \\ 0 & B_{ref,WT}^{12x2} & 0 \\ 0 & 0 & B_{ref,BESS}^{12x4} \\ 0^{12x2} & 0^{12x2} & 0^{12x4} \end{bmatrix} + \begin{bmatrix} B_{GEN} \\ B_{GRID} \\ B_{LOAD} \end{bmatrix} \begin{bmatrix} 0^{12x8} \\ D_{\omega,BESS}^{1x8} \end{bmatrix} \right] \tag{6.12}$$

$$D_{\omega,BESS} = \begin{bmatrix} 0 & 0 & 0 & 0 & d_{1,1} & d_{1,2} & 0 & 0 \end{bmatrix} \tag{6.13}$$

For both with and without the DGS the C matrix of the full system is given as:

$$C_{mg} = \begin{bmatrix} R_n \cdot M_{GEN} C_{GEN} & R_n \cdot M_{GRID} & R_n \cdot M_{LOAD} \\ & M_\omega & \end{bmatrix} \tag{6.14}$$

The case without the DGS also has a D matrix given as:

$$D_{mg} = \begin{bmatrix} 0^{12x8} \\ D_{\omega,BESS}^{1x8} \end{bmatrix} \tag{6.15}$$

From this derivation, it is now possible to analyse the entire system in terms of stability and sensitivity.

6.2 Stability and Sensitivity Analysis

Defining operating points

As mentioned in the introduction of this chapter, an analysis of the microgrid eigs is performed. This is done by producing the eigs of the two state matrices assembled in the previous section, both at two extreme operating points. The extreme operating points are defined below:

- C1.1: DGS on, High load, low production. BESS supplying power
- C1.2: DGS on, Low load , high production. BESS absorbing power
- C2.1: DGS off, High load, low production. BESS supplying with power
- C2.2: DGS off, Low load , high production. BESS absorbing power

C1.1 is an operating point where the peak demand $P_{load} = 88kW$ and the production is low relative to the load. This operating point forces the BESS to support the load with power, close to its maximum. C1.2 is an operating point with excess power production, forcing the BESS to store power from the production units. These operating points are defined to asses the stability of the microgrid, when the BESS is charging and discharging close to its maximum of 80 kW in order to balance the power; hence showcasing scenarios with high and low load/production. C2.1 and C2.3 are a repetition of C1.1 and C1.2 with the difference of having the DGS turned off. This will indicate the stability when the system is fully inverter-based.

The two operating points are defined in Table 6.1, for both microgrid models. The operating points have been made for a fixed power factor of $PF = 0.97$ for the production units and $PF = 0.95$ for the load. The initial conditions are again given by the Newton-Rhapson load flow used in Subsection 5.3.4.

Table 6.1: Four Microgrid operation scenarios

Unit	PV	WT	BESS		DGS	Load
	P $[kW]$	P $[kW]$	P $[kW]$	Q $[kVAr]$	P $[kW]$	P $[kW]$
C1.1	5	10	69	24	5	88
C1.2	30	50	-73	-15	5	10
C2.1	5	10	75	26	0	88
C2.2	30	55	-75	-14	0	10

Critical eigenvalues of the A-matrix

The first part of this analysis focuses on revealing whether the A-matrix of the microgrid model has negative eigenvalues (referred to as eig or eigs). The eigs for C1.1, C1,2 are plotted in Figure 6.1, and C2.1 and C2,2 are plotted in Figure 6.2 where it should be noted that the x-axis is logarithmic.

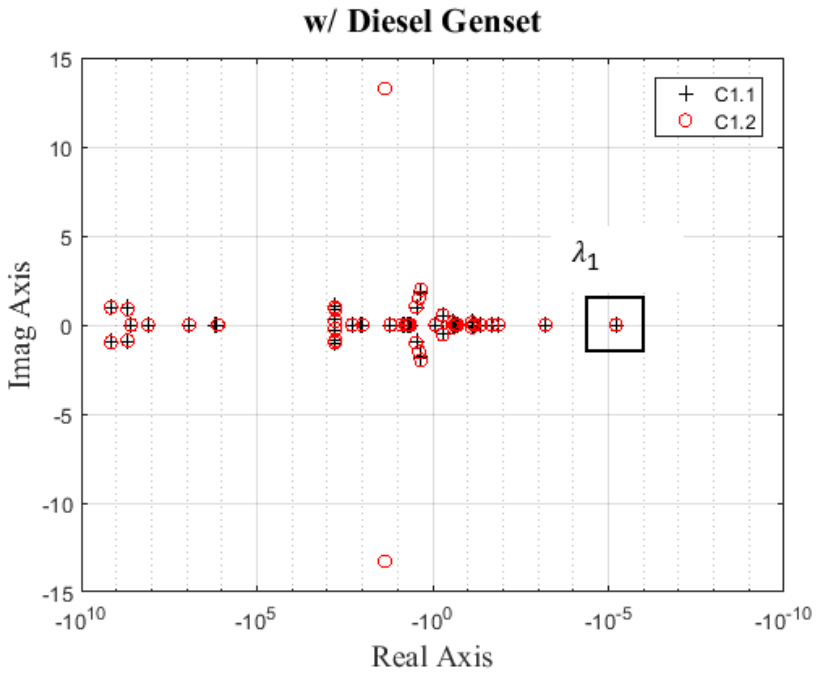

Figure 6.1: Logarithmic eigenvalue plot for C1.1 and C1.2

Figure 6.1, which is the case with DGS, it is seen that all all eigs are negative and hence C1.1 and C1.2 are stable operational points. The changes between the two operational points are in general seen to be negligible. Two interesting eigs, defined as λ_1, are marked in the figure, laying almost on top of each other. These are the ones closest to the imaginary axis, and hence may have the highest influence on the system according to the theory explained in Appendix C. For this reason, these will be analysed in the next step as this will give valuable insight about the dominant factors in the system. It should be noted, that two complementary eigs are found with an imaginary value of ± 13. This pair only appears in case of C1.2, low load and high production. However, when analysing the damping ratio of this eigenvalue it is seen to be $\zeta = 0.8$, and therefore accepted. In fact, the lowest damping ratio for both C1.1 and C1.2 is seen to be 0.5, which is accepted in this study.

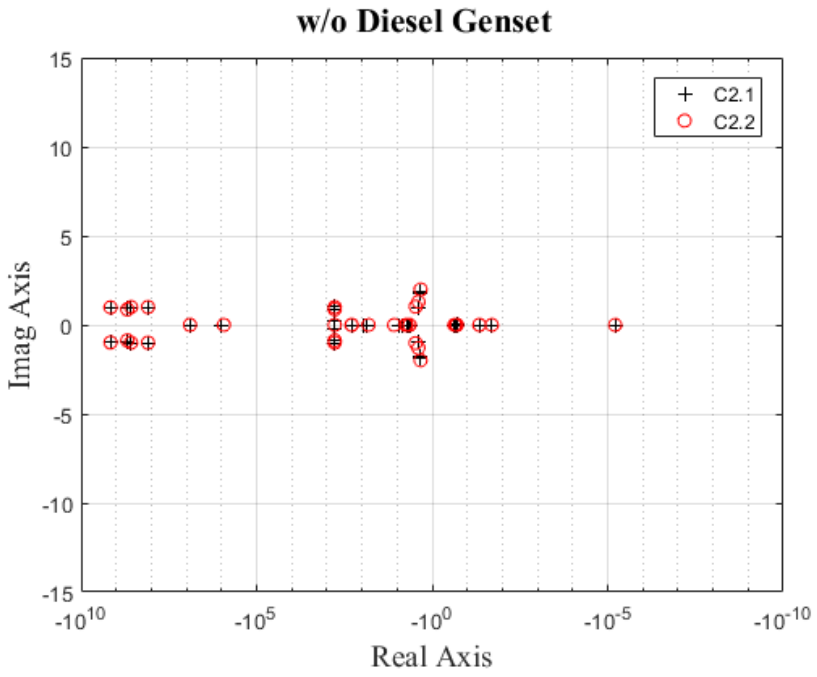

Figure 6.2: Logarithmic eig plot for C2.1 and C2.2

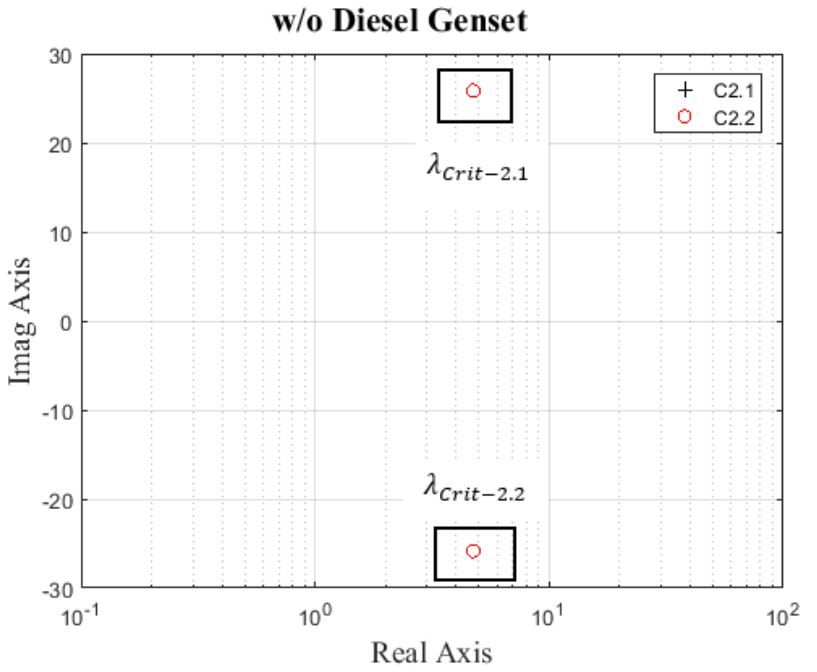

Figure 6.3: Zoom of C2.2 positive eig.

For the second set of cases in Figure 6.2, it is found that for C2.1 the system is stable, but for C2.2 one complex eig pair is moved to the right half plane and the system is at an unstable point, as seen in Figure 6.3. The set of unstable eigs are noted as critical eigs $\lambda_{Crit-2.1}$, $\lambda_{Crit-2.2}$. These critical eigs are seen to have almost the same absolute imaginary value as the ones appearing in C1.2. This suggests that whenever the BESS is charging a relatively large amount of power, when production is high and load is low, it may be a critical scenario. Furthermore, whenever the DGS is turned off, the system is more susceptible to changes and becoming unstable. Apart from this, the differences between case C2.1 and C2.2 are seen to be negligible. λ_1 is also seen in these two cases.

Allocating states to the Critical eigenvalues

The next step is now to allocate the critical eigs with states and parameters that affect them.

For λ_1 and the set $\lambda_{Crit-2.1}$,$\lambda_{Crit-2.2}$ the participation matrix described in Appendix C is produced to find the states that influence these eigs the most. In Table 6.2 the results from the participation analysis are shown.

Table 6.2: Participation factors for the critical eigs and their influencing states

	$\lambda_{43} = \lambda_1$	$\lambda_{24} = \lambda_{Crit-2.1}$	$\lambda_{25} = \lambda_{Crit-2.2}$
Value	-6.13e^{-6}	4.74+25.85i	4.74-25.85i
$p_{ki,max}$	0.348$\angle$0 deg	0.280$\angle$96 deg	0.00261$\angle$63 deg
Influencing State	ϕ_{pll} from WT and PV	V_{oq} from PV	ϕ_{pll} from WT

It is found that for λ_1, the most influential state is the PLL state of the WT and PV. It is expected that the PLL may have a high influence on the total system as this control loop is one of the slowest in the system. As suggested by the previous analysis of C1.1-C2.2, this eigenvalue did not change, hence instability due to this value is not expected. However, clearly the PLL has a high influence on the system, and is also likely to affect other control loops. Regarding the PLL the most important parameter is how fast it reaches a new value, hence its settling time. Therefore, the settling time of the PLL is varied in order to see how this affects the system stability. It is expected, that a too fast PLL will make the system unstable, since reactions to fast changes will affect the voltage and current control loops.

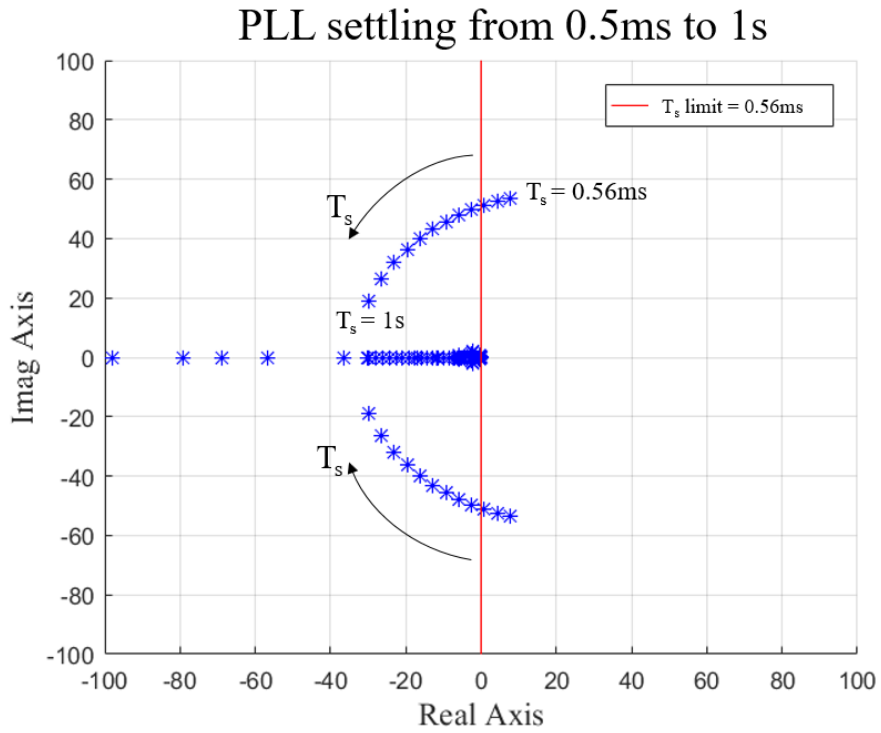

Figure 6.4: Variation of PLL settling time, impact on system stability.

As seen in Figure 6.4 clearly, the system does become unstable. The two marked eigs moves toward the right half plane when the settling time is reduced. Even with a very slow PLL $T_s = 1$s, the system is still stable, and as expected with a too fast settling time, the system becomes unstable. Therefore, care should be taken when designing the PLL. As explained in Section 5.2, the PLL settling time is 2.35ms when following the design procedure given in [Sezi, 2010].

Now analysing $\lambda_{Crit-2.1}$ and $\lambda_{Crit-2.2}$, the most influential states are seen to be V_{oq} and ϕ_{pll} from the WT and PV. However, the value of the $p_{ki,max}$ for $\lambda_{Crit-2.1}$ is very small, indicating that several states have a very small influence on this value. Due to the small value, the sensitivity with regards to the PLL is negligible. A higher influence is however seen from the measured output filter value of V_{oq}. However, this value is again small and it can therefore not be solely due to this measurement filter. Analysing the operational point itself, it is seen that whenever the BESS is absorbing power at a relatively large scale, a positive eigenvalue appears.

In order to check this hypothesis, different operational points with both high/low production and load demand is investigated. The common tendency noted here is

that the positive eigenvalue appears even with high loads and production, as long as the BESS is absorbing a relatively large amount of power, this amount being decreased with increasing load and production. Therefore, indications of instability are seen due to the BESS. This is something that was not seen in the previous chapter, Section 5.4.2, where the BESS was investigated solely. An explanation for this could be, that the BESS still had open loop voltage controllers, as it was not connected to the grid. Hence the influence of these gains were not showcased, as described in Section 5.4.2.

For these reasons the BESS voltage controller gains are assessed, with the intention of observing its influence on this positive eigenvalue. This reveals that the K_{pv} gain actually has an influence on the positive eigenvalue which can be seen in Figure 6.5. The gain K_{pv} is varied from 0.8 to 2.5, the original value found as described in Section 5.2 is 1.2178.

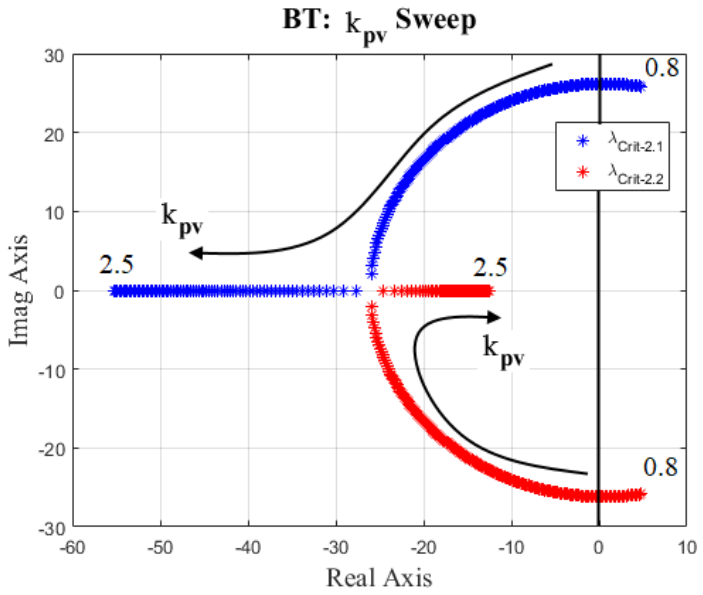

Figure 6.5: The variation of $\lambda_{Crit-2.1}$ and $\lambda_{Crit-2.2}$ for a sweep in BESS voltage controller gain K_{pv}, varied from varied from 0.8 to 2.5.

It is interesting to note that these poles go from being complex conjugates to only having a real part, which will as a result reduce oscillations from these eigs. It is found that the change of K_{pv} affect the overshoot of the voltage controller, while the settling time remains unchanged. The limit for stable operation is found to be $K_{pv} = 1.54$ corresponding to an overshoot of 7.5%. The new K_{pv} is selected to be twice the original value equal to 2.43, which results in an over-damped response.

The response of the BESS voltage control is dependent on the system operating point (eq. load size and power delivered from BESS), and the new K_{pv} ensures high enough damping that the response will be over-damped in any set point.

The comparison between the eigs with the new and old controller gain value is shown in Figure 6.6. The plot with the old K_p value does not show the unstable poles $\lambda_{Crit-2.1}$ and $\lambda_{Crit-2.2}$, because a logarithmic x-axis is used in order to properly show all other eigs. No significant changes are seen besides a new complex conjugate pair. However, this pair is seen to have $\zeta = 0.81$ which is not a problem. This same tendency is seen for the new eig plot of the grid with DGS turned on, seen in Figure C.1 in Appendix C.3.

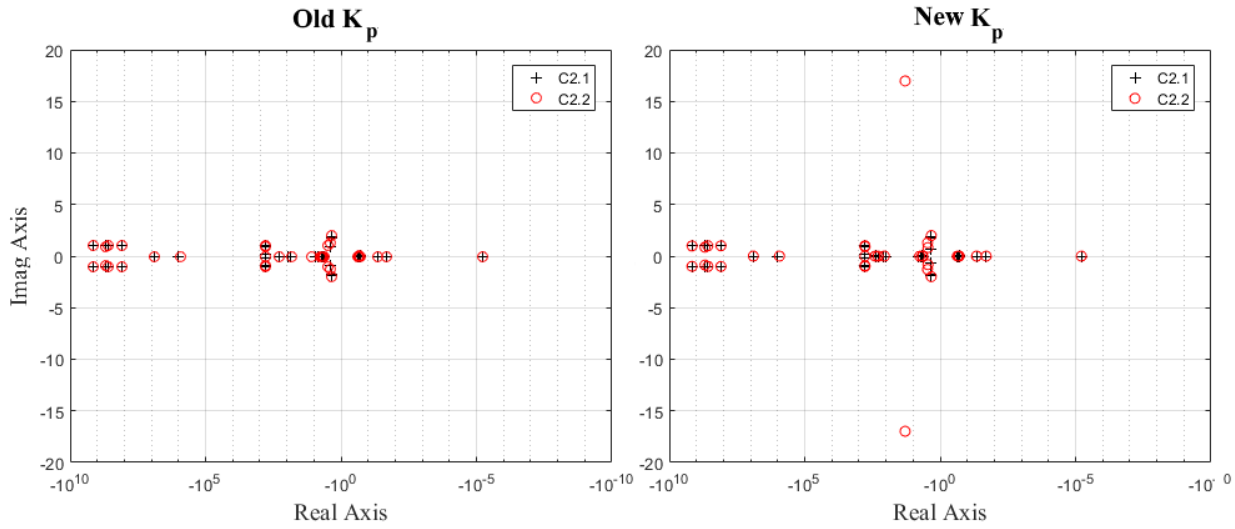

Figure 6.6: Eigenvalue plot for the new and old K_{pv} value

In order to exemplify the instability due to the positive eigenvalue, the state space model is used to show the time response of the model when subject to a small change in the system. This is seen in Figure 6.7, where a step of $0.1p.u.$ and $0.01p.u.$ is given at the operational point C2.2 where the positive eigenvalue appeared. A step in the power from the PV is made. The voltage at common connection point is investigated.

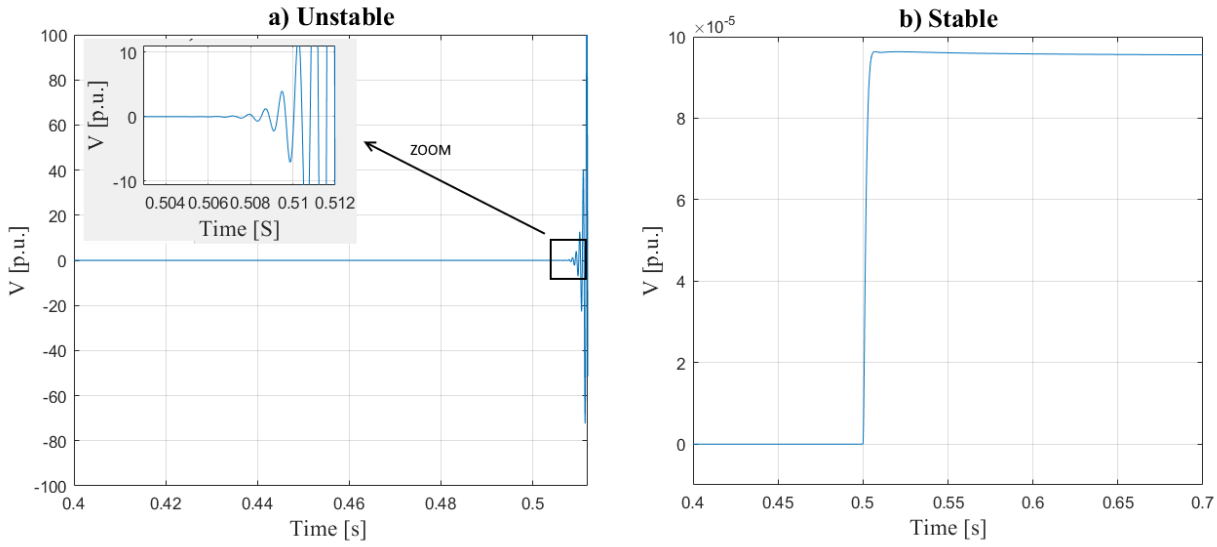

Figure 6.7: State space model response in Case C2.2 with an unstable eigenvalue in the system, a) for a power step of 0.1 , b) for a power step of 0.01.

The figure shows, that a step of $0.01p.u.$ does not result in instability. However, a step of $0.1p.u.$ clearly indicates an unstable system. It could be that 0.1 is too large a step due to the linearisation of the model, where higher order terms where neglected. Hence, the state space response is shown again with the new gain value, seen in Figure 6.8 for a step of $0.1p.u.$. Furthermore, this is compared with the dynamic model of the system to see, if the state space model is valid for a step this size. The dynamic model is explained in Appendix E.

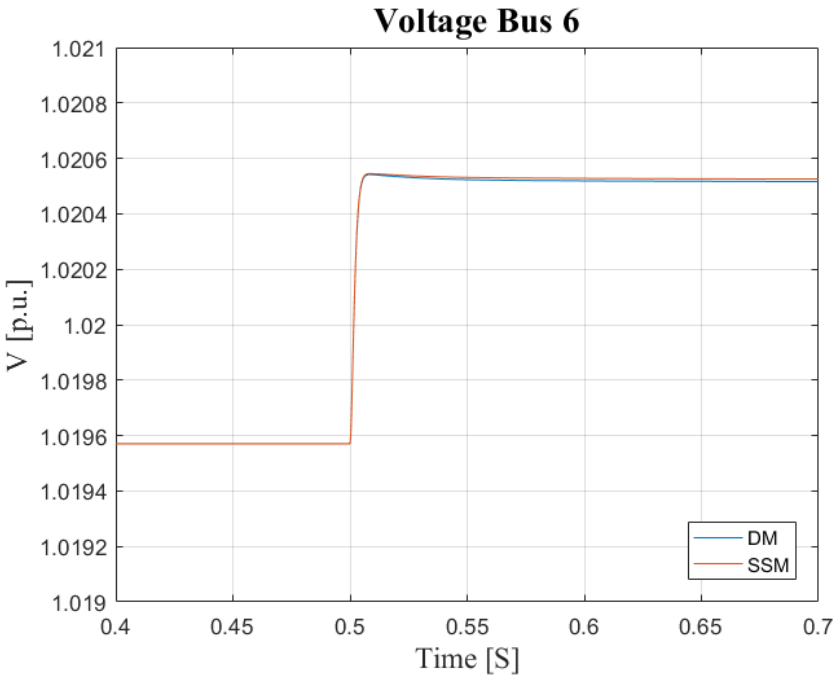

Figure 6.8: Dynamic model response in Case C2.2 with an unstable eigenvalue in the system

Clearly, both systems are stable and give the same response for a change in the system. Tuning the K_{pv} gain in the voltage control of the BESS to be 2 times higher, yielded only left half plane eigs as seen in Figure 6.6, hence this value is used in the subsequent parts of this project.

During the stability and sensitivity analysis of the two entire models it was found that the model including the DGS was stable, and non-sensitive to different operating points. However, it was found that the PLL of PV and WT was the most influential state in both systems and the response time of the PLL was varied to reveal which ranges are stable. Moreover the K_{pv} of the BESS voltage controller was seen to have an impact on the system without the DGS, as it was found to produce an unstable eigenvalue. The locus of the eig was made, varying K_{pv} and a new value was set. To ensure that the system was stable the state space model was used to check the response, and it was seen that with the new value of K_{pv}, the system became stable. The response with the new K_{pv} value was compared to the dynamic model and showed good agreement. Hereby the two grid layouts is stated to be stable, and the dynamic model is seen to work properly. This leads to the next chapter, where the network level control considerations will be assessed.

Network Control Design and Tests

7

The entire system has been proven to be stable as shown in Chapter 6 for several operating points. This chapter will then describe how a Network Level Control (NLC) can be made using the complete state space model together with a dynamic model of the system. Firstly, an analysis of typical and expected operational points in the system will be described and tested with the dynamic model. This will reveal which control loops that should be considered by the NLC. Secondly, the relevant I/O transfer functions will be analysed an tuned using SISOTOOL. Finally, the same scenarios described in the first part will be analysed with the closed loop control and a discussion will be made on the considerations needed for NLC.

The most practical part of having the system in state space form will come to show in this chapter. As seen from the previous chapter, two different control models are present, one with and without the DGS. As discussed in Section 4.5, the DGS should be used to a minimum. It therefore serves as a backup to the system. Furthermore, as it was seen in the stability analysis Section 6.2, the system is more critical whenever the DGS is turned off, as the system will be fully inverter-based.

For these reasons and in order to give an example of how the system NLC can be made, the system without the DGS is considered solely, in this chapter. Figure 7.1 shows the network level control as explained in 4.5 without the DGS. The control signals and their latency should be considered when designing the NLC. If some of the signals already exist in the system, this should be utilized in regards to the microgrid operators goal.

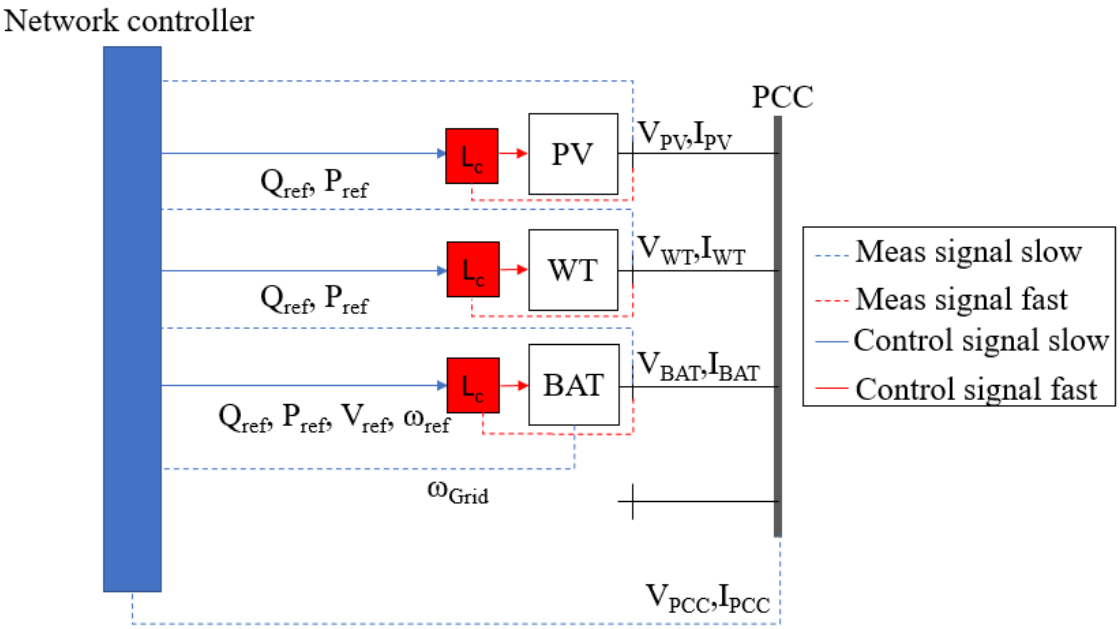

Figure 7.1: The device and network level control capabilities and required speed of measured and control signals with DGS turned off. L_c is the local control.

7.1 Test Case

Now, in order to understand the shortfalls of the Device Level control, and hence the required control from the network level, the system is analysed with the dynamic model described in Appendix E. The operating point is chosen to be a "base case" meaning that this operating point will be one of the most likely and normal to have in the system. The reason for choosing such a point and not an extreme is that the base case will depict the shortfalls of the device level control, whereas in extreme points this may not show as the point itself is critical. Considering that the system has a high penetration of renewable energy compared to the load, such a base case would fulfil the following statements:

- Available power from PV and WT is higher or close to the load demand
- PV and WT have power reserve
- BESS is controlling the frequency
- BESS' SoC is neither close to being fully charged or discharged.

This will be the base case if the DGS is turned off, under the assumption that a supervisory level control has predicted that the production from RES is higher than the load demand for a certain timespan. The base case chosen is depicted in Table

7.1. It is seen that the PV and WT have $PF = 1$, which may be a base case in order to utilize the maximum amount of active power from the unit. However, changing this will not alter the results seen in the next section.

Table 7.1: Initial operating point for the case with DGS turned off

DGS: On	PV	WT	BESS	DGS	Load
P kW	25	25	0	0	50
Q $kVAr$	0	0	14	0	12.5

In order to check the system response it is only necessary to change the load of the system. Doing so will reveal how the device level control behaves and reacts whenever such change appears in the system. Therefore, the simulation to be made, will be with the load increasing with 30 kW, at a fixed power factor of $PF = 0.97$. The load is set to ramp up over a timespan of 2 seconds, assuming that a load of this size could be a motor, controlled by a soft starter. This is a fast and large change, and will reveal if the BESS can handle such extreme changes without the DGS. The PV and WT is set to only deliver active power. This is done to ensure that the BESS handles both reactive and active power balance before and after the load increase.

7.2 Test Results

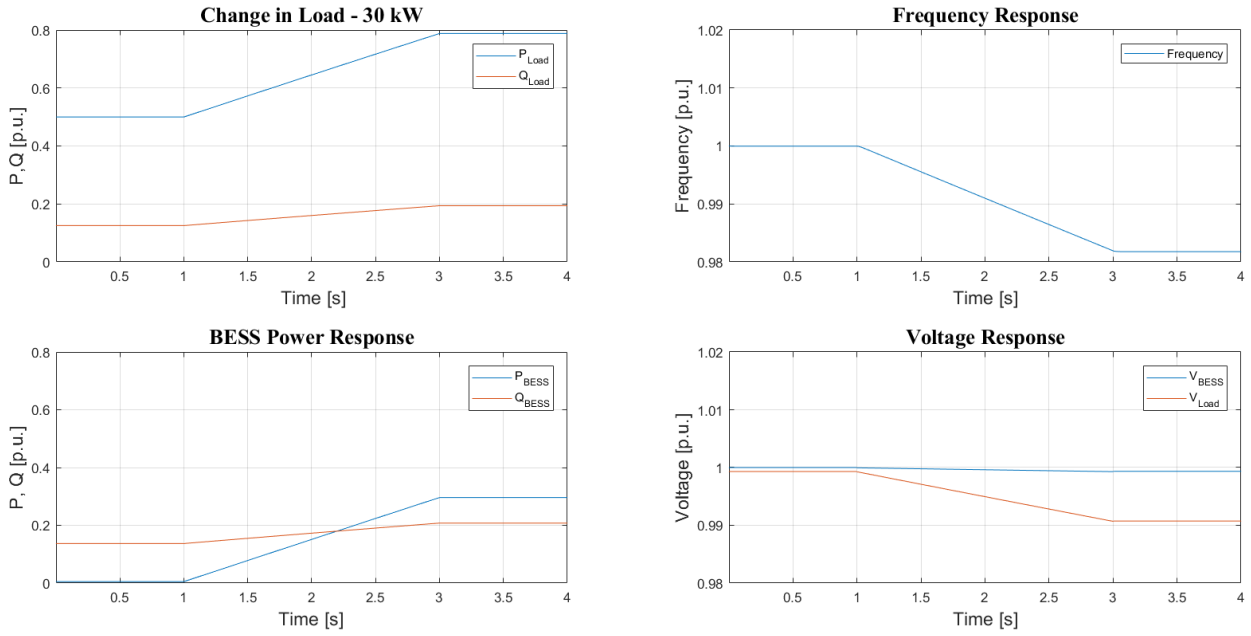

Figure 7.2: Responses due to a load increase of 30 kW. a) P and Q change in the load, b) frequency response from BESS, c) BESS power response, d) Voltage change at BESS bus and Load bus

In Figure 7.2, the test results are seen for the load increase which starts at $t = 1s$. From 7.2a) and 7.2c) it is seen, that as soon as the change in the load happens, the voltage and frequency will drop resulting in the BESS changing its P and Q output. This suggests that the control from the BESS is fast and can act on a large sudden change, as the one made in this test.

From 7.2b) and 7.2d) the frequency and voltage are now seen, respectively. As expected, a steady state error occurs, which is due to the droops of the device level control. Clearly, this exemplifies the need for a NLC that can correct this value without working against the device level control. The voltages do not deviate much. This is due to the fast response from the BESS which adjusts its response to the sudden load change. The frequency response shows that the system stabilizes at the new operating point, however with a frequency error around $f_{err} \approx 0.018p.u. = 0.9Hz$ which is not acceptable.

Now it should be considered, how the NLC should adjust the voltage and frequency

back to nominal values. Starting with the frequency, this parameter is controlled by adjusting P_{BESS} in the device level control. It will therefore make sense to update this active power reference with the NLC in a slower control loop. As seen in Figure 7.1, fast measurement is not needed for the frequency in NLC. Generally, recommendations for grids suggest that in a period of 10 s, the average frequency (sampled every 5 periods) must not deviate more than ±1% [DEFU, 2011]. Considering this, it is reasonable to have the NLC adjust the frequency with a settling time of 1-2 seconds.

Considering the voltages, the V_{Load} is deviating more than V_{BESS}. This is due to the fact that the BESS voltage control is based on the measured voltage on its own bus, and thereby changing the reactive power setpoint to keep this bus voltage constant. A discussion would be to consider where the NLC should receive its voltage reference from, to eliminate the steady state error. Again as discussed in Section 4.5, it makes sense to place the physical NLC unit at the site of the BESS and DGS. Then, information from the load bus would require additional communication between the two sites. Furthermore, as seen from Figure 7.1, fast measurement is achieved at the BESS bus compared to the load bus. Using the bus voltage at the BESS to correct the voltage error therefore seems more intuitive as this value will already be available to the NLC. However, this might not solve the steady state error at the bus voltage of the load bus. To check this hypothesis, firstly the two control loops to control the frequency with P_{BESS} and the voltage at V_{BESS} with Q_{BESS} will be tuned and analysed.

7.2.1 Tuning G_{wP} and G_{VQ}

As seen from the previous section $\frac{\omega(s)}{P_{BESS}(s)} = G_{wP}$ and $\frac{V_{BESS}(s)}{Q_{BESS}(s)} = G_{VQ}$ need to be analysed and tuned in order to cancel the voltage and frequency errors. The control loops for each plant is seen in Figure 7.3. To do this, the state space model needs to be transformed to transfer functions. As explained in Section 3.1, this is where the state space model has an advantage due to its ease of obtaining transfer functions and thereby analyse the system in the frequency and time domain and tune controllers. This is achieved by using the *ss2tf* (State Space to Transfer Function) command in Matlab. The respective transfer functions are then analysed and tuned with SISOTOOL (Single Input Single Output Tool), which will depict the changes to the root locus, bode plot or step response when subject to different proportional-integral (PI) controllers. The results from the SISOTOOL tuning are seen in Table 7.2. It is seen that SISOTOOL has proposed an integral (I)-controller as sufficient for the needed responses.

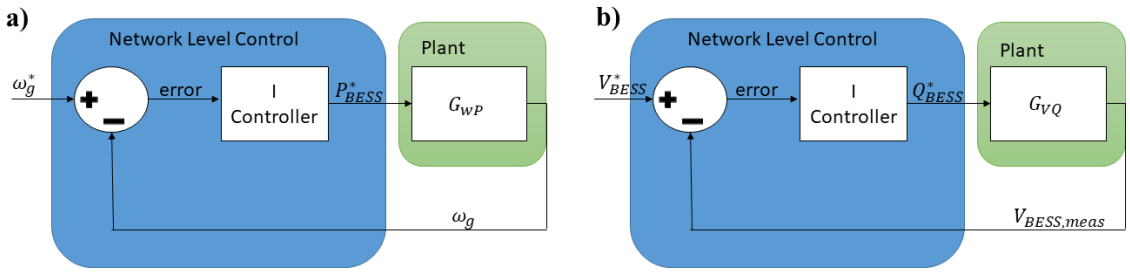

Figure 7.3: The NLC control loops for a) G_{wP} and b) G_{VQ} transfer functions

Table 7.2: The results obtained from tuning with SISOTOOL for G_{wP} and G_{VQ} in NLC

TF	Settling Time (sec)	PO (%)	Rise Time (sec)	I Controller
G_{wP}	1.9	0	1	$\frac{39.98}{s}$
G_{VQ}	5.3	0	3	$\frac{90.42}{s}$

As wanted, the G_{wP} controller has a slower settling time than the device level control of the BESS, but it is still fast enough to account for the frequency error. Furthermore, the rise time for this control loop is designed to be fast ($1s$) in order to quickly achieve the range of desired values.

G_{VQ} is designed to have a slower settling and rise time than the other loop. This is done such that the P and Q responses do not counteract each other. The rise time is not the most critical parameter for the voltage and is therefore set to $3s$, as this will ensure no overshoot.

7.2.2 Results with NLC for G_{wP} and G_{VQ}

Going back to the dynamic model, the same base case is tested with the NLC controller. The frequency and voltage response are seen in Figure 7.4 and 7.5, respectively.

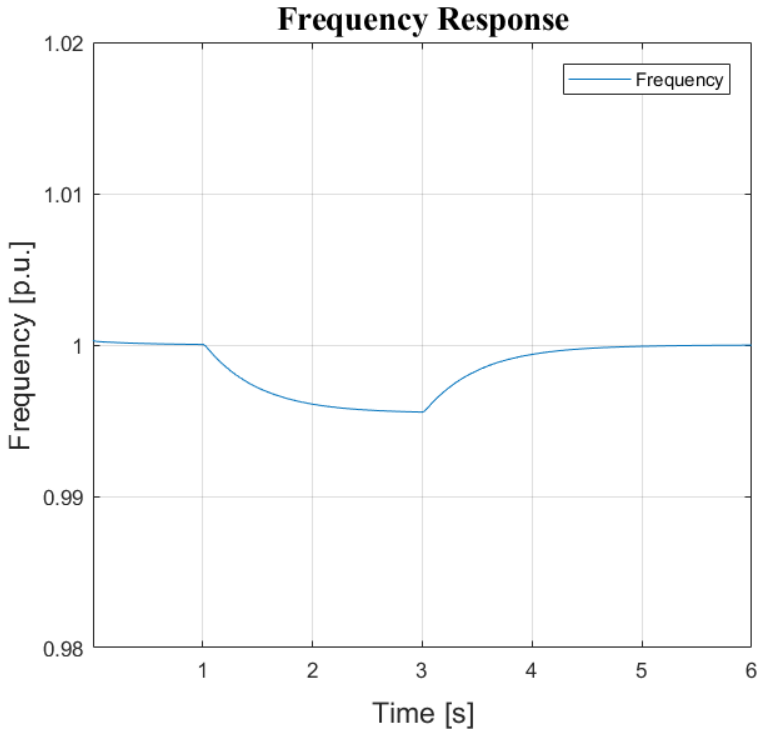

Figure 7.4: Frequency response with NLC

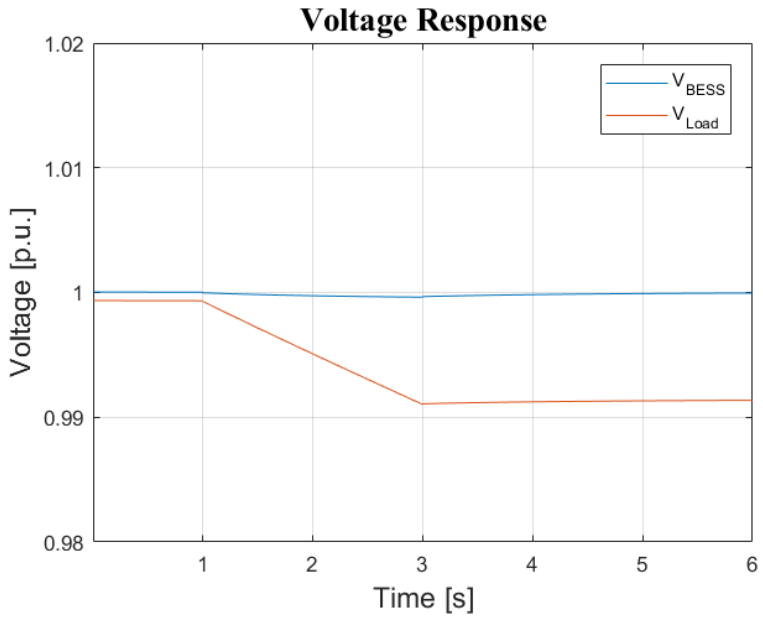

Figure 7.5: Voltage response at BESS and load with NLC

From the frequency response it is clear, that the NLC adjusts the frequency in a smooth manner due to the much slower loop of the NLC. In this way the NLC is supporting the device level control from time $1s$ to $3s$ where the load is changing, such that the frequency does not reach the critical value as before. When the load has stopped changing, the full effect of the NLC is shown as it changes the error in approx. $2s$, which is the expected settling time.

The V_{BESS} (blue line) in Figure 7.5 is seen to be adjusted by the NLC to 1 $p.u.$ The change in both voltages are even less severe due to the external control. The V_{load} change is however seen to still have a steady state error. It is only slightly affected by the NLC control. It should be noted, that the line between the BESS bus and load is only 100 m, indicating that higher distances would create even higher errors. The hypothesis is then confirmed. It is not a critical value for the load bus, however, several operational changes throughout the day might lead to higher errors, as the resistance is increased. For this reason it is deemed necessary to account for this error. This is however not cumbersome in case of receiving measurement signals, as seen from Figure 7.1, since only slow measurement signals are required for this purpose.

In order to check if the tuned controller can be used in different operating points, the step response will be tested in the extreme points analysed in Section 6.2. This is shown in Figure 7.6 and 7.7 for G_{wP} and G_{VQ}, respectively. Clearly, both step responses are the same in case C2.1 and C2.2, hence it is assumed that the controller can be used in all operational points.

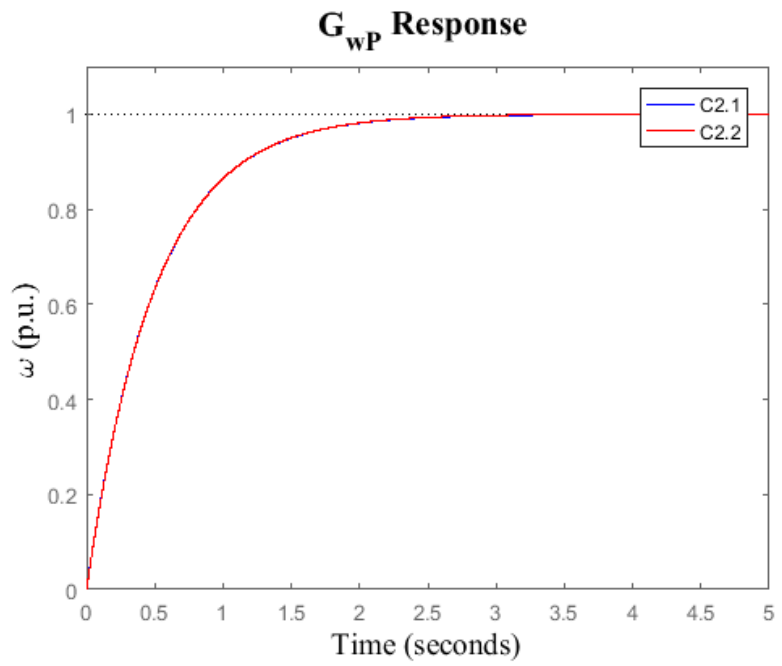

Figure 7.6: Step response for case C2.1 and C2.2 for the transfer function G_{wP}

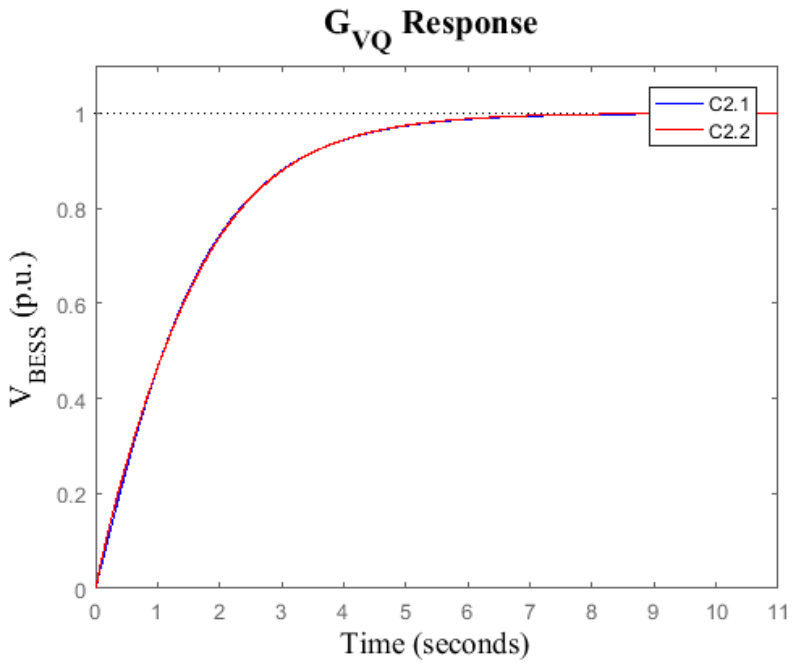

Figure 7.7: Step response for case C2.1 and C2.2 for the transfer function G_{VQ}

7.2.3 Adjusting the Load Voltage

As explained in previous subsection, the load voltage needs to be controlled. One way to do this without altering and disturbing the existing NLC, could be to change the nominal voltage reference of the BESS V_0 of the BESS, which is one of the inputs to the total state space model. As seen from Equation 7.1, this will change the v^* and hence the BESS will change its nominal voltage to be higher and thereby achieving 1 p.u. at the load bus.

$$v^* = V^* - n_v(Q_{avg} - Q^*) \tag{7.1}$$

The transfer function to be controlled is therefore $\frac{V_{load}(s)}{V_{BESS}(s)} = G_{VV_{Load}}$. Obviously, this control loop has to be much slower than the control of G_{VQ}. Hence a settling time that is 5x higher than G_{VQ}s control will be applied. Again, going back to the state space model, the relevant I/O transfer function is obtained and tuned using SISOTOOL. The results are seen in Table 7.3.

Table 7.3: The results obtained from tuning with SISOTOOL for $G_{VV_{Load}}$ in NLC

TF	Settling Time (sec)	PO (%)	Rise Time (sec)	PI Controller
$G_{VV_{Load}}$	23	0	12	$\frac{0.17027}{s}$

To check if this controller can be defined uniquely, a step response of the C2.1 and C2.2 operational points are checked. This is seen in Figure 7.8, which clearly shows that this controller can be used uniquely for this loop.

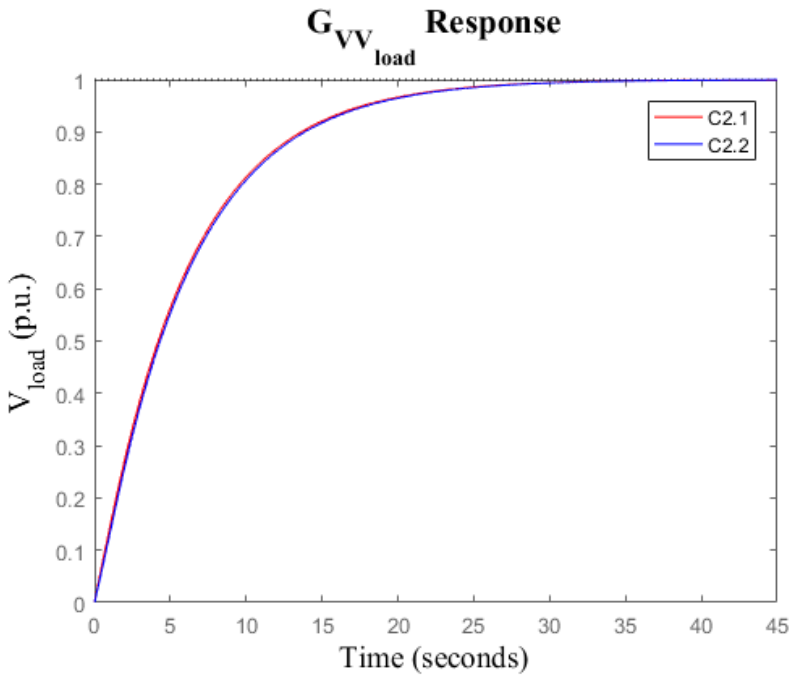

Figure 7.8: Step response for case C2.1 and C2.2 for the transfer function $G_{VV_{Load}}$

The controller is now implemented in the dynamic state space model, and the base case with the load increase is simulated again with the new loop added to the NLC. The results are shown in Figure 7.9.

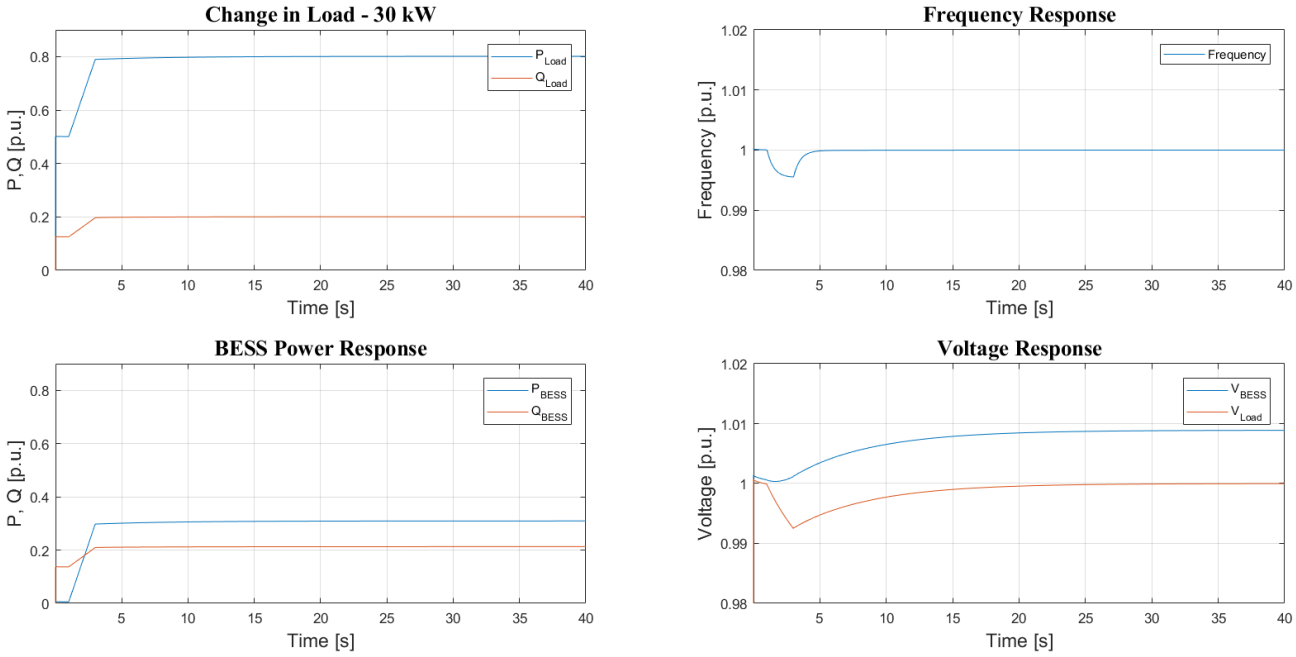

Figure 7.9: Responses due after Network Level Control with control of $G_{VV_{Load}}$

As expected, the control of the load bus is slowly boosting the voltage after the load change with the settling time of approx. $23s$, in order to get 1 $p.u.$ at the bus. This is done by increasing the voltage at the BESS. It is seen that the BESS is adjusting the current such that the same P and Q is delivered as in the case without control on the load bus.

This example clearly shows that the steady state errors of the system can be cancelled by tuning relevant I/O transfer functions with appropriate responses. It can then be concluded that for a base case such as the one considered in this example the NLC together with the device level control, can keep the voltage and frequency stable when subject to large sudden changes in the system. From here on, the grid operator should analyse and define how the system should operate in other scenarios and follow the same procedure as given here, in order to design the rest of the NLC.

Given the system dynamic model and the state space model, it was shown that NLC could be easily designed. The dynamic model reveals which problems will or can occur in the system, and hereby different control strategies can be implemented using the state space model (transfer functions) to tune control loops. This clearly states why a state space model is useful when designing NLC for microgrids.

Guideline for Control in Isolated Microgrids 8

This project has been structured in a way that has simplified and made the assessment of device and network level intuitive and practical. Therefore, as a summary of this procedure; a guideline on how to asses device and network level control in isolated microgrids will be given.

The core of this project has been to exploit the possibilities that exists in the system in scope and look at "what is there" in order to see "what can be done". This is a method that is inverse to what has been seen in the state of the art literature in Section 2.3. However, as clearly seen from the previous chapters, such a method simplifies and makes the decision of using the proper control architectures intuitive, instead of forcing one control method on to the system. This guideline is therefore seen as the best way to asses device and network level control and can be used as preliminary studies to understand the grid dynamics, capabilities and stability criteria.

Step 1: Specify the main goal of the microgrid

- This is the foundation for how the microgrid should be controlled.
- Goals can be economical, optimal dispatch, exploit renewable energy etc.
- Considerations about location, country and living standard of the society, to determine the dependency of stable power supply.
- Done in Section 4.5

Step 2: Discuss the capabilities of each unit in the system

- This is where the physical capabilities of the units are assessed.
- Consider the following for each unit: size, placement, response time, reliability.
- Which unit can be grid forming/following?
- Done in Section 4.5

Step 3: Define critical scenarios

- Define scenarios that may counteract with the main goal.
- If relevant, grid codes should be considered.
- This can be done by considering high/low production/consumption.
- Done in Section 4.5

Step 4: Initial discussion and outline of the proposed control method

- The previous 3 steps should be considered in total for this step.
- This will reveal the most beneficial way of controlling the system.
- Define if the units control are based on droops, communication etc. (again based on Step 1-3).
- E.g. the battery is chosen to be placed with the diesel genset to control V/f.
- Done in Section 4.5

Step 5: Design state space model of the individual units

- Design should be made according to Step 4 conclusions.
- Design should be made in state space, in a modular manner including the grid and load
- The individual reference frames should be considered, and how to relate them to on another.
- Individual control loops should be tuned according to required response (e.g. based on grid codes).
- Done in Section 5.1.

Step 6: Model Verification

- Define test scenarios
- Compare the linearised state space models with EMT models, load flow solver etc. before proceeding.
- Done in Section 5.3.

Step 7: Individual model analysis

- This is done to see individual behaviour of the models
- Sensitivity Analysis: understanding R/X ratio, P/Q influence, critical buses, tuning device level droops
- Analyse eigenvalues at various operational points, e.g. at critical values of V, PQ and PF
- Check their frequencies, relate them to control loops. Understand influence of V, PQ and PF on these values.

- If any unstable eigenvalues are found, retune the gains that influence these eigenvalues to prevent instability.
- This will ensure proper tuning of Device level control.
- Proceed when no unstable eigevalues appear at different operational points.
- Done in Section 5.4.

Step 8: Full System Analysis

- Define relevant critical cases
- Analyse the eigenvalues, frequencies and damping ratios, check if acceptable in relation to Step 4.
- Use participation factors to identify influence on critical eigenvalues.
- Find the limits on the critical eigenvalues in order to retune the control loops that can make them unstable.
- The knowledge obtained in this analysis will reveal how the system behaves, which units can make the system unstable etc.
- Done in Section 6.2.

After these steps, it is easy to understand the system. A clear understanding of what influences the system, what makes it unstable and how to prevent this will be evident. This can then be acted on with proper network level control.

Step 9: Network Level Design

- Define base cases and critical cases with the knowledge obtained in Step 6 and 7.
- Identify how the Network level should be made in order to achieve goal in Step 1, using dynamic model simulations.
- Tune relevant controllers to eliminate steady state errors etc. using state space model and transfer functions.
- Check the system with Network level control using dynamic models. Show that Step 3 scenarios are avoided.
- An example is given in Chapter 7.

A graphical example of this method is given in Figure 8.1.

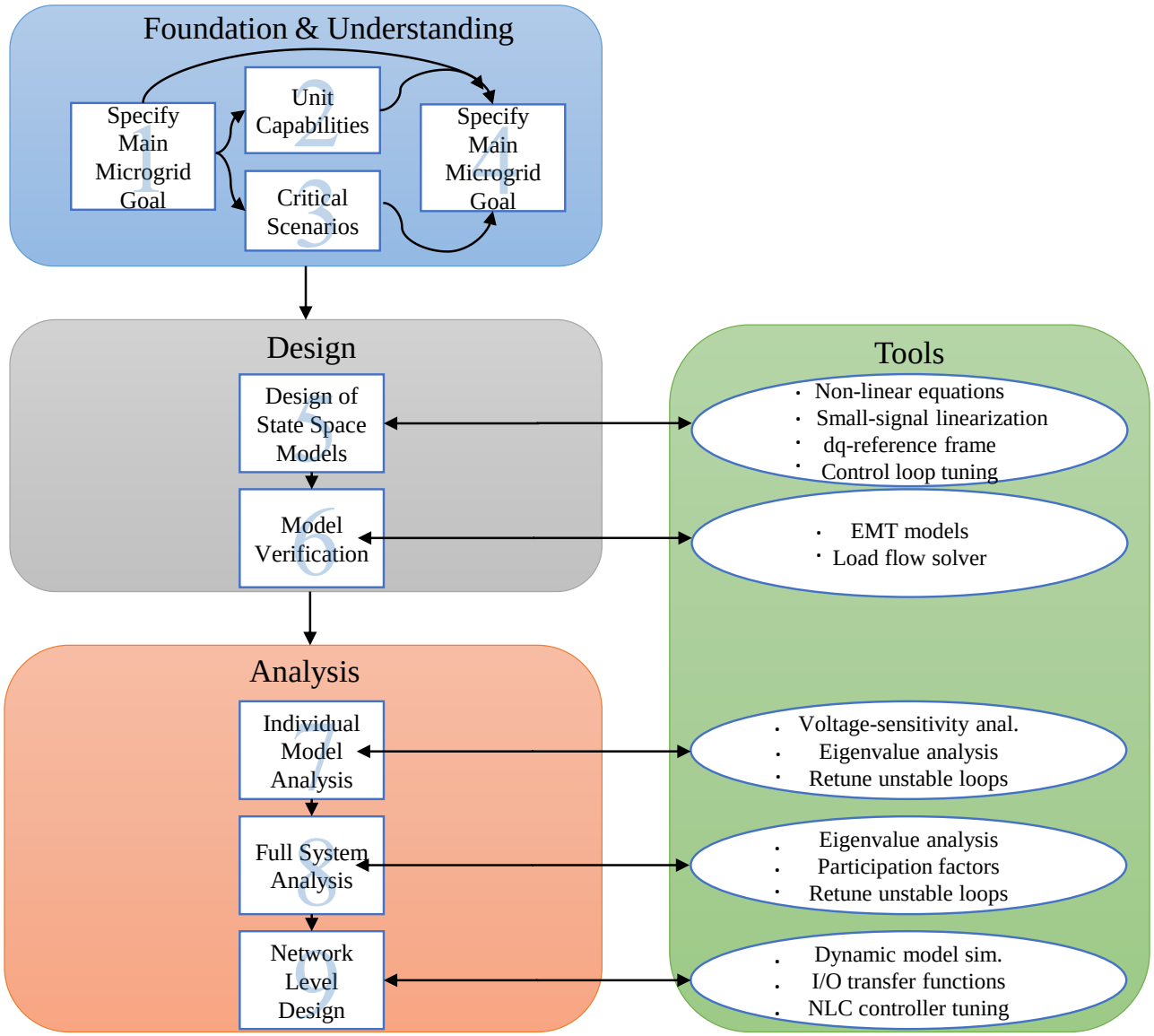

Figure 8.1: Graphical depiction of the step-by-step guide given in this project.

Conclusion & Outlook 9

The thesis conclusion will be presented in this chapter, followed by the outlook, which will discuss the further work that could be done. The conclusion will answer the following problem statement:

"How can the device and network level of a LV isolated hybrid power plant be designed in a simple and practical manner, that can be used by existing and future microgrid operators?"

9.1 Conclusion

From the SoA review it was seen, that the literature lacks a structured way of designing device and network level control. Therefore, this project is structured in an opposite way, by firstly looking at the system components, their capabilities and the system critical scenarios. From this discussion, it is concluded that the WTs and PVs should be controlled as grid-following units due to their intermittent behaviour, their dispersed placement and the interest of utilizing renewable energy to the most. Furthermore, the BESS is chosen to be grid-forming, unless energy from RES are not sufficient, in which case the DGS is turned on and will control the frequency with P. The battery will control V with reactive power and it will follow the DGS frequency reference, in this case. It is known, that the system has high R/X ratio, however, having a DGS in the system will require P/f and Q/V control. The BESS will control V and f when the DGS is turned off by using droops, which makes it able to mimic a DGS control. This control method is based on the fact, that the BESS and DGS will be placed at the same site. In this way, the NLC unit is placed at this site as well.

Each individual unit, including the grid and load, was modelled in state space. This requires a thorough analysis of the differential non-linear equations that represents each unit. The inner loop controllers are designed based on criteria deemed appropriate for device level control, as there are no grid codes for island microgrids. The

models are then verified using EMT models in SimScape (Simulink) and load flow solvers. All the models are concluded to be suitable for this study, as the deviations are negligible.

A voltage sensitivity analysis is made as this will help gain knowledge needed for the device level and network level control. It is concluded, that active power has most influence on the system voltages. However, active power and reactive power control from each unit to the load bus is seen to have the same influence, therefore all units can be used to control the load bus with approx. the same droops. The residual values are used in the BESS droop control. Each individual model is now analysed for stability, e.g. analysing eigenvalues, damping ratios, frequencies etc., at different operational points. The influence of V, PF and PQ is checked for each model. It is concluded that the models are stable at nominal and extreme operating points. Furthermore, voltage changes have influence on all the units, however the influence is not seen on the BESS, since its voltage control loops are open. Active power changes are seen to affect the DGS only. PF does not change the eigenvalues of the models. The changes in eigenvalues are not seen to cause instability and retuning of internal loops are therefore not needed at this point.

The system is now assembled, and the total state matrix is analysed for stability. Again, extreme points are evaluated. The system when the DGS is turned off is seen to have a positive eigenvalue at one operation point. By use of participation factor and intuition it is concluded that the voltage control loop in the BESS has to be retuned. The affect of this on the stability is analysed and the loop is retuned. Furthermore, the PLL is seen to have a high influence on the total system. Settling time of the PLL control vs. stability is analysed, and it is concluded that this unit should not have faster settling time than 0.5 ms, which will lead to instability. This chapter concludes then, that the system is stable with the retuned control loops.

Finally, the network level control is assessed. In this project, an example is given on how this control could be made. This is done for the case where the DGS is turned off, as this was seen to be more critical, and this will also be the base case in this system. Firstly, a base case is considered, which will represent a typical operational point. Then a load change is defined, which will be a large sudden change. This is to check the limits of the device level control.

When analysing the system in time domain with dynamic models, the voltages at the BESS bus and load bus along with the frequency have a steady state error. This leads to the proper I/O transfer functions that should be found and tuned. An outer P/f loop is considered. An integral-controller is tuned for this purpose

which is seen to cancel the steady state error. A discussion is made on which bus to control the voltage on with the network level control. It is seen, that if only the BESS bus is controlled, a steady state error still occur on the load bus. This is then eliminated, by making a control loop that controls the bus at the load by changing the voltage reference at the BESS. Hence a slightly higher voltage point is achieved at the BESS, however this will not lead to unstable operation.

It is therefore concluded, that the approach given in this project will help to understand the system at hand, and based on this the control of the device and network level control can be achieved. It is seen that even for a sudden large load change, the voltages and frequency are kept within the allowed range for stable operation by using the knowledge attained from the several analysis made both in frequency and time domain. Thereby the problem statement and sub-questions have been answered and the success criteria met.

9.2 Outlook

In this chapter four topics will be presented, which was out of scope of this project, but is still relevant for the overall topic, and important for achieving a fully functional microgrid. A short description will be given of each topic, including why they are important and what new information they could provide.

DGS Tests
For the further work, test of the dynamic model should be performed showing how the NLC works when the DGS is turned on, and thereby is the grid-forming unit. Chapter 6 reveals that the system is stable when the DGS is turned on, however it would be interesting to see how the power is shared between the DGS and the BESS, whenever the load changes. This could be used to make the NLC take care of the power sharing in the system, as an example if the BESS takes care of the power mismatch as a first response, the NLC should update the power reference to the DGS, such that the SoC of the BESS can be maintained. The frequency response should be investigated such that the two models can be compared. The NLC could then be designed to have the same response for the case without the DGS, such that components in the system will experience the same frequency response for both cases.

Furthermore, the NLC should take care of the transition between the two modes of operation. The decision whether to turn the DGS on/off would be made in a higher control layer. Based on weather and load forecasting from the supervisory control, the NLC should receive a go signal and ensure safe and slow transition to the new mode of operation. In cases of faults, loss of communication or similar, the DGS could be turned on as well, since it is designed without any communication to solely control the grids frequency and voltage. Simulations showing this transition would be a part of the future work.

Implementation in AAU - Smart Energy Systems Laboratory
In order to further test the control and stability of the grid, the models presented in this project should be implemented in a real time (Hardware-in-the-loop) simulator, available at Aalborg University "*Smart Energy Systems Laboratory*". This will give the possibility of testing with load emulators and including a realistic communication network and data traffic, which can be used to further test and optimize the control.

Battery state of charge model
The battery state of charge (SoC) is very critical to the control methodology proposed in this project. When the diesel genset is turned off, the grid relies on the

BESSs ability to either consume or deliver power, in order to keep stable voltage and frequency. This however requires the battery SoC to be kept in a range around 50%, never fully charged or discharged. Therefore, a battery model representing the battery SoC needs to be included. Testing with this model can be used to design a part of the NLC, which keeps the SoC within a healthy range. In this regard, it will also be relevant to look at the specific battery type and how the lifetime of this unit will be affected by the wanted control from the NLC.

Practical implementation

Investigations towards the practical implementation of the system in scope is also considered as future work. In the project, the migrogrid central controller is suggested to be placed together with the BESS and DGS, and furthermore this should be close to the main bus of the system. As an example, it would be relevant to look into the needed ICTs for the proposed control method and how this can be achieved. The practical considerations would also be to investigate how fast the communication between the microgrid controller, BESS and DGS could be made. For instance, considering if its possible to keep the distance short enough between these units, such that the shaft speed sensor of the DGS could be wired directly to each units control. This would enable the units to have the exact same frequency reference, and thereby no latency difference. Investigations with regards to choosing the exact units, such as WTs, PV, BESS and all measurements, are also seen as relevant future work.

Bibliography

Andrzej Grzegorz Adamezyk. Damping of Low Frequency Power System Oscillations with Wind Power Plants. PhD thesis, Aalborg university, 2012.

Anderson and Abdel-Aziz, **1977**. Paul Anderson and Fouad Abdel-Aziz. *Power System Control and Stability*. The Iowa State University Press, first edition, 1977. ISBN 0-8138-1245-3.

Bergen, **1999**. Arthur R. Bergen. *Power Systems Analysis*. Prentice-Hall, 1999.

Caterpillar, **2016**. Caterpillar. *DIESEL GENERATOR SET*, 2016.

DEFU, **2011**. DEFU. *Rekommandation 16 Spaendingskvalitet i lavspaendingsnet 4. udgave, August 2011*, Dansk Energi Forskning og Udvikling, 2011.

Díaz et al., **2017a**. NELSON Díaz, Juan Vasquez and Josep Guerrero. *A Communication-less Distributed Control Architecture for Islanded Microgrids with Renewable Generation and Storage*. IEEE Transactions on Power Electronics, pages 1–1, 2017. ISSN 0885-8993. doi: 10.1109/TPEL.2017.2698023. URL `http://ieeexplore.ieee.org/document/7911341/`.

Díaz et al., **2017b**. Nelson L. Díaz, Adriana Carolina Luna, Juan C. Vasquez and Josep M. Guerrero. *Centralized Control Architecture for Coordination of Distributed Renewable Generation and Energy Storage in Islanded AC Microgrids*. IEEE Transactions on Power Electronics, 32(7), 5202–5213, 2017. ISSN 08858993. doi: 10.1109/TPEL.2016.2606653.

Díaz et al., **2017c**. Nelson Leonardo Díaz, Jose Guillermo Guarnizo, Martin Mellado, Juan C. Vasquez and Josep M. Guerrero. *A robot-soccer-coordination inspired control architecture applied to islanded microgrids*. IEEE Transactions on Power Electronics, 32(4), 2728–2742, 2017. ISSN 08858993. doi: 10.1109/TPEL.2016.2572262.

Energinet, **2016a**. Energinet. *Teknisk forskrift 3.2.5 for vindkraftanlaeg stoerre end 11 kW*, Energinet, 2016a.

Energinet, **2016b**. Energinet. *Teknisk forskrift 3.3.1 for batterianlaeg*, Energinet, 2016b.

Farrokhabadi et al., **2017**. M. Farrokhabadi, S. Koenig, C.A. Canizares, K. Bhattacharya and T. Leibfried. *Battery Energy Storage System Models for Microgrid Stability Analysis and Dynamic Simulation.* IEEE Transactions on Power Systems, 33(2), 2301–2312, 2017. ISSN 08858950. doi: 10.1109/TPWRS.2017.2740163.

Foruzan et al., **2017**. Elham Foruzan, Marcelo C. Algrain and Sohrab Asgarpoor. *Decentralized controller design for microgrids in islanded and grid-connected modes.* IEEE International Conference on Electro Information Technology, pages 28–33, 2017. ISSN 21540373. doi: 10.1109/EIT.2017.8053325.

Fronius, **2017**. Fronius. *Fronius Symo Technical Data of Inverters.* Fronius, 2017.

Gao, **2015**. David Wenzhong Gao. *Energy Storage for Sustainable Microgrid.* Elsevier, 2015.

Gkountaras, **2017**. Aris Gkountaras. *Modeling techniques and control strategies for inverter dominated microgrids.* 2017. ISBN 9783798328723. doi: 10.14279/depositonce-5520.

Guerrero et al., **2004**. Josep M. Guerrero, Luis Garcia De Vicuia, Jose Matas, Jaume Miret and Miguel Castilla. *Output impedance design of parallel-connected UPS inverters.* IEEE International Symposium on Industrial Electronics, 2(4), 1123–1128, 2004. ISSN 02780046. doi: 10.1109/ISIE.2004.1571971.

Guerrero et al., **2011**. Josep M. Guerrero, Juan C. Vasquez, José Matas, Luis García De Vicuña and Miguel Castilla. *Hierarchical control of droop-controlled AC and DC microgrids - A general approach toward standardization.* IEEE Transactions on Industrial Electronics, 58(1), 158–172, 2011. ISSN 02780046. doi: 10.1109/TIE.2010.2066534.

Hatziargyriou, **2014**. Nikos Hatziargyriou. *Microgrids Architectures and Control.* John Wiley and Sons Ltd, 2014.

Hayden, **2013**. Ernie Hayden. *Introduction to Microgrids.* Internet, 2013. URL `http://www.securicon.com/sites/default/files/Introduction%20to%20Microgrids%20-%20Securicon%20-%202013_1.pdf`.

IEC-62898-1, **2017**. IEC-62898-1. *Microgrids - Part 1: Guidelines for microgrid projects planning and specification*, IEC, 2017.

Karimi et al., **2017**. M. Karimi, R. Azizipanah-Abarghooee, H. Uppal, Q. Hong, C. Booth and V. Terzija. *Smart integrated adaptive centralized controller for islanded microgrids under minimized load shedding*. ICSG 2017 - 5th International Istanbul Smart Grids and Cities Congress and Fair, pages 41–45, 2017. doi: 10.1109/SGCF.2017.7947633.

Per Karlsson. DC Distributed Power Systems - Analysis, Design and Control for a Renewable Energy System. PhD thesis, Lund University, 2002.

Kim et al., **2016**. Yun Su Kim, Chul Sang Hwang, Eung Sang Kim and Changhee Cho. *State of charge-based active power sharing method in a standalone microgrid with high penetration level of renewable energy sources*. Energies, 9(7), 2016. ISSN 19961073. doi: 10.3390/en9070480.

Kundur, **1994**. Prabha Kundur. *Power System Stability and Control*. McGraw-Hill Education, 1994.

Lou et al., **2017**. Guannan Lou, Wei Gu, Liufang Wang, Bin Xu, Ming Wu and Wanxing Sheng. *Decentralised secondary voltage and frequency control scheme for islanded microgrid based on adaptive state estimator*. IET Generation, Transmission & Distribution, 11(15), 3683–3693, 2017. ISSN 1751-8687. doi: 10.1049/iet-gtd.2016.1910. URL `http://digital-library.theiet.org/content/journals/10.1049/iet-gtd.2016.1910`.

Lund, **2007**. Per Lund. *The Danish Cell Project - Part 1: Background and General Approach*. 2007.

Maitra and Simmins, **2015**. A. Maitra and J. Simmins. *Grid Interactive Microgrid Controllers and the Management of Aggregated Distributed Energy Resources (DER)*, EPRI, 2015.

Miller, **2017**. Thomas Ackermann & Thibault Prevos & Vijay Vittal & Andrew J. Roscoe & Julia Matevosyan & Nicholas Miller. *Paving the way*. IEEE Energy and Power Magazine, 2017.

Mondal et al., **2017**. Gopal Mondal, Joachim Bamberger, Michael Bernhard Buhl and Sebastian Nielebock. *Voltage source operation of parallel PV/wind inverters-stabilized hybrid power plants in "diesel off-mode"-an experimental verification*. 2017 IEEE 8th International Symposium on Power Electronics for Distributed Generation Systems, PEDG 2017, 2017. doi: 10.1109/PEDG.2017.7972452.

JACOB ANDREAS Mueller. Small-Signal Modeling of Grid-Supporting Inverters in Droop Controlled Microgrids. Master's thesis, Missouri University of science and technology, 2014.

Petersen and Iov, **May 2018**. Lennart Petersen and Florin Iov. *Optimal and Modular Configuration of Wind Integrated Hybrid Power Plants for Off-Grid Systems*. Energynautics, page 10, 2018. ISSN 978-3-9816549-7-4.

Phillips and Parr, **2010**. Charles L. Phillips and John M. Parr. *Feedback Control Systems*. Pearson Education (Us), 2010.

Phillips and Parr, **2011**. Charles L. Phillips and John M. Parr. *Feedback Control Systems, 5th Edition*. Pearson, 2011.

Platform, **2006**. European SmartGrids Technology Platform. *Vision and Strategy for Europe's Electricity Networks of the Future*, European commission, 2006.

Pogaku et al., **2007**. Nagaraju Pogaku, Milan Prodanovic and Timothy C. Green. *Modeling, Analysis and Testing of Autonomous Operation of an Inverter-Based Microgrid*. IEEE TRANSACTIONS ON POWER ELECTRONICS, 22(2), 613–625, 2007.

R&D, **2011**. Vestas Wind Systems Technology R&D. *General Specification V112-3.0 MW 50/60 Hz*, 2011. Class 1.: Document no.: 0011-9181 V05.

Rocabert et al., **2012**. Joan Rocabert, Alvaro Luna, Frede Blaabjerg and Invited Paper. *Control of Power Converters in AC Microgrids.pdf*. IEEE Transactions on Power Electronics, 27(11), 4734–4749, 2012. ISSN 0885-8993. doi: 10.1109/TPEL.2012.2199334.

SA. LEM International SA. *Industry Current & Voltage Transducers*. LEM International SA.

Sezi, **2010**. Tevfik Sezi. *Fast and Accurate Measurement of Power System Frequency*. Power and Energy Society General Meeting, 2010 IEEE, 2010.

Shafiee et al., **2012**. Qobad Shafiee, Juan C. Vasquez and Josep M. Guerrero. *Distributed secondary control for islanded MicroGrids - A networked control systems approach*. IECON 2012 - 38th Annual Conference on IEEE Industrial Electronics Society, pages 5637–5642, 2012. ISSN 1553-572X. doi: 10.1109/IECON.2012.6389034. URL `http://ieeexplore.ieee.org/lpdocs/epic03/wrapper.htm?arnumber=6389034`.

Tameghe et al., 2015. Tommy Tameghe, Rene Wamkeue and Innocent Kamwa. *Diesel Generator Modelling for Microgrid Power Plant Parameters Assessment.* ResearchGate, 2015.

Tecknology, 2017. FKI Energy Tecknology. *Data Sheets Three phase Syncronous Generators*, 2017.

Teodorescu et al., 2011. Remus Teodorescu, Marco Liserre and Pedro Rodriguez. *Grid Converters for Photovoltaic and Photovoltaic and.* John Wiley and Sons Ltd, 2011. ISBN 9780470057513. doi: 10.1002/9780470667057.

Village. *Engineering Village.* URL `https://www.engineeringvillage.com/search/quick.url`.

Wang et al., 2017. Shike Wang, Zeng Liu, Jinjun Liu, Baojin Liu, Xin Meng and Ronghui An. *Modeling and Analysis of Droop Based Hybrid Control Strategy for Parallel Inverters in Islanded Microgrids.* pages 3462–3469, 2017. doi: 10.1109/APEC.2017.7931194.

Wang et al., 2016. Yunping Wang, Ying Li and Xinbo Ruan. *High-Accuracy and Fast-Speed MPPT Methods for PV String Under Partially Shaded Conditions.* IEEE TRANSACTIONS ON INDUSTRIAL ELECTRONICS vol 63 No. 1, 2016.

Williams and Lawrence, 2007. Robert L. Williams and Douglas A. Lawrence. *Linear state-space control systems.* John Wiley & Sons, Inc., Hoboken, New Jersey, 2007.

Wu et al., 2014a. D. Wu, F. Tang, T. Dragicevic, J. Vasquez and J. Guerrero. *Autonomous active power control for islanded ac microgrids with photovoltaic generation and energy storage system, IEEE Transactions on Energy Conversion.* IEEE Transactions on Energy Conversion, 29(4), 882–892, 2014.

Wu et al., 2014b. Dan Wu, Fen Tang, Josep M. Guerrero, Juan C. Vasquez, Guoliang Chen and Libing Sun. *Autonomous active and reactive power distribution strategy in islanded microgrids.* Conference Proceedings - IEEE Applied Power Electronics Conference and Exposition - APEC, pages 2126–2131, 2014. ISSN 1048-2334. doi: 10.1109/APEC.2014.6803600.

Yamashita et al., 2011. K Yamashita, S Martinaz Villanueva and JV Milanovic. *Initial results of international survey on industrial practice on power system load modelling conducted by CIGRE WG C4. 605.* CIGRE, 2011.

Zhang et al., **2016**. Huaguang Zhang, Sunghyok Kim, Qiuye Sun and Jianguo Zhou. *for Accurate Reactive Power Sharing Based on Consensus Control in Microgrids*. IEE Transactions on Smart Grid, 8(4), 1749–1761, 2016. ISSN 1949-3053. doi: 10.1109/TSG.2015.2506760.

Zhou et al., **2015**. Sizhan Zhou, Jinjun Liu, Linyuan Zhou and Hongwei She. *Cross-coupling and decoupling techniques in the current control of grid-connected voltage source converter*. 2015 IEEE Applied Power Electronics Conference and Exposition (APEC), pages 2821–2827, 2015. doi: 10.1109/APEC.2015.7104750. URL `http://ieeexplore.ieee.org/document/7104750/`.

System Characterisation Parameters and PQ-maps

A

This Appendix will give the system parameters as described in Chapter 4.

A.1 Diesel Generator

The diesel genset is manufactured by Caterpillar, and the parameters are found in their datasheet [Caterpillar, 2016], while the synchronous generator is from Marelli Generators and the parameters are found in their datasheet [Tecknology, 2017]. The right side of Table A.1, depicts the common parameters for the entire genset and the generator. The notation x is the reactances, with the subscript d and q, for the d and q axis. The notation with x' is the transient reactances and x'' is the subtransient reactance. The same notation is applied for the time constants T, along with the subscript T_o being the open circuit time constant.

The most important parameter for the diesel generator is the inertia of the entire system, since this is closely related to the dynamic response to a change in frequency. Due to the assumption that the two datasheets are correlated, it is approximated that the values from the generator can be applied with the total inertia given by the diesel genset datasheet.

Table A.1:

Genset Parameters				Genset/SG Parameters		
I	FC	S	P	f	V	ω_m
$kg \cdot m^2$	L/h	kVA	kW	hz	V	RPM
1.14	13.7	60	48	50	400/230	1500

Table A.2:

Synchronous Generator Parameters													
S	P	x_d	x_q	x'_d	x''_d	x''_q	x_2	x_0	T'_{d0}	T'_d	T''_d	T_a	r_S
kVA	kW	pu	pu	pu	pu	pu	pu	pu	s	s	s	s	Ω
62	49.6	2.7	1.5	0.22	0.109	0.13	0.119	0.05	0.6	0.06	0.01	0.011	0.14

PQ-map Synchronous Generator

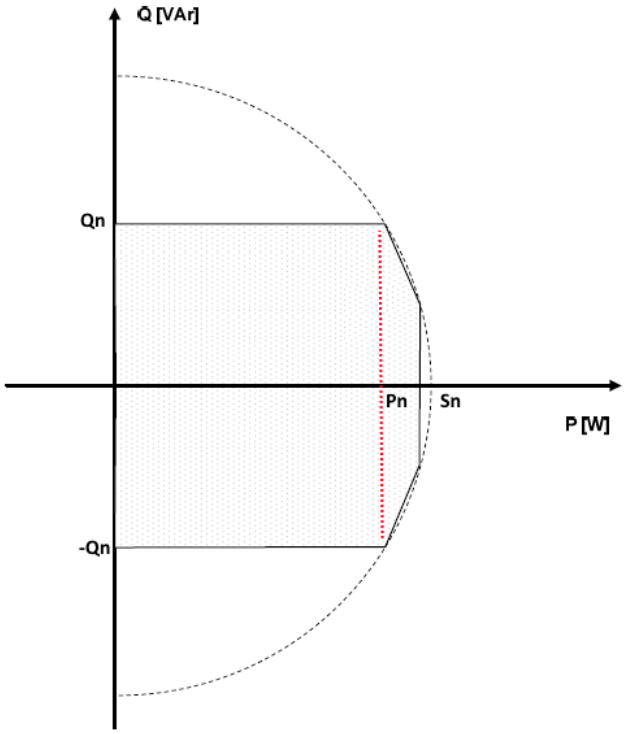

Figure A.1: Synchronous generator PQ-map. $P_n = 45kW$, $S_n = 60kVA, Q_n = 40kVAr$

AVR

AVR parameters are given here, where K_F and K_A are the gains of the feedback and amplifier, respectively. T_F is the response time of the feedback.

Table A.3:

AVR - Parameters			
K_A	T_A	K_F	T_F
$-$	s	$-$	s
400	0.02	0.03	1

A.2 PV

Parameters for the PV:

Table A.4: PV plant specifications.

Parameter	symbol	Value
Rated power	P_n	40kW
Rated voltage	V_r	400V (phase-phase) RMS
Rated Current	I_r	57.7A RMS
DC link voltage	V_{dc}	1000V DC
Switching frequency	f_s	5000kHz
DC link capacitor	C_{dc}	4.5mF
Output filter inductor	L_f	2.3mH
Transformer inductance	L_t	0.168mH LV side
Total output inductor	L_{ft}	2.468mH

PQ-map PV

The PQ map for the PV-inverter is irrelavant to show as it is found from a datasheet for Fronius 20 kW inverter, that the power factor can be regulated from $0-1 ind./cap.$ [Fronius, 2017].

A.3 WT

Parameters for the WT:

Table A.5: WT unit specifications.

Parameter	symbol	Value
Rated power	P_n	80kW
Rated voltage	V_r	400V (phase-phase) RMS
Rated Current	I_r	115.5A RMS
DC link voltage	V_{dc}	1000V DC
Switching frequency	f_s	5000kHz
DC link capacitor	C_{dc}	9mF
Output filter inductor	L_f	1.1mH
Transformer inductance	L_t	0.29mH LV side
Total output inductor	L_{ft}	1.39mH

PQ-map WT Important to notice is that this is the minimum requirement as described in [Energinet, 2016a] for a WT larger than 50 kW and up to 1.5 MW.

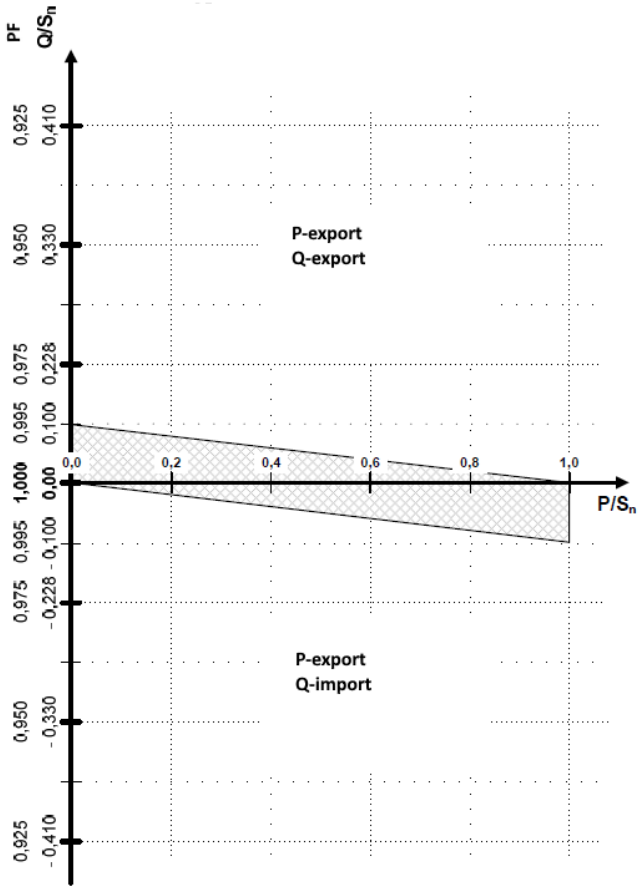

Figure A.2: The minimum requirements for group C WT. Danish Grid code for WT's from [Energinet, 2016a].

A.4 BESS

Parameters for the battery:

Table A.6: BESS plant specifications.

Parameter	symbol	Value
Rated power	P_n	80kW
Rated voltage	V_r	400V (phase-phase) RMS
Rated Current	I_r	115.5A RMS
DC link voltage	V_{dc}	1000V DC
Switching frequency	f_s	5000kHz
output filter inductor	L_f	1.1mH

PQ-map BESS Minimum reactive power capabilities, for BESS bigger than $P = 50kW$ and smaller than $1.5MW$ as described in [Energinet, 2016b].

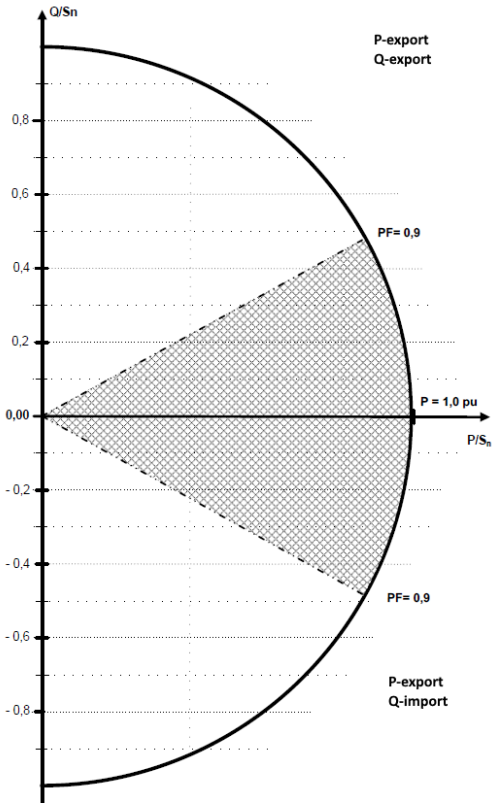

Figure A.3: PQ-map for BESS minimum requirements [Energinet, 2016b]

State Space representations B

B.1 State space matrixes for the Grid and Load Model

$$A_{grid} = \begin{bmatrix} A_{grid1} & 0 & ... & 0 \\ 0 & A_{grid2} & ... & 0 \\ ... & ... & ... & 0 \\ 0 & 0 & 0 & A_{grid_n} \end{bmatrix}, A_{gridi} = \begin{bmatrix} \frac{-R_{linei}}{L_{linei}} & \omega_0 \\ -\omega_0 & \frac{-R_{linei}}{L_{linei}} \end{bmatrix}, B_{1grid} = \begin{bmatrix} B_{1grid_1} \\ B_{1grid_2} \\ ... \\ B_{1grid_n} \end{bmatrix}$$

$$B_{1gridi} = \begin{bmatrix} ... & \frac{1}{L_{gridi}} & 0 & ... & \frac{-1}{L_{gridi}} & 0 & ... \\ ... & 0 & \frac{1}{L_{gridi}} & ... & 0 & \frac{-1}{L_{gridi}} & ... \end{bmatrix}, B_{2grid} = \begin{bmatrix} B_{2grid_1} \\ B_{2grid_2} \\ ... \\ B_{2grid_n} \end{bmatrix}, B_{2gridi} = \begin{bmatrix} I_{lineQi} \\ -I_{lineDi} \end{bmatrix}$$

$$A_{load} = \begin{bmatrix} A_{load1} & 0 & ... & 0 \\ 0 & A_{load2} & ... & 0 \\ ... & ... & ... & 0 \\ 0 & 0 & 0 & A_{load_n} \end{bmatrix}, A_{loadi} = \begin{bmatrix} \frac{-R_{loadi}}{L_{loadi}} & \omega_0 \\ -\omega_0 & \frac{-R_{loadi}}{L_{loadi}} \end{bmatrix}$$

$$B_{1load} = \begin{bmatrix} B_{1load_1} \\ B_{1load_2} \\ ... \\ B_{1load_p} \end{bmatrix}, B_{1loadi} = \begin{bmatrix} ... & \frac{1}{L_{loadi}} & 0 & ... \\ ... & 0 & \frac{1}{L_{loadi}} & ... \end{bmatrix}, B_{2load} = \begin{bmatrix} B_{2load_1} \\ B_{2load_2} \\ ... \\ B_{2load_p} \end{bmatrix}, B_{2loadi} = \begin{bmatrix} I_{loadQi} \\ -I_{loadDi} \end{bmatrix}$$

B.2 State space matrixes for PV & WT model

$$A = \begin{bmatrix} 0 & 0 & 0 & 0 & 0 & 0 & a_{1,7} & 0 & 0 & 0 & 0 & 0 & a_{1,13} \\ 0 & 0 & 0 & 0 & 0 & 0 & 0 & 0 & a_{2,9} & 0 & 0 & 0 & 0 \\ 0 & a_{3,2} & 0 & 0 & 0 & 0 & 0 & 0 & a_{3,9} & a_{3,10} & 0 & 0 & 0 \\ 0 & 0 & 0 & 0 & 0 & 0 & 0 & 0 & 0 & 0 & a_{4,11} & a_{4,12} & 0 \\ a_{5,1} & a_{5,2} & a_{5,3} & 0 & 0 & a_{5,6} & 0 & 0 & a_{5,9} & a_{5,10} & a_{5,11} & a_{5,12} & 0 \\ a_{6,1} & 0 & 0 & a_{6,4} & a_{6,5} & 0 & 0 & 0 & 0 & a_{6,10} & a_{6,11} & a_{6,12} & a_{6,13} \\ 0 & 0 & 0 & 0 & 0 & 0 & 0 & 0 & 0 & 0 & 0 & 0 & a_{7,13} \\ 0 & 0 & 0 & 0 & 0 & 0 & 0 & a_{8,8} & 0 & 0 & 0 & 0 & 0 \\ a_{9,1} & 0 & 0 & 0 & a_{9,5} & a_{9,6} & 0 & 0 & a_{9,9} & 0 & 0 & 0 & 0 \\ 0 & 0 & 0 & 0 & a_{10,5} & 0 & 0 & 0 & 0 & a_{10,10} & 0 & 0 & 0 \\ 0 & 0 & 0 & 0 & 0 & a_{11,6} & 0 & 0 & 0 & 0 & a_{11,11} & 0 & 0 \\ a_{12,1} & 0 & 0 & 0 & 0 & 0 & 0 & 0 & 0 & 0 & 0 & a_{12,12} & 0 \\ a_{13,1} & 0 & 0 & 0 & 0 & 0 & 0 & 0 & 0 & 0 & 0 & 0 & a_{13,13} \end{bmatrix}$$

$a_{1,7} = ki_{pll}$, $a_{1,13} = kp_{pll}$, $a_{2,9} = 1$, $a_{3,2} = ki_V$,

$a_{3,9} = kp_V$,$a_{3,10} = -1$, $a_{4,11} = -1$, $a_{4,12} = -\frac{{Q_0}^*}{V_{GD,0}^2}$,

$a_{5,1} = -\frac{1}{L_{ft}}(-V_{gD,0}sin(s_0) + V_{gQ,0}cos(s_0))$, $a_{5,2} = \frac{1}{L_{ft}kp_{id}ki_V}$

$a_{5,3} = \frac{1}{L_ft}ki_{id}$, $a_{5,6} = \omega_{g,0}$, $a_{5,9} = \frac{1}{L_{ft}}kp_{id}kp_V$, $a_{5,10} = -\frac{1}{L_{ft}}kp_{id}$

$a_{5,11} = -\omega_n$, $a_{5,12} = \frac{1}{L_{ft}}$, $a_{6,1} = -\frac{1}{L_{ft}}(-V_{gD,0}cos(s_0) - V_{gQ,0}sin(s_0))$

$a_{6,4} = \frac{1}{L_{ft}}ki_{iq}$, $a6,5 = -\omega_{g,0}$, $a6,10 = \omega_n$, $a_{6,11} = -\frac{1}{L_{ft}}kp_{iq}$

$a_{6,12} = \frac{1}{L_{ft}}kp_{iq}(-{Q_0}^2/V_{GD,0}^2)$, $a_{6,13} = \frac{1}{L_{ft}}$, $a_{7,13} = 1$, $a_{8,8} = -\omega_p$

$a_{9,1} = -(-V_{gD,0}sin(s_0)+V_{gQ,0}cos(s_0))\frac{i_{od,0}}{C_{DC}V_{DC,0}} - (-V_{gD,0}cos(s_0)-V_{gQ,0}sin(s_0))\frac{i_{oq,0}}{C_{DC}V_{DC,0}}$

$a_{9,5} = -\frac{v_{gd,0}}{C_{DC}V_{DC,0}}$, $a_{9,6} = -\frac{v_{gq,0}}{C_{DC}V_{DC,0}}$, $a_{9,8} = \frac{1}{C_{DC}V_{DC,0}}$, $a_{9,9} = \frac{{P_0}^*}{C_{DC}V_{DC,0}^2} - \frac{v_{gd,0}i_{od,0} + v_{gq,0}i_{oq,0}}{C_{DC} * V_{DC,0}^2}$

$a_{10,5} = \omega_{mi}$, $a_{10,10} = -\omega_{mi}$, $a_{11,6} = \omega_{mi}$, $a_{11,11} = -\omega_{mi}$

$a_{12,1} = (-V_{gD,0}sin(s_0) + V_{gQ,0}cos(s_0))\omega_{mv}$, $a_{12,12} = -\omega_{mv}$

$a_{13,1} = (-V_{gD,0}cos(s_0) - V_{gQ,0}sin(s_0))\omega_{mv}$, $a_{13,13} = -\omega_{mv}$

$$B = \begin{bmatrix} 0 & 0 & 0 & 0 & b_{1,5} & 0 \\ 0 & 0 & 0 & 0 & 0 & b_{2,6} \\ 0 & 0 & 0 & 0 & 0 & b_{3,6} \\ 0 & b_{4,2} & 0 & 0 & 0 & 0 \\ 0 & 0 & b_{5,3} & b_{5,4} & b_{5,5} & b_{5,6} \\ 0 & b_{6,2} & b_{6,3} & b_{6,4} & b_{6,5} & 0 \\ 0 & 0 & 0 & 0 & 0 & 0 \\ b_{8,1} & 0 & 0 & 0 & 0 & 0 \\ b_{9,1} & 0 & b_{9,3} & b_{9,4} & 0 & 0 \\ 0 & 0 & 0 & 0 & 0 & 0 \\ 0 & 0 & 0 & 0 & 0 & 0 \\ 0 & 0 & b_{12,3} & b_{12,4} & 0 & 0 \\ 0 & 0 & b_{13,3} & b_{13,4} & 0 & 0 \end{bmatrix}$$

$b_{1,5} = -1$, $b_{2,6} = -1$, $b_{3,6} = -kp_V$, $b_{4,2} = -\dfrac{1}{V_{GD,0}}$

$b_{5,3} = -\dfrac{1}{L_{ft}cos(s_0)}$, $b_{5,4} = -\dfrac{1}{L_{ft}sin(s_0)}$, $b_{5,5} = i_{oq,0}$

$b_{5,6} = -kp_V * kp_{id}\dfrac{1}{L_{ft}}$, $b_{6,2} = \dfrac{1}{L_{ft}}kp_{iq} - \dfrac{1}{V_{GD,0}}$

$b_{6,3} = \dfrac{1}{L_{ft}}sin(s_0)$, $b_{6,4} = -\dfrac{1}{L_{ft}}cos(s_0)$, $b_{6,5} = -i_{od,0}$

$b_{8,1} = \omega_p$, $b_{9,1} = -(\dfrac{i_{od,0}cos(s_0)}{C_{DC}V_{DC,0}} - \dfrac{i_{oq,0}sin(s_0)}{C_{DC} * V_{DC,0}})$

$b_{9,3} = -(\dfrac{i_{od,0}sin(s_0)}{C_{DC}V_{DC,0}} + \dfrac{i_{oq,0}cos(s_0)}{C_{DC}V_{DC,0}})$, $b_{9,4} = \dfrac{1}{C_{DC}V_{DC,0}}$,

$b_{12,3} = \omega_{mv}cos(s_0)$, $b_{12,4} = \omega_{mv}sin(s_0)$

$b_{13,3} = -\omega_{mv}sin(s_0)$, $b_{13,4} = \omega_{mv}cos(s_0)$

$$C = \begin{bmatrix} c_{1,1} & 0 & 0 & 0 & c_{1,6} & c_{1,7} & 0 & 0 & 0 & 0 & 0 & 0 & 0 \\ c_{1,2} & 0 & 0 & 0 & c_{2,6} & c_{2,7} & 0 & 0 & 0 & 0 & 0 & 0 & 0 \end{bmatrix}$$

$c_{1,1} = (-i_{od,0}sin(s_0) - i_{oq0}cos(s_0))\frac{P_{base,unit}}{P_{base,global}}$, $c_{1,6} = cos(s_0)\frac{P_{base,unit}}{P_{base,global}}$, $c_{1,7} = -sin(s_0)\frac{P_{base,unit}}{P_{base,global}}$

$c_{1,2} = (i_{od,0}cos(s_0) - i_{oq,0}sin(s_0))\frac{P_{base,unit}}{P_{base,global}}$, $c_{2,6} = sin(s_0)\frac{P_{base,unit}}{P_{base,global}}$, $c_{2,7} = cos(s_0)\frac{P_{base,unit}}{P_{base,global}}$

B.3 State space matrixes for BESS model

$$A = \begin{bmatrix} a_{1,1} & 0 & 0 & 0 & 0 & 0 & 0 & 0 & a_{1,9} & a_{1,10} & a_{1,11} & a_{1,12} \\ 0 & a_{2,2} & 0 & 0 & 0 & 0 & 0 & 0 & a_{2,9} & a_{2,10} & a_{2,11} & a_{2,12} \\ 0 & a_{3,2} & 0 & 0 & 0 & 0 & 0 & 0 & a_{3,9} & 0 & 0 & 0 \\ 0 & 0 & 0 & 0 & 0 & 0 & 0 & 0 & 0 & a_{4,10} & 0 & 0 \\ 0 & a_{5,2} & a_{5,3} & 0 & 0 & 0 & 0 & 0 & a_{5,9} & 0 & a_{5,11} & 0 \\ 0 & 0 & 0 & a_{6,4} & 0 & 0 & 0 & 0 & 0 & a_{6,10} & 0 & a_{6,12} \\ 0 & a_{7,2} & a_{7,3} & 0 & a_{7,5} & 0 & 0 & a_{7,8} & a_{7,9} & 0 & a_{7,11} & a_{7,12} \\ 0 & 0 & 0 & a_{8,4} & 0 & a_{8,6} & a_{8,7} & 0 & 0 & a_{8,1} & a_{8,11} & a_{8,12} \\ 0 & 0 & 0 & 0 & 0 & 0 & 0 & 0 & a_{9,9} & 0 & 0 & 0 \\ 0 & 0 & 0 & 0 & 0 & 0 & 0 & 0 & 0 & a_{10,10} & 0 & 0 \\ 0 & 0 & 0 & 0 & 0 & 0 & a_{11,7} & 0 & 0 & 0 & a_{11,11} & 0 \\ 0 & 0 & 0 & 0 & 0 & 0 & 0 & a_{12,8} & 0 & 0 & 0 & a_{12,12} \end{bmatrix}$$

$a_{1,1} = -\omega_c$, $a_{1,9} = \omega_c I_{od,0}$, $a_{1,10} = \omega_c I_{oq,0}$, $a_{1,11} = \omega_c v_{gd,0}$

$a_{1,12} = \omega_c v_{gq,0}$, $a_{2,2} = -\omega_c$, $a_{2,9} = -\omega_c I_{oq,0}$

$a_{2,10} = \omega_c I_{od,0}$, $a_{2,11} = \omega_c v_{gq,0}$, $a_{2,12} = -\omega_c v_{gd,0}$

$a_{3,2} = -n_v$, $a_{3,9} = -1$, $a_{4,10} = -1$, $a_{5,2} = -n_v kp_{id}$

$a_{5,3} = ki_{vd}$, $a_{5,9} = -kp_{vd}$, $a_{5,11} = -1$

$a_{6,4} = ki_{vq}$, $a_{6,10} = -kp_{vq}$, $a_{6,12} = -1$

$a_{7,2} = -\frac{1}{L_{ft}} kp_{id} kp_{vd} n_v$, $a_{7,3} = \frac{1}{L_{ft}} kp_{id} ki_{vd}$, $a_{7,5} = \frac{1}{L_{ft}} ki_{id}$

$a_{7,8} = \omega_{g,0}$, $a_{7,9} = \frac{1}{L_{ft}} - kp_{id}\frac{1}{L_{ft}} kp_{vd}$, $a_{7,11} = -\frac{1}{L_{ft}} kp_{id}$

$a_{7,12} = -\omega_n$, $a_{8,4} = \frac{1}{L_{ft}} kp_{iq} ki_{vq}$, $a_{8,6} = \frac{1}{L_{ft}} ki_{iq}$, $a_{8,7} = -\omega_{g,0}$

$a_{8,10} = \frac{1}{L_{ft}} - \frac{1}{L_{ft}} kp_{iq} kp_{vq}$, $a_{8,11} = \omega_n$, $a_{8,12} = -\frac{1}{L_{ft}} kp_{iq}$

$a_{9,9} = -\omega_{mv}$, $a_{10,10} = -\omega_{mv}$, $a_{11,7} = \omega_{mi}$, $a_{11,11} = -\omega_{mi}$,

$a_{12,8} = \omega_{mi}$, $a_{12,12} = -\omega_{mi}$

$$B = \begin{bmatrix} 0 & 0 & 0 & 0 & 0 & 0 & 0 \\ 0 & 0 & 0 & 0 & 0 & 0 & 0 \\ 0 & 0 & b_{3,3} & b_{3,4} & 0 & 0 & 0 \\ 0 & 0 & 0 & 0 & 0 & 0 & 0 \\ 0 & 0 & b_{5,3} & b_{5,4} & 0 & 0 & 0 \\ 0 & 0 & 0 & 0 & 0 & 0 & 0 \\ 0 & 0 & b_{7,3} & b_{7,4} & b_{7,5} & 0 & b_{7,7} \\ 0 & 0 & 0 & 0 & 0 & b_{8,6} & b_{8,7} \\ 0 & 0 & 0 & 0 & b_{9,5} & 0 & 0 \\ 0 & 0 & 0 & 0 & 0 & b_{10,6} & 0 \\ 0 & 0 & 0 & 0 & 0 & 0 & 0 \\ 0 & 0 & 0 & 0 & 0 & 0 & 0 \end{bmatrix}$$

$b_{3,3} = n_v$, $b_{3,4} = 1$, $b_{5,3} = kp_{vd} n_v$, $b_{5,4} = kp_{vd}$

$b_{7,3} = \frac{1}{L_{ft}} kp_{id} kp_{vd} n_v$, $b_{7,4} = \frac{1}{L_{ft}} kp_{id} kp_{vd}$, $b_{7,5} = -\frac{1}{L_{ft}}$, $b_{7,7} = i_{oq,0}$

$b_{8,6} = -\frac{1}{L_{ft}}$, $b_{8,7} = -i_{od,0}$, $b_{9,5} = \omega_{mv}$, $b_{10,6} = \omega_{mv}$

$$C = \begin{bmatrix} c_{1,1} & 0 & 0 & 0 & 0 & 0 & 0 & 0 & 0 & 0 & 00 & \\ 0 & 0 & 0 & 0 & 0 & 0 & c_{2,11} & 0 & 0 & 0 & 0 & 0 \\ 0 & 0 & 0 & 0 & 0 & 0 & 0 & c_{3,12} & 0 & 0 & 0 & 0 \end{bmatrix}$$

$c_{1,1} = -m_f$, $c_{2,11} = 1$, $c_{3,12} = 1$

$$D = \begin{bmatrix} d_{1,1} & d_{1,2} & 0 & 0 & 0 & 0 & 0 \\ 0 & 0 & 0 & 0 & 0 & 0 & 0 \\ 0 & 0 & 0 & 0 & 0 & 0 & 0 \end{bmatrix}$$

$d_{1,1} = 1$, $d_{1,2} = m_f$

B.4 State space matrixes for DG model and constants

The three models (Governor, Generator and AVR) are assembled in the following A, B and C matrices. The A matrix has been broken into sub-blocks as in B.1. Where each matrix is products of the C and B matrices that goes from having input/outputs to being closed resulting in the total A-matrix. The notation and subscribes applied for a connection between the diesel engine and the synchronous generator, is $Q_{de,sg}$, while if an entrance for example 1,3 from the diesel engine input matrix is used, the notation $B_{de1,3}$ is applied. The sub-blocks of A_{DG} is found in B.2 to B.4

$$A_{DGS} = \begin{bmatrix} A_{SG}^{6\times6} & Q_{de,sg}^{6\times4} & Q_{avr,sg}^{6\times2} \\ Q_{sg,de}^{4\times6} & A_{DE}^{4\times4} & 0^{4\times2} \\ 0^{2\times6} & 0^{2\times4} & A_{AVR}^{2\times2} \end{bmatrix} \tag{B.1}$$

$$Q_{sg,de} = \begin{bmatrix} 0 & 0 & 0 & 0 & 0 & 0 \\ 0 & 0 & 0 & 0 & 0 & 0 \\ 0 & 0 & 0 & 0 & 0 & B_{de1,3} \\ 0 & 0 & 0 & 0 & 0 & B_{de4,1} \end{bmatrix} \tag{B.2}$$

$$Q_{de,sg} = \begin{bmatrix} 0 & 0 & 0 & 0 \\ 0 & 0 & 0 & 0 \\ 0 & 0 & 0 & 0 \\ 0 & 0 & 0 & 0 \\ 0 & 0 & 0 & 0 \\ B_{sg6,6} \cdot C_{de1} & 0 & 0 & 0 \end{bmatrix} \tag{B.3}$$

$$Q_{avr,sg} = \begin{bmatrix} -B_{sg1,2} \cdot C_{avr1,1} & -B_{sg1,2} \cdot C_{avr2,1} \\ -B_{sg2,2} \cdot C_{avr1,1} & -B_{sg2,2} \cdot C_{avr2,1} \\ -B_{sg3,2} \cdot C_{avr1,1} & -B_{sg3,2} \cdot C_{avr2,1} \\ 0 & 0 \\ 0 & 0 \\ 0 & 0 \end{bmatrix} \tag{B.4}$$

The B matrix is shown in B.5

$$B_{DGS} = \begin{bmatrix} B_{sg1,1} \cdot H_1 & B_{sg1,2} \cdot H_2 & 0 & 0 & 0 & 0 \\ B_{sg2,1} \cdot H_1 & B_{sg2,2} \cdot H_2 & 0 & 0 & 0 & 0 \\ B_{sg3,1} \cdot H_1 & B_{sg3,2} \cdot H_2 & 0 & 0 & 0 & 0 \\ B_{sg4,1} \cdot H_3 & B_{sg4,2} \cdot H_4 & 0 & 0 & 0 & 0 \\ B_{sg5,1} \cdot H_3 & B_{sg5,2} \cdot H_4 & 0 & 0 & 0 & 0 \\ 0 & 0 & 0 & 0 & 0 & 0 \\ 0 & 0 & 0 & 0 & 0 & 0 \\ 0 & 0 & 0 & 0 & 0 & 0 \\ 0 & 0 & 0 & B_{de3,2} & B_{de3,3} & 0 \\ 0 & 0 & 0 & B_{de4,2} & B_{de4,3} & 0 \\ 0 & 0 & 0 & 0 & 0 & 0 \\ B_{dg12,1} & B_{dg12,2} & 1 & 0 & 0 & 1 \end{bmatrix} \tag{B.5}$$

Where H_1, H_2, H_3, H_4, is the entrances of the transformation matrix as in B.6.

$$P_{dq-qd} = \sqrt{3} \begin{bmatrix} cos(-\pi/2 - (\delta - \beta) - \delta_{grid}) & -sin(-\pi/2 - (\delta - \beta) - \delta_{grid}) \\ -sin(-\pi/2 - (\delta - \beta) - \delta_{grid}) & -cos(-\pi/2 - (\delta - \beta) - \delta_{grid}) \end{bmatrix} = \begin{bmatrix} H_1 & H_2 \\ H_3 & H_4 \end{bmatrix} \tag{B.6}$$

The C matrix is shown in B.7

$$C_{DGS} = \begin{bmatrix} C_1 & 0 & 0 & C_2 & 0 & 0 & 0 & 0 & 0 & 0 & 0 & 0 \\ C_3 & 0 & 0 & C_4 & 0 & 0 & 0 & 0 & 0 & 0 & 0 & 0 \\ 0 & 0 & 0 & 0 & 0 & 1 & 0 & 0 & 0 & 0 & 0 & 0 \end{bmatrix} \tag{B.7}$$

Where C_1, C_2, C_3, C_4, is the entrances of the inverse transformation matrix shown in B.8.

$$P^{-1}_{dq-qd} = \frac{1}{\sqrt{3}} \begin{bmatrix} cos(-\pi/2 - (\delta - \beta) - \delta_{grid}) & -sin(-\pi/2 - (\delta - \beta) - \delta_{grid}) \\ -sin(-\pi/2 - (\delta - \beta) - \delta_{grid}) & -cos(-\pi/2 - (\delta - \beta) - \delta_{grid}) \end{bmatrix} = \begin{bmatrix} C_1 & C_2 \\ C_3 & C_4 \end{bmatrix} \tag{B.8}$$

B.4.1 Constants of the K and M Matrix

$l_d = x_l$, $l_q = x_l$, $L_d = x_d$, $L_q = x_q$, $L^*_d = x^*_d$, $L^{**}_d = x^{**}_d$, $L^{**}_q = x^{**}_q$, $L^*_q = x^*_q$

$L_{AD} = L_d - l_d$, $k_{MF} = L_{AD}$, $k_{MD} = L_{AD}$, $M_R = L_{AD}$, $L_{AQ} = L_q - l_q$

$k_{MQ} = L_{AQ}$, $l_F = L_{AD} \cdot \frac{L_d^* - l_d}{L_d - L_d^*}$, $L_F = l_F + L_{AD}$, $l_D = L_{AD} \cdot l_F \cdot \frac{L_d^{**} - l_d}{L_{AD} \cdot l_F - L_F \cdot (L_d^{**} - l_d)}$

$l_Q = L_{AQ} \cdot \frac{L_q^{**} - l_q}{L_q - L_q^{**}}$, $L_{AQ} = L_q - l_q$, $L_D = l_D + L_{AD}$, $L_Q = L_{AQ} + l_Q$

$r_s = r_{120} = rs * \frac{234.5+120}{234.5+20}$, $r_F = \frac{L_F}{T_{do}^*}$, $r_D = \frac{(L_D \cdot L_F - L_{AD}^2) \cdot L_d^{**}}{T_d^{**} \cdot L_F \cdot L_d^*}$, $r_Q = L_q^{**} \cdot \frac{L_Q}{L_q \cdot T_q^{**}}$

B.5 Model initialization

WT & PV

The models are initialized assuming the PLL has settled meaning in local frame $v_{oq} = 0$. Therefore given initial inputs P_0, Q_0 and v_{od} equal to bus voltage magnitude. The initial currents are calculated as:

$$i_{od,0} = \frac{P_0}{V_{od}} \quad i_{oq,0} = \frac{Q_0}{-V_{od}} \tag{B.9}$$

The DC-link is considered balanced initially $V_{DC,0} = 1p.u.$. The reference frame transformation is initialized with $s_0 = tan^{-1}(v_{gq,0}^{global} / v_{gd,0}^{global})$. The outputs of all LPF are initially set equal to the inputs so eq. $V_{GD,0} = v_{gd,0}$.

BESS

The BESS is initialized similarly to the PV and WT model using equation (B.9), given initial v_{od}, P_0 and Q_0 further it is assumed $v_{oq} = 0$.

Diesel Generator

For the initialization 3 values must be determined to start the initialization, u_{t0}, PF, P_0, δ_{grid}, terminal voltage magnitude, power factor, initial loading and bus voltage angle.

$\phi = cos^{-1}(PF)$, $i_{t0} = \frac{P_0}{PF \cdot u_{t0}}$, $I_r = it0 \cdot cos(\phi)$, $I_x = i_{t0} \cdot sin(-\phi)$

$\delta - \beta = tan^{-1} \frac{x_q \cdot I_r + r_s * Ix}{u_{t0} + r_s \cdot I_r - x_q \cdot I_x}$, $V_{d0} = -u_{t0} \cdot sin(\delta - \beta)$

$v_{d0} = \sqrt{3} * V_{d0}$, $V_{q0} = u_{t0} * cos(\delta - \beta)$, $v_{q0} = \sqrt{3} \cdot V_{q0}$, $I_{d0} = -it0 * sin(\delta - \beta + \phi)$

$i_{d0} = \sqrt{3} * I_{d0}$, $I_{q0} = i_{t0} \cdot cos(\delta - \beta + \phi)$, $i_{q0} = \sqrt{3} * I_{q0}$

$E_{fd} = V_{q0} + r_s \cdot I_{q0} - x_d \cdot I_{d0}$, $i_F = \sqrt{3} \frac{E_{fd}}{L_{AD}}$, $\lambda_{d0} = L_d \cdot i_{d0} + k_{MF} \cdot i_F$, $\lambda_{q0} = \frac{L_q}{i_{q0}}$, $\omega_0 = 1$

Control Theory and Analysis Results

C

C.1 Stability Analysis

In [Kundur, 1994], Kundur describes small signal stability as *"the ability of the power system to maintain synchronism when subject to small disturbances"*, which is what will be analysed in this section. An unstable system would therefore be, when the small changes results in oscillations of increasing amplitude. The system will be analysed around an equilibrium point. This is a point where all the derivatives of the states are simultaneously zero. Such a point can be obtained by a load flow solver, in this project a Newton-Rhapson load flow solver is used to estimate these points. It should be noted, that a non-linear system, such as the one considered here, will have multiple isolated equilibrium states, each with distinctive stability properties.

Local stability is when the system remains stable after small perturbations. Finite stability, is when the system remains stable within a finite region R. In both cases, if the system returns back to its initial state when $t \rightarrow \infty$ it is called asymptotically stable, either locally or in a finite region R.

There are several ways to check whether the system is asymptotically stable or not. One way is to analyse the poles of the system, which will be equal to the eigenvalues of the state matrix [Kundur, 1994].

- If the state matrix eigenvalues have negative real parts, the system is said to be asymptotically stable.

This method cannot be used in cases where one or more eigenvalues have real parts equal to zero. In this case, the direct method, also called Lyapunov's second method, can be used.

- If a positive definite Lyapunov function $V(x_1, x_2, ..., x_n)$ exists and its total

derivative with respect to $\dot{x} = f(x, u)$ is negative semi-definite, then the system is stable, if negative definite the system is asymptotically stable

This can be clarified in a more intuitive way as done in [Williams and Lawrence, 2007]: *For any symmetric positive definite matrix Q, the Lyapunov matrix equation*

$$A^T P + PA = -Q$$

has a unique symmetric positive definite solution P if and only if A is asymptotically stable. In order to check this, Q is usually chosen to be an identity matrix, which obviously is positive definite and symmetric. Then P is found and it is checked whether the system symmetric matrix is positive definite or not. Positive definiteness can be concluded by Sylvester's Criterion which says that if the submatrix determinants

$$p_{11} \quad \begin{vmatrix} p_{11} & p_{12} \\ p_{12} & p_{22} \end{vmatrix} \quad \begin{vmatrix} p_{11} & p_{12} & p_{13} \\ p_{12} & p_{22} & p_{23} \\ p_{13} & p_{23} & p_{33} \end{vmatrix} \quad \cdots \quad \begin{vmatrix} p_{11} & p_{12} & \cdots & p_{1n} \\ p_{12} & p_{22} & \cdots & p_{2n} \\ \vdots & \vdots & \ddots & \vdots \\ p_{1n} & p_{2n} & \cdots & p_{nn} \end{vmatrix}$$

are all positive, then the matrix is positive definite [Williams and Lawrence, 2007].

C.2 Participation Factor

The participation matrix can be found for the system, which will reveal the amount of influence each state has on the eigenvalues. This matrix can be found as shown in Equation C.1, where n is the number of states.

$$P = [P_1 \ P_2 \ ... \ P_n] \tag{C.1}$$

(C.2)

$$p_i = \begin{bmatrix} p_{1i} \\ p_{2i} \\ ... \\ p_{ni} \end{bmatrix} = \begin{bmatrix} \phi_{1i}\psi_{i1} \\ \phi_{2i}\psi_{i2} \\ ... \\ \phi_{ni}\psi_{in} \end{bmatrix}$$

This will produce a matrix with participation factors given as $p_{ki} = \frac{\delta\lambda_i}{\delta a_{kk}}$, which tells how sensitive the eigenvalue is to the diagonal elements of the state matrix.

C.3 Results

The following tables are firstly presented for the nominal cases, where the eigenvalues should be negative or zero. After this, tables will be given for the operating range interval, and how the frequency of the eigenvalues vary in this range.

Nominal operating point:

Table C.1: Eigenvalue (in increasing order), natural frequency, damping ratio and time constant of the WT system matrix at equilibrium point with nominal power and PF=0.9

λ_{no}	λ	f_n $[p.u.]$	f _n $[Hz]$	ζ	τ $[s]$	Origin
λ_1	-595.5+1.008i	94.77	$29.78e^3$	1	$5.346e^{-6}$	ω_{mi}
λ_2	-595.5-1.008i	94.77	$29.78e^3$	1	$5.346e^{-6}$	ω_{mi}
λ_3	-200.0+0.000i	31.83	$10.00e^3$	1	$15.92e^{-6}$	ω_{mv}
λ_4	-194.6+0.000i	31.83	$9.730e^3$	1	$15.92e^{-6}$	ω_{mv}
λ_5	-5.443+0.000i	$866.3e^{-3}$	272.2	1	$584.8e^{-6}$	-
λ_6	-4.488+0.000i	$714.2e^{-3}$	224.4	0.7485	$94.76e^{-3}$	-
λ_7	-2.133+1.889i	$453.5e^{-3}$	142.5	0.7485	$1.493e^{-3}$	L_{fc}
λ_8	-2.133-1.889i	$453.5e^{-3}$	142.5	1	$1.117e^{-3}$	L_{fc}
λ_9	-0.2234+0.000i	$35.56e^{-3}$	11.17	1	$14.25e^{-3}$	V_dc control
λ_{10}	-0.045459+0.000i	$7.235e^{-3}$	2.273	1	$70.02e^{-3}$	I_d
λ_{11}	-0.04500+0.000i	$7.162e^{-3}$	2.250	1	$70.73e^{-3}$	I_q
λ_{12}	-0.02+0.000i	$3.183e^{-3}$	1	1	$159e^{-3}$	ω_p
λ_{13}	$-6.136e^{-6}$+0.000i	$97.68e^{-6}$	$30.69e^{-3}$	1	518.8	PLL

Table C.2: Eigenvalue (in increasing order), natural frequency, damping ratio and time constant of the PV system matrix at equilibrium point with nominal power and PF=0.9

λ_{no}	λ	f_n $[p.u.]$	f _n $[Hz]$	ζ	τ $[s]$	Origin
λ_1	-595.5+1.008i	94.77	$29.78e^3$	1	$5.346e^{-6}$	ω_{mi}
λ_2	-595.5-1.008i	94.77	$29.78e^3$	1	$5.346e^{-6}$	ω_{mi}
λ_3	-200.0+0.000i	31.83	$10.00e^3$	1	$15.92e^{-6}$	ω_{mv}
λ_4	-194.6+0.000i	31.83	$9.730e^3$	1	$15.92e^{-6}$	ω_{mv}
λ_5	-5.443+0.000i	$866.3e^{-3}$	272.2	1	$584.8e^{-6}$	-
λ_6	-4.488+0.000i	$714.2e^{-3}$	224.4	0.7485	$94.76e^{-3}$	-
λ_7	-2.133+1.889i	$453.5e^{-3}$	142.5	0.7485	$1.493e^{-3}$	L_{fc}
λ_8	-2.133-1.889i	$453.5e^{-3}$	142.5	1	$1.117e^{-3}$	L_{fc}
λ_9	-0.2234+0.000i	$35.56e^{-3}$	11.17	1	$14.25e^{-3}$	V_dc control
λ_{10}	-0.045459+0.000i	$7.235e^{-3}$	2.273	1	$70.02e^{-3}$	I_d
λ_{11}	-0.04500+0.000i	$7.162e^{-3}$	2.250	1	$70.73e^{-3}$	I_q
λ_{12}	-0.002+0.000i	$0.3183e^{-3}$	0.1	1	1.59	ω_p
λ_{13}	$-6.136e^{-6}$+0.000i	$97.68e^{-6}$	$30.69e^{-3}$	1	518.8	PLL

Table C.3: Eigenvalue (in increasing order), natural frequency, damping ratio and time constant of the Battery system matrix at equilibrium point with nominal power and PF=0.9

λ_{no}	λ	f_n $[p.u.]$	f _n $[Hz]$	ζ	τ $[s]$	Origin
λ_1	-595.5+1.008i	94.77	$29.78e^3$	1	$5.346e^{-6}$	ω_{mi}
λ_2	-595.5+1.008i	94.77	$29.78e^3$	1	$5.346e^{-6}$	ω_{mi}
λ_3	-200.0+0.000i	31.83	$10.00e^3$	1	$15.92e^{-6}$	ω_{mv}
λ_4	-200.0-0.000i	31.83	$10.00e^3$	1	$15.92e^{-6}$	ω_{mv}
λ_5	$-4.488+7.660e^{-3}$i	$714.3e^{-3}$	224.4	1	$709.2e^{-6}$	Output Filter
λ_6	$-4.488-7.660e^{-3}$i	$714.3e^{-3}$	224.4	1	$709.2e^{-6}$	Output Filter
λ_7	-0.2000+0.000i	$31.83e^{-3}$	10.00	1	$15.92e^{-3}$	I_d
λ_8	-0.2000-0.000i	$31.83e^{-3}$	10.00	1	$15.92e^{-3}$	I_q
λ_9	$-45.46e^{-3}+3.460e^{-6}$i	$7.235e^{-3}$	2.273	1	$70.02e^{-3}$	Output Filter
λ_{10}	$-45.46e^{-3}-3.460e^{-6}$i	$7.235e^{-3}$	2.273	1	$70.02e^{-3}$	Output Filter
λ_{11}	0	0	0	1	-Inf	-
λ_{12}	0	0	0	1	-Inf	-

Table C.4: Eigenvalue (in increasing order), natural frequency, damping ratio and time constant of the diesel genset system matrix at equilibrium point with nominal power and PF=0.9

λ_{no}	λ	f_n $[p.u.]$	f_n $[Hz]$	ζ	τ	Origin
λ_1	-15.92+0.000i	2.533	795.45	1	$0.2000e^{-3}$	T_A (GOV)
λ_2	-5.258+0.000i	0.8369	262.9	1	$0.6054e^{-3}$	AVR
λ_3	-0.6583+0.8905i	0.1763	55.37	0.5945	$4.835e^{-3}$	SG
λ_4	-0.6583-0.8905i	0.1763	55.37	0.5945	$4.835e^{-3}$	SG
λ_5	-0.8359+0.000i	0.1330	41.80	1	$3.808e^{-3}$	K_I (GOV)
λ_6	-0.2833+0.1056i	$48.12e^{-3}$	15.12	0.9371	$11.23e^{-3}$	SG
λ_7	-0.2833-0.1056i	$48.12e^{-3}$	15.12	0.9371	$11.23e^{-3}$	SG
λ_8	-0.07794+0.1279i	$23.83e^{-3}$	7.490	0.5205	$40.84e^{-3}$	GOV
λ_9	-0.07794-0.1279i	$23.83e^{-3}$	7.490	0.5205	$40.84e^{-3}$	GOV
λ_{10}	-0.05962+0.000i	$9.488e^{-3}$	2.981	1	$53.39e^{-3}$	SG
λ_{11}	-0.01358+0.000i	$2.160e^{-3}$	0.6786	1	$234.5e^{-3}$	SG
λ_{12}	$-0.1927e^{-3}$+0.000i	$30.67e^{-6}$	$9.635e^{-3}$	1	16.52	AVR

Percentage change of eigenvalues in the operating range:

Table C.5: The percentage change of the eigenvalues (in the same order as above) when subject to V, PF and P changes. The colour red indicates the critical changes, that might lead to instability

	C1-C2: V Sweep				C1-C3: PF Sweep				C1-C5 P Sweep			
λ_{no}	BESS	DG	WT	PV	BESS	DG	WT	PV	BESS	DG	WT	PV
λ_1	0	0	0	0	0	0	0	0	0	0	0	0
λ_2	0	0	0	0	0	0	0	0	0	0	0	0
λ_3	0	0,49	0	0	0	0	0	0	0	0,14	0	0
λ_4	0	0,49	-0,31	-0,31	0	0	0	0	0	0,14	0	0
λ_5	0	1,93	36,67	36,67	0	0	0	0	0	-0,02	0	0
λ_6	0	0,01	0	0	0	0	0	0	0	-1,08	0	0
λ_7	0	1,15	15,8	15,77	0	0	0	0	0	-1,08	0	0
λ_8	0	1,15	15,8	15,77	0	0	0	0	0	6,73	0	0
λ_9	0	1,93	-4,2	-4,17	0	0	0	0	0	6,73	0	0
λ_{10}	0	-22,55	0	0	0	0	0	0	0	-55,25	0	0
λ_{11}	0	12,31	0	0	0	0	0	0	0	27,36	0	0
λ_{12}	0	0	0	0	0	0	0	0	0	0	0	0
λ_{13}	-	-	-0,01	-0,01	-	-	0	0	-	-	0	0

The other cases are not depicted as they show the same tendencies and deviations, and the highest changes are seen in this Table. A big change in the lower part of the table (which depicts the eigenvalues closest to 0) will be more severe than changes in the upper part of the table. It is therefore clear that the red coloured parts may be critical for stability. It is clear, that PF do not change the eigenvalues. Only the Diesel Genset is susceptible to P change, since the PV, WT and BAT are based on power electronics and hence can operate efficiently and fast in almost the whole range of loading. This is however not true for the genset, as it will be most efficient at its nominal operating point. The voltage has an influence on the all the units.

The whole system matrix

The eigenvalues of the microgrid system matrix is given in Table C.6.

Table C.6: The eigenvalues of the total microgrid system state matrix A_{mg}

λ	Eigenvalues	λ	Eigenvalues
1	-0.2 + 0i	32	-2.1313 + 1.8518i
2	-1.451e+09 + 0.99132i	33	-2.1313 - 1.8518i
3	-1.451e+09 - 0.99132i	34	-2.5564 + 0.9068i
4	-4.8247e+08 + 0.9795i	35	-2.5564 - 0.9068i
5	-4.8247e+08 - 0.9795i	36	-4.3287 + 0i
6	-3.7813e+08 + 0i	37	-4.5085 + 0.0086567i
7	-3.782e+08 + 0i	38	-4.5085 - 0.0086567i
8	-1.2528e+08 + 0i	39	-4.4893 + 0i
9	-1.255e+08 + 0i	40	-0.83479 + 0i
10	-8.5657e+06 + 0i	41	-0.52435 + 0.49155i
11	-8.6547e+06 + 0i	42	-0.52435 - 0.49155i
12	-1.4358e+06 + 0i	43	-0.26848 + 0.12671i
13	-1.4974e+06 + 0i	44	-0.26848 - 0.12671i
14	-598.27 + 0.37826i	45	-0.076309 + 0.12218i
15	-598.27 - 0.37826i	46	-0.076309 - 0.12218i
16	-595.48 + 1.0035i	47	-0.23409 + 0i
17	-595.48 - 1.0035i	48	-0.21264 + 0i
18	-595.79 + 0.93651i	49	-0.19881 + 0i
19	-595.79 - 0.93651i	50	-0.065805 + 0i
20	-115.01 + 0i	51	-0.013277 + 0i
21	-130.83 + 0i	52	-0.00059973 + 0i
22	-235.34 + 0i	53	-6.1359e-06 + 7.7278e-11i
23	-234.21 + 0i	54	-6.1359e-06 - 7.7278e-11i
24	-199.46 + 0i	55	-0.045459 + 0i
25	-194.03 + 0i	56	-0.045462 + 0i
26	-15.915 + 0i	57	-0.045003 + 0i
27	-6.2139 + 0i	58	-0.045003 + 0i
28	-5.3571 + 0i	59	-0.044997 + 0i
29	-5.2595 + 0i	60	-0.044992 + 0i
30	-2.2382 + 1.8072i	61	-0.2 + 0i
31	-2.2382 - 1.8072i	62	-0.02 + 0i

EV map with new Kpv value:

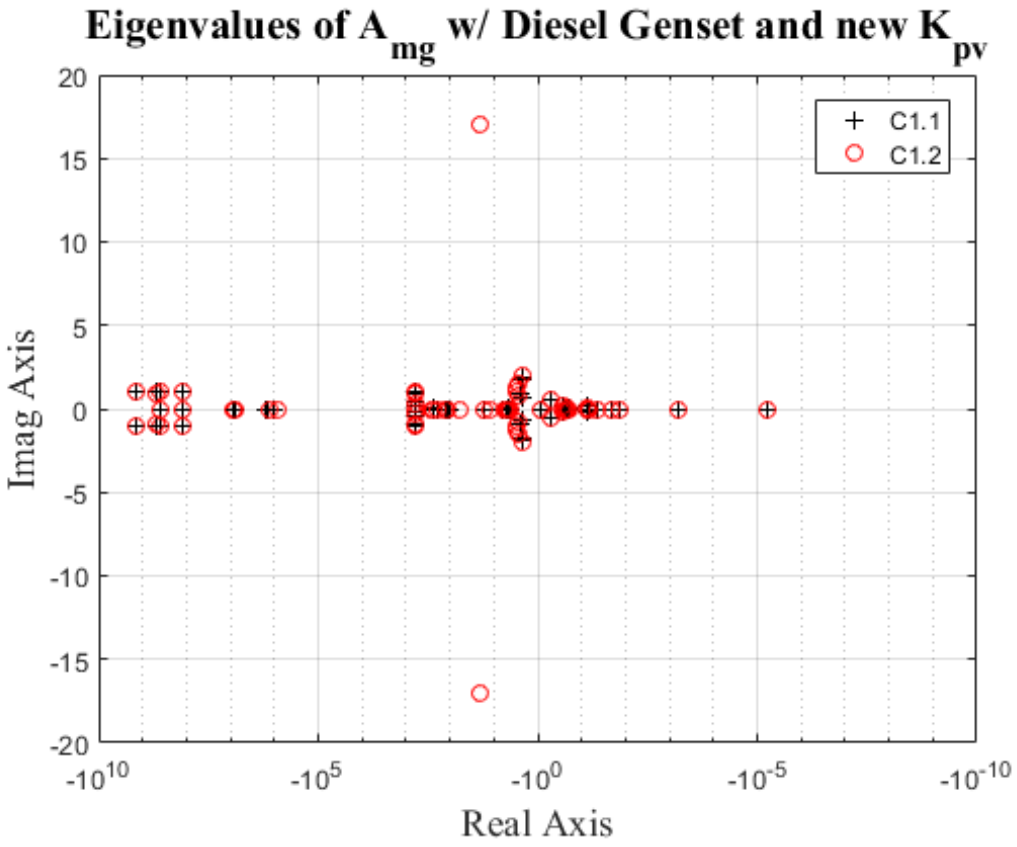

Figure C.1: Logarithmic EV plot for C1.1 and C1.2 with new K_{pv} gain in the voltage controller of the battery.

Voltage Sensitivity Results

The sensitivity matrix for Test 1 is seen in Figure C.3

```
Sresidue =

    0.0465    0.0458    0.0453    0.0018    0.0017   -0.0455   -0.0386   -0.0388   -0.0256   -0.0257
    0.0455    0.0458    0.0453    0.0018    0.0017   -0.0387   -0.0387   -0.0388   -0.0256   -0.0257
    0.0456    0.0458    0.0463    0.0018    0.0018   -0.0387   -0.0386   -0.0455   -0.0256   -0.0257
    0.0063    0.0063    0.0063    0.0077    0.0040   -0.0248   -0.0248   -0.0248   -0.0492   -0.0253
    0.0062    0.0062    0.0062    0.0039    0.0039   -0.0249   -0.0249   -0.0249   -0.0253   -0.0253
    0.0397    0.0327    0.0323    0.0229    0.0239    0.0474    0.0464    0.0463    0.0034    0.0037
    0.0326    0.0328    0.0323    0.0230    0.0240    0.0465    0.0466    0.0465    0.0034    0.0037
    0.0324    0.0326    0.0394    0.0228    0.0239    0.0463    0.0463    0.0472    0.0034    0.0037
    0.0229    0.0230    0.0227    0.0472    0.0240    0.0035    0.0035    0.0034    0.0071    0.0037
    0.0234    0.0235    0.0232    0.0235    0.0245    0.0036    0.0036    0.0035    0.0035    0.0038
```

Figure C.2: Sensitivity matrix test 1.

The sensitivity matrix for Test 2 is seen in Figure C.3

```
Sresidue =

    0.0524    0.0514    0.0513    0.0038    0.0038   -0.0479   -0.0400   -0.0400   -0.0267   -0.0267
    0.0514    0.0514    0.0513    0.0038    0.0038   -0.0400   -0.0400   -0.0400   -0.0267   -0.0267
    0.0514    0.0514    0.0524    0.0038    0.0038   -0.0400   -0.0400   -0.0479   -0.0267   -0.0267
    0.0043    0.0043    0.0043    0.0082    0.0041   -0.0266   -0.0266   -0.0266   -0.0536   -0.0266
    0.0043    0.0043    0.0043    0.0040    0.0040   -0.0266   -0.0266   -0.0266   -0.0266   -0.0266
    0.0472    0.0394    0.0393    0.0268    0.0269    0.0519    0.0509    0.0509    0.0042    0.0042
    0.0394    0.0394    0.0394    0.0268    0.0269    0.0509    0.0509    0.0509    0.0042    0.0042
    0.0394    0.0394    0.0471    0.0268    0.0269    0.0508    0.0509    0.0519    0.0042    0.0042
    0.0268    0.0268    0.0268    0.0534    0.0269    0.0042    0.0042    0.0042    0.0083    0.0042
    0.0268    0.0268    0.0268    0.0269    0.0270    0.0042    0.0042    0.0042    0.0042    0.0042
```

Figure C.3: Sensitivity matrix test 2.

Model Parameters D

In this appendix the parameter values used in the models are listed. The values are given for both state space model and EMT model.

D.1 PV model

The base values used in the model is listed below.

- P_{base} = 40kW
- $V_{base,AC}$ = 400V RMS
- $V_{base,DC}$ = 1000V
- $I_{base} = P_{base}/(\sqrt{3}V_{base,AC}) = 57.735$A
- $Z_{base,AC} = V_{base,AC}^2/P_{base} = 4\Omega$
- $Z_{base,DC} = V_{base,DC}^2/P_{base} = 25\Omega$
- $\omega_{base} = 2\pi 50 = 314.1593\,\mathrm{rad/s}$
- $t_{base} = 1/t_{base} = 0.0032$s
- $\omega_{base,EMT} = 2\pi 50 = 314.1593\,\mathrm{rad/s}$
- $t_{base,EMT}$ =1s
- $L_{base} = Z_{base,AC}/\omega_{base}$ = 12.7mH
- $C_{base} = 1/(Z_{base,DC}\omega_{base})$ = 0.125mF

The values of all model parameters is given in the table below. The values are given in p.u. the only difference between the state space and EMT model, is the state space is in p.u. time while the EMT model is in absolute time, and the EMT model uses real values for C_{dc} and L_{ft}. It should be noted that the gains for the PLL controller found as described in Section 5.2 are meant for real values and must be converted to p.u. to fit the models. The base for the PLL gains is $\frac{\omega_{base}}{\hat{V}_{ph-n}}$, furthermore in the EMT model the output of the PLL must be the actual frequency in rad/s, therefore in the EMT model the gains have been multiplied with ω_{base} after the conversion to p.u.. In the state space model the integral gain Ki_{PLL} must be divided by ω_{base} because the model is running in p.u. time.

Table D.1: PV plant specifications.

Parameter	State space model	EMT model
C_{DC}	42.12	5.4mF
L_{ft}	0.1936	2.3mH
Kp_{idq}	0.8713	0.8713
Ki_{idq}	0.0392	12.3174
Kp_v	84.2532	84.2532
Ki_v	16.8506	$5.2938 \cdot 10^3$
Kp_{PLL}	5.29	1663.4
Ki_{PLL}	$3.24 \cdot 10^{-5}$	3.206
ω_n	1	314.1593rad/s
T_{unit}	5	0.016s
ω_{mv}	200	$3.1416 \cdot 10^3$rad/s
ω_{mi}	600	$6.2832 \cdot 10^3$rad/s

D.2 WT model

The base values used in the model is listed below.

- P_{base} = 80kW
- $V_{base,AC}$ = 400V RMS
- $V_{base,DC}$ = 1000V
- $I_{base} = P_{base}/(\sqrt{3}V_{base,AC}) = 115.47$A
- $Z_{base,AC} = V^2_{base,AC}/P_{base} = 2\Omega$
- $Z_{base,DC} = V^2_{base,DC}/P_{base} = 12.5\Omega$
- $\omega_{base} = 2\pi 50 = 314.1593\,\mathrm{rad/s}$
- $t_{base} = 1/t_{base} = 0.0032$s
- $\omega_{base,EMT} = 2\pi 50 = 314.1593\,\mathrm{rad/s}$
- $t_{base,EMT}$ =1s
- $L_{base} = Z_{base,AC}/\omega_{base}$ = 6.35mH
- $C_{base} = 1/(Z_{base,DC}\omega_{base})$ = 0.25mF

The values of all model parameters is given in the table below. The values are given in p.u. the only difference between the state space and EMT model, is the state space is in p.u. time while the EMT model is in absolute time, and the EMT model uses real values for C_{dc} and L_{ft}. The PLL gains is found as described for the PV.

Table D.2: WT plant specifications.

Parameter	**State space model**	**EMT model**
C_{DC}	42.12	10.7mF
L_{ft}	0.226	1.4mH
Kp_{idq}	1.0169	1.0169
Ki_{idq}	0.0458	14.3759
Kp_v	84.2532	84.2532
Ki_v	16.8506	$5.2938 \cdot 10^3$
Kp_{PLL}	5.29	1663.4
Ki_{PLL}	$3.24 \cdot 10^{-5}$	3.206
ω_n	1	314.1593rad/s
T_{unit}	50	0.16s
ω_{mv}	200	$3.1416 \cdot 10^3$rad/s
ω_{mi}	600	$6.2832 \cdot 10^3$rad/s

D.3 BESS model

The base values used in the model is listed below.

- P_{base} = 80kW
- $V_{base,AC}$ = 400V RMS
- $V_{base,DC}$ = 1000V
- $I_{base} = P_{base}/(\sqrt{3}V_{base,AC}) = 115.47$A
- $Z_{base,AC} = V_{base,AC}^2/P_{base} = 2\Omega$
- $\omega_{base} = 2\pi 50 = 314.1593\,\mathrm{rad/s}$
- $t_{base} = 1/t_{base} = 0.0032$s
- $\omega_{base,EMT} = 2\pi 50 = 314.1593\,\mathrm{rad/s}$
- $t_{base,EMT}$ =1s
- $L_{base} = Z_{base,AC}/\omega_{base}$ = 12.7mH

The values of all model parameters is given in the table below. The values are given in p.u. the only difference between the state space and EMT model, is the state space is in p.u. time while the EMT model is in absolute time, and the EMT model uses real values for C_{dc} and L_{ft}.

Table D.3: BESS plant specifications.

Parameter	State space model	EMT model
L_{ft}	0.1804	1.mH
Kp_{idq}	0.8119	0.8119
Ki_{idq}	0.0365	11.4779
Kp_{vdq}	1.2178	1.2178
Ki_{vdq}	10.9606	$3.4434 \cdot 10^3$
ω_n	1	314.1593rad/s
ω_{mv}	200	$3.1416 \cdot 10^3$rad/s
ω_{mi}	600	$6.2832 \cdot 10^3$rad/s
ω_c	0.2	62.8319rad/s
m_f	$1 \cdot 10^{-4}$	$1 \cdot 10^{-4}$
n_v	$1 \cdot 10^{-4}$	$1 \cdot 10^{-4}$

D.4 DG model

The base values used in the model is listed below.

- $S_{base} = 60kVA$
- $V_{base,AC} = 400/\sqrt{3}VRMS$
- $I_{base} = S_{base}/V_{base,AC}) = 86.603A$
- $Z_{base,AC} = V_{base,AC}/I_{base} = 2.6667\Omega$
- $\omega_{base} = 2\pi 50 = 314.1593\,\mathrm{rad/s}$
- $t_{base} = 1/t_{base} = 0.0032s$
- $\omega_{base,EMT} = 2\pi 50 = 314.1593\,\mathrm{rad/s}$
- $t_{base,EMT} = 1s$
- $L_{base} = Z_{base,AC}/\omega_{base} = 8.49mH$
- $H = (0.5 * J * \omega^2)/S_base = 0.2344s$

Table D.4: Genset plant specifications used for models.

Parameter	**State space model**	**EMT model**
Diesel Engine		
KI	0.25	78.54
R	0.05	0.05
T_a	1.2566 $p.u.$	0.004 s
T_c	5.2465 $p.u.$	0.0167 s
T_d	0.062832 $p.u.$	0.0002 s
Synchronous Generator		
T'_{do}	188.5	0.6 s
T'_d	18.85	0.06 s
T''_d	3.1416	0.01 s
T''_q	T''_d	T''_d
AVR		
K_A	400	400
T_A	6.2832	0.02
K_F	12.566	0.04
T_F	157.08	0.5

Dynamic model E

The Dynamic model of the full microgrid, with genset off, used for analysis in Chapter 6 and 7 is presented here. The model is implemented in Matlab/SIMULINK.

The model is functioning similarly to the state space model in dq frame, with all generation units modelled as current sources, the load as a constant impedance and the grid model outputs the bus voltages dependent on the generation and load currents. The model of each unit is based on the non-linear equations presented in Chapter 5, which was used to derive the linear state space models. For this reason the model does not require validation, because the validation of state space models, have validated these equations.

The Model is shown in Figure E.1. The load impedance is calculated based on specified P and Q at initial voltage.

The model is initialized using a matlab script containing newton-Raphson load flow solver which gives the bus voltages and line currents. Based on this the initial integrator states of each unit can be calculated.

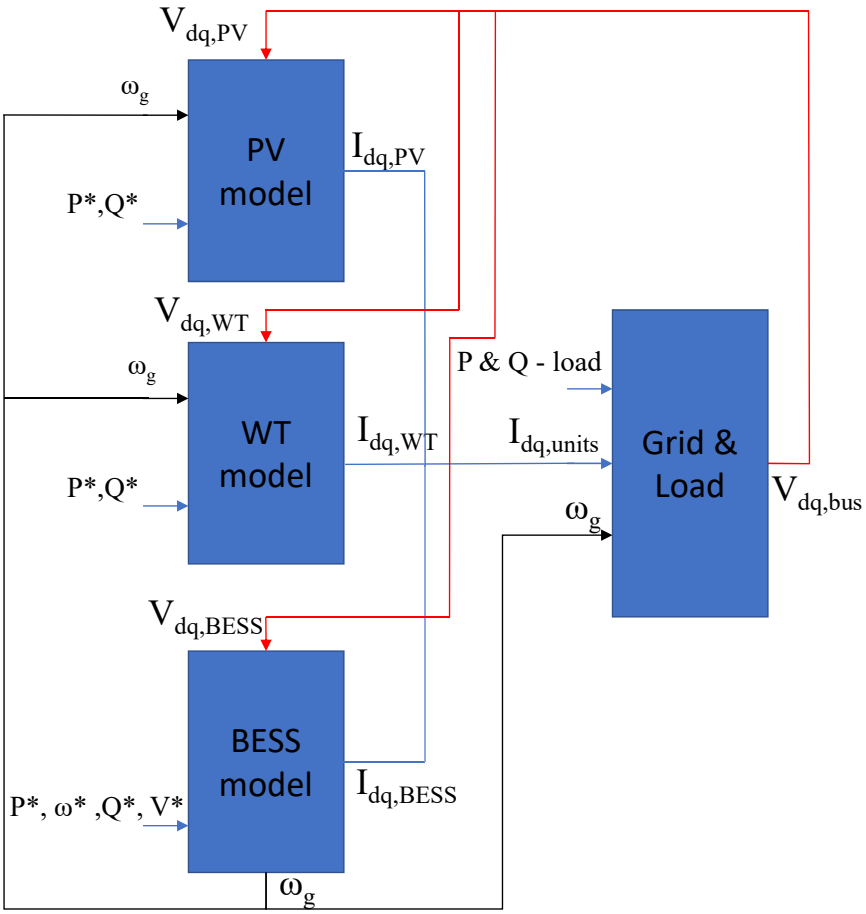

Figure E.1: Structure of the dynamic model.